SELECTIVE OXIDATION OF ACTIVATED CARBON SUPPORTED VANADIUM BASED OXIDE CATALYSTS

By

PRAKAS PALANYCHAMY

A dissertation submitted to the Department of Chemical Engineering,
Lee Kong Chian Faculty of Engineering and Science,
Universiti Tunku Abdul Rahman,
in partial fulfilment of the requirements for the degree of
Master of Engineering and Science
January 2016

I dedicate this dissertation to my beloved family members who gave moral encouragement and support throughout the duration of my study.

ABSTRACT

SELECTIVE OXIDATION OF ACTIVATED CARBON SUPPORTED VANADIUM BASED OXIDE CATALYSTS

Prakas Palanychamy

Four series of vanadium phosphorus oxide (VPO) catalysts were synthesised via dihydrate method and activated in a reaction flow of 0.75% *n*-butane/air mixture. VPO catalysts in the first series were synthesised implying various volume combination of 1-butanol and ethanol as reducing agents. The activated catalysts showed improved physico-chemical, reactivity and catalytic performances as the volume of ethanol was increased from 0 to 60 ml. However, when the volume of ethanol was increased from 90 to 150 ml, the catalyst exhibited lower surface area and poorer catalytic properties due to the formation of deleterious β-$VOPO_4$ phase. The optimal volume combination of reducing agents was determined as 90 ml 1-butanol and 60 ml ethanol within the range of study conducted. The formation of dihydrate precursor from various duration of ultrasound irradiation was investigated in the second series. As the duration of ultrasound irradiation increased from one to three hours, smaller and thinner crystal platelets were produced, enhancing the development of (0 2 0) plane, which is vital in improving the catalytic performances. Three hours of ultrasound irradiated VPO catalysts exhibited superior characteristics of physico-chemical, reactivity and catalytic performances as compared to those

less sonicated VPO catalysts. Coconut shell activated carbon (CSAC) was used as a catalyst support to disperse the VPO synthesised via conventional reflux and ultrasound irradiation in the third and fourth series, respectively. As the VPO loading increased from 10 to 40 wt% in both series, more active $(VO)_2P_2O_7$ phase was present on the support to catalyse the reaction. All the CSAC supported VPO catalysts showed better catalytic performances as compared to bulk VPO catalysts due to higher dispersion of the active phase. VPO synthesised implying ultrasound irradiation technique and supported on CSAC exhibited better catalytic properties as compared to the VPO prepared via conventional reflux method and supported on CSAC.

ACKNOWLEDGEMENTS

I praise God, the almighty for providing me this opportunity and granting me the capability to complete this research successfully. This thesis appears in its current form due the assistance and guidance from several people and I would like to express my heart felt gratitude to those who had helped me complete this project.

First and foremost, I would like to sincerely thank my supervisor, Asst. Prof. Dr. Leong Loong Kong and my co-supervisor, Asst. Prof. Dr. Gulnaziya Issabayeva from Universiti Tunku Abdul Rahman (UTAR), for providing me with an opportunity to undertake this research. Their wisdom, diligence and patience encouraged me to move past failures and obstacles throughout the research.

I also would like to take this opportunity to thank Ms. Kang Jo Yee and Mr. Lim Kuan Hoe for their excellent instrumentation skills and help throughout my project. I am also indebted to Kekwa Indah Sdn. Bhd. for providing me with KI Coconut Shell Activated Carbon, which was crucial in my research. Last but not least, I would like to thank my family members for standing by my side despite all the hardship faced and encouraged me to complete this project successfully.

APPROVAL SHEET

This dissertation entitled "**SELECTIVE OXIDATION OF ACTIVATED CARBON SUPPORTED VANADIUM BASED OXIDE CATALYSTS"** was prepared by PRAKAS PALANYCHAMY and submitted as partial fulfilment of the requirements for the degree of Master of Engineering and Science at Universiti Tunku Abdul Rahman.

Approved by:

_____

(Asst. Prof. Dr. Leong Loong Kong) Date: ……..
Supervisor
Department of Chemical Engineering
Faculty of Engineering and Science
Universiti Tunku Abdul Rahman

_____

(Asst. Prof. Dr. Gulnaziya Issabayeva) Date: ……..
Co-supervisor
Department of Chemical Engineering
Faculty of Engineering and Science
Universiti Tunku Abdul Rahman

FACULTY OF ENGINEERING AND SCIENCE

UNIVERSITI TUNKU ABDUL RAHMAN

Date: _____

SUBMISSION OF DISSERTATION

It is hereby certified that **Prakas Palanychamy** (ID No: **12UEM06906**) has completed this dissertation entitled "SELECTIVE OXIDATION OF ACTIVATED CARBON SUPPORTED VANADIUM BASED OXIDE CATALYSTS" under the supervision of Asst. Prof. Dr. Leong Loong Kong (Supervisor) from the Department of Chemical Engineering, Faculty of Engineering and Science, and Asst. Prof. Dr. Gulnaziya Issabayeva (Co-Supervisor)* from the Department of Chemical Engineering, Faculty of Engineering and Science.

I understand that University will upload softcopy of my dissertation in pdf format into UTAR Institutional Repository, which may be made accessible to UTAR community and public.

Yours truly,

_____

(Prakas Palanychamy)

DECLARATION

I hereby declare that the dissertation is based on my original work except for quotations and citations which have been duly acknowledged. I also declare that it has not been previously or concurrently submitted for any other degree at UTAR or other institutions.

_____

(PRAKAS PALANYCHAMY)

Date _____

TABLE OF CONTENTS

LIST OF TABLES

LIST OF FIGURES

LIST OF ABBREVIATION

α_I	Alpha I
α_{II}	Alpha II
β	Beta
δ	Delta
ε	Epsilon
γ	Gamma
ω	Omega
AC	Activated carbon
BET	Brunauer-Emmett-Teller
C_2H_4	Ethylene
C_2H_6	Ethane
Cl^*	Chlorine free radicals
CSAC	Coconut shell activated carbon
EDX	Energy dispersive x-ray
GAC	Granular activated carbon
H_2	Hydrogen
HCl	Hydrochloric acid
H_2SO_4	Sulphuric acid
H_3PO_4	Phosphoric acid
ICP-OES	Inductively coupled plasma optical emission spectrometry
JCPDS	Joint committee on powder diffraction standards
$KMnO_4$	Potassium permanganate
MA	Maleic anhydride

O_2	Oxygen
O_3	Ozone
PAC	Powdered activated carbon
PO_4	Phosphate
SO_2	Sulphur dioxide
SO_3	Sulphur trioxide
TPR	Temperature programmed reduction
UPR	Unsaturated polyester resins
V^{3+}	Vanadium(III)
V^{4+}	Vanadium(IV)
V^{4+}-O^{-}	Oxygen associated with vanadium(IV) phase
V^{5+}	Vanadium(V)
V^{5+}-O^{2-}	Oxygen associated with vanadium(V) phase
V_2O_5	Vanadium pentoxide
VO_6	Vanadium hexaoxide
$VOHPO_4 \cdot 0.5H_2O$	Hemihydrate precursor
$VOHPO_4 \cdot 1.5H_2O$	Sesquihydrate precursor
$VOPO_4 \cdot 2H_2O$	Dihydrate precursor
$VO(H_2PO_4)_2$	Oxo-vanadium(IV) dihydrogen phosphate
$VO(PO_3)_2$	Vanadyl phosphite
$(VO)_2P_2O_7$	Vanadyl pyrophosphate
VPA	Aqueous method
VPD	Dihydrate method
VPO	Vanadium phosphorus oxide
XRD	X-ray diffraction

CHAPTER ONE

INTRODUCTION

1.1 Fundamentals of Catalysis

The existence of catalyst was discovered by Berzelius in 1836. He proposed the word “catalytic power” and rationalised it as the substance that is able to awake affinities, which are asleep at a specific temperature by their mere presence. The catalyst concept was improvised throughout the century until a final acceptable definition that it is a chemical substance that accelerates the rate of a chemical reaction until equilibrium is reached by lowering the activation energy required for the reaction to take place without being consumed in the reaction itself (Viswanathan et al., 2002).

The process of a catalyst assisting a chemical reaction is known as catalysis. The presence of a positive catalyst speeds up the chemical reaction while the presence of negative catalyst known as inhibitors, slows down the reaction. The rate of reaction differs with the presence of catalyst and this is due to the alterations that the catalysts exerts on the kinetics of the reaction. Interacting with the reactant catalyst enters into the reaction cycle, but is regenerated in its last step, hence not consumed in its course (Viswanathan et al., 2002).

1.2 Types of Catalyst

1.2.1 Heterogeneous Catalyst

Heterogeneous catalyst are commonly used in the industry where the catalyst, usually in solid phase while the reactants are either in liquid or gaseous phase. Heterogeneous catalysis implies that the catalyst and the reactants are in different phase and are frequently used due to its high separation efficiency. Higher separation efficiency of heterogeneous catalyst accounts to its higher reaction activity (Clark, 2012).

Heterogeneous catalyst also has a higher percentage of catalyst recovery as the catalyst and the reactants are in different phase. This makes the product separation less tedious and widens the catalyst's application (Fadhel et al., 2010).

The manufacturing process of sulphuric acid (H_2SO_4) is an example of heterogeneous catalysis. Solid vanadium pentoxide (V_2O_5) is used as a catalyst in the reaction between sulphur dioxide (SO_2) and oxygen (O_2) to form sulphur trioxide (SO_3) where all the reactants and products formed are in gaseous phase (Clark, 2012).

The equation for the formation of sulphur trioxide in the manufacturing of sulphuric acid is shown in Equation 1.1:

$$2SO_{2\,(g)} + O_{2\,(g)} \xrightarrow[V_2O_5]{} 2SO_{3\,(g)} \qquad (1.1)$$

(Clark, 2012)

1.2.2 Homogeneous Catalyst

Homogeneous catalyst is molecularly dispersed in the reactants, either in liquid or gaseous state. Homogeneous catalysis implies both catalyst and reactant are in the same phase. The separation of homogeneous catalyst from the final product is very tedious, hence resulting it to be its major drawback (Fadhel et al., 2010).

One of the most common example of homogeneous catalysis is the decomposition of ozone (O_3) in the atmosphere by chlorine free radicals ($Cl^{\star}$). The ozone is decomposed to oxygen by chlorine free radicals, which act as the catalyst and are regenerated when it leaves the reaction cycle. Both chlorine free radical and ozone are in gaseous phase (Clark, 2012).

The equations for the decomposition of ozone by chlorine free radical are shown in Equation 1.2, 1.3 and 1.4, respectively:

$$Cl^{\star}_{(g)} + O_{3\,(g)} \rightarrow ClO_{3\,(g)} \quad (1.2)$$

$$ClO_{3\,(g)} \rightarrow ClO_{(g)} + O_{2\,(g)} \quad (1.3)$$

$$ClO_{(g)} + O_{(g)} \rightarrow Cl^{\star}_{(g)} + O_{2\,(g)} \quad (1.4)$$

(Clark, 2012)

1.2.3 Biocatalyst

Biocatalyst are often referred to as catalyst which occurs naturally and the most prominent examples of biocatalyst would be enzymes. Enzyme plays an essential role in converting any substrate to a specific product with high conversion rate. The specificity of the enzyme's structure allows the catalyst to attach to a specific substrate. This increases the selectivity of the reaction as enzymes are very shape specific reacting with the desired substrate only (Prather, 2004).

An example of a biocatalyst is illustrated in Figure 1.1, where the substrate, a sucrose is bonded to the enzyme's active site to form an enzyme-substrate complex. The active site breaks down the substrate and produces glucose and fructose, the monomers of sucrose. The enzyme returns to its original structure and is available to catalyse the next reaction (Prather, 2004).

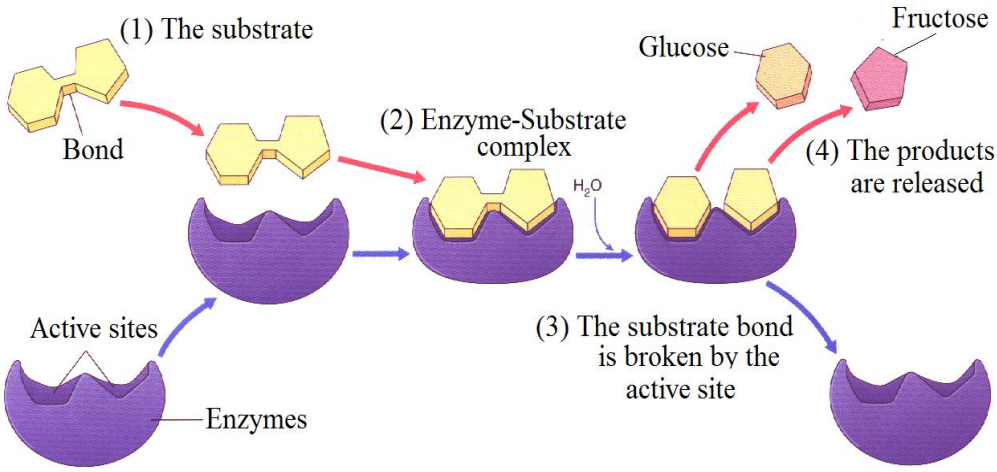

Figure 1.1: Enzyme – substrate interaction

1.3 The Mechanism of Catalysis

Every catalyst adheres to a series of steps in their catalytic reaction. Although various types of catalyst are used in different reactions, the general mechanism would be the same involving three elementary steps: initiation, formation and desorption. Hydrogenation of ethylene on a heterogeneous catalyst shown in Figure 1.2 is used to explain this basic principle. In the initiation step, the reactants, in this case hydrogen (H_2) and ethylene (C_2H_4) are adsorbed on the catalyst surface. The bond between the molecules are broken and an intermediate bond is formed between the atoms of the reactants and the surface of the catalyst. The individual atom reacts with each other to form the product ethane (C_2H_6) completing the formation cycle. The product formed has a weak intermediate bond with the surface of the catalyst, which is broken and the product is detached from the catalyst (Vollhardt and Schore, 2009).

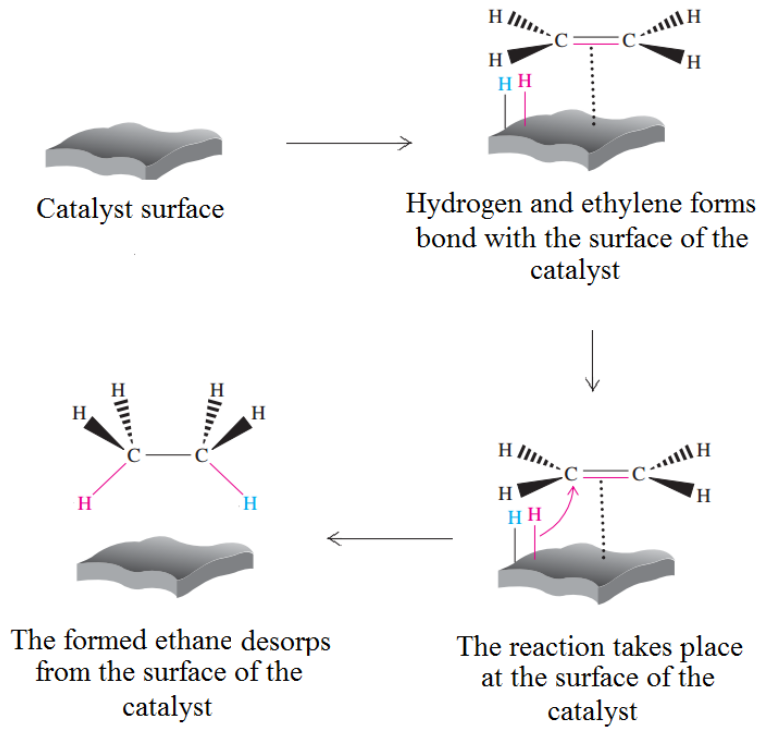

Figure 1.2: Mechanism of catalytic hydrogenation of ethylene

1.4 Problem Statement

Vanadium phosphorus oxide (VPO) catalyst have been reported to be efficient heterogeneous catalysts for oxyfunctionalisation of C_2-C_5 alkanes. However, the system had been successfully applied at commercial level only for the oxidation of *n*-butane to maleic anhydride (MA). It is the only example of an industrially practiced selective oxidation reaction involving alkane activation (Lopez, 2006).

Maleic anhydride, $C_4H_2O_3$, is chemically known as 2,5-furandione. Today, it is a chemical of significant industrial importance in the fields of petrochemicals and polymer feedstock. The production of maleic anhydride from *n*-butane oxidation relies on the efficiency of VPO catalyst. The highest activity and selectivity obtained from VPO catalyst in the selective oxidation of *n*-butane was 65 % and 82 %, respectively. However, the method used in synthesising the catalyst involves the usage of benzyl alcohol which is not an environmentally friendly reagent. It also requires a longer duration to synthesise the VPO catalyst (BASF Malaysia, 2013).

1.5 Research Aims and Objectives

1.5.1 Research Aims

The research aim is to synthesise VPO catalysts using more environmental friendly and shorter duration synthetic route as to improve the physical, chemical, reactivity and catalytic performances of the catalysts.

1.5.2 Objectives

1. To study the effect of various volume combination of more environmentally friendly reducing agents for the synthesis of VPO catalyst.
2. To investigate the effect of ultrasound irradiation on the physico-chemical, reactivity and catalytic performances of VPO catalysts.
3. To analyse the effect of various weight percentages of VPO synthesised via conventional reflux and ultrasound irradiation and supported on activated carbon catalyst support via incipient wetness impregnation method.

CHAPTER TWO

LITERATURE REVIEW

2.1 Selective Oxidation of *n*-Butane

For many decades, oxidation of benzene was the primary route to produce maleic anhydride (MA). Vaporised benzene and air are mixed and heated before passed over vanadium pentoxide (V_2O_5) catalyst dispersed in the reactor. However, the rising cost of benzene and the threat it pose as a carcinogenic compound had made the process obsolete. The principle reaction of benzene oxidation is summarised in Figure 2.1 (Luciani, 2009).

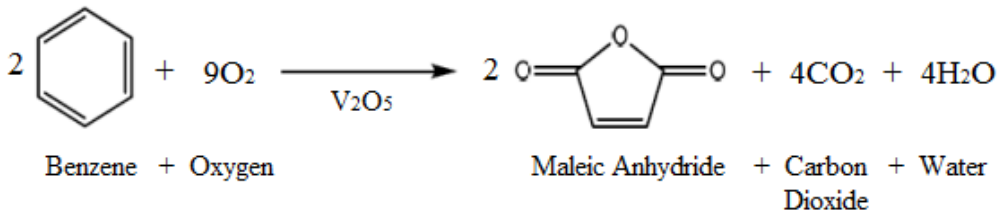

Figure 2.1: Benzene oxidation

The production of MA only requires four carbons, thus the earlier raw material is substituted by *n*-butane. Selective oxidation of *n*-butane was established as there was no carbon lost, lower price for the feedstock, higher availability in many regions and its non-hazardous property. These factors led to the production of maleic anhydride using *n*-butane at Monsanto's plant in 1974 (Felthouse et al., 2001).

The reaction of *n*-butane to form MA is a 14 electron oxidation which occurs on the catalyst surface. In this 14 electron oxidation reaction, eight hydrogen atoms are removed, while three oxygen atoms are inserted and a ring closure is performed. The principle reaction of *n*-butane oxidation is summarised in Figure 2.2 (Felthouse et al., 2001).

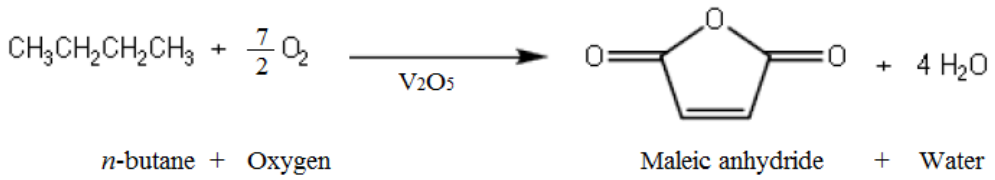

Figure 2.2: *n*-butane oxidation

The mechanism of *n*-butane oxidation can be broken down into several steps, beginning with *n*-butane as the starting material. This selective oxidation process goes through a series of reactions with an intermediate product formed at the end of each reaction. Table 2.1 shows the proposed steps in the oxidation of *n*-butane to MA. Figure 2.3 outlines the mechanism of *n*-butane oxidation (Guliants and Carreon, 2005).

Table 2.1: Proposed steps in the oxidation of *n*-butane to maleic anhydride

Product / Intermediates	Type of Reaction
n-butane → 1-butene	Oxidative dehydrogenation
1-butene → 1,3-butadiene	Allylic oxidation
1,3-butadiene → 2,5-dihydrofuran	1-4 Oxygen insertion
2,5-dihydrofuran → Furan	Allylic oxidation
Furan → Butyrolactone	Electrophilic oxygen insertion
Butyrolactone → Maleic anhydride	Electrophilic oxygen insertion

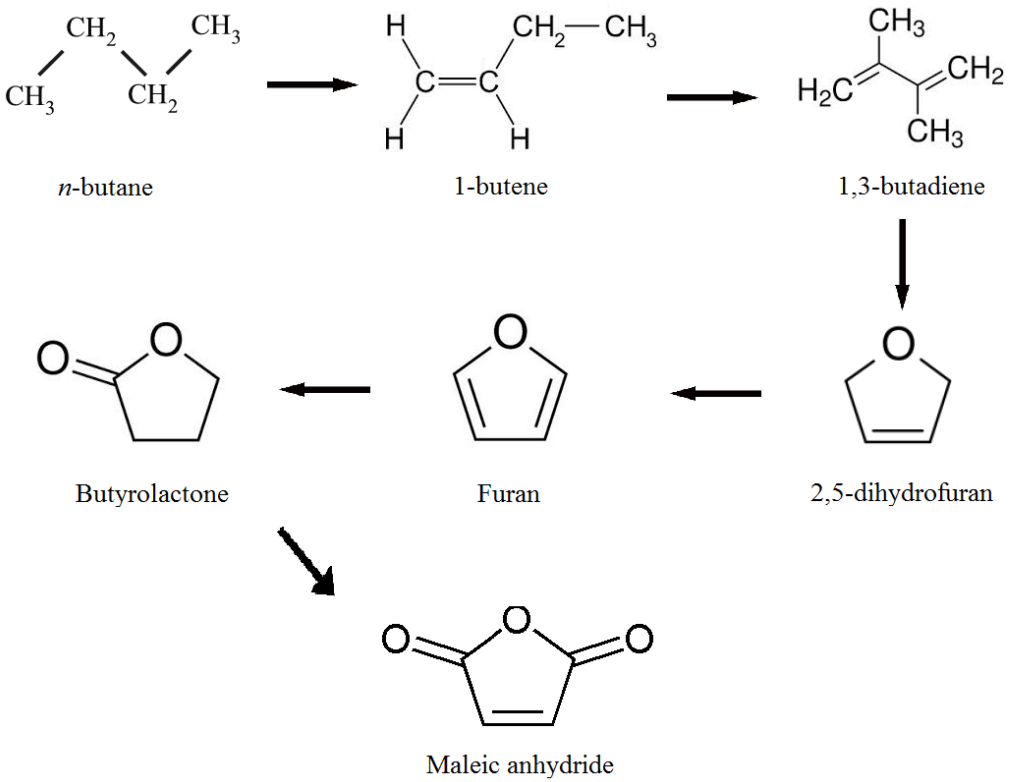

Figure 2.3: Mechanism of *n*-butane Oxidation

2.2 Maleic Anhydride

2.2.1 Properties and Applications

Maleic anhydride (MA) is a versatile monomer which can provide reactive anhydride or carboxylic groups with nucleophilic molecules. It is an excellent joining and cross linking agent as it consists of three actives sites, namely two carboxyl group and one double bond. It is also known as cis-butenedioic anhydride, 2,5-furandione and toxilic anhydride. Table 2.2 shows the physical properties of maleic anhydride (Zhou et al., 2004).

Table 2.2: Physical properties of maleic anhydride

Properties	Maleic Anhydride
Formula	$C_4H_2O_3$
Molecular weight	98.06 g mol^{-1}
Melting point	52.6° C
Boiling point	202° C
Flammability Limit	1.4 % (Lower)
	7.1 % (Upper)
Solubility in water (25° C)	79 g / 100 ml

It is an important intermediate in the engineering polymer sectors. MA has extremely low tendency to homopolymerise in a radical polymerisation condition, on contrary it copolymerises with a variety of donor monomers. The anhydride groups in the polymer chain make it very reactive and commonly used in various fields (Nasirtabrizi et al., 2013).

The dominant end use of MA is in the production of unsaturated polyester resins. These laminating resins, which have high structural strength and good dielectric properties have a variety of applications in automobile bodies, building panels, moulded boats, chemical storage and lightweight pipes (Nasirtabrizi et al., 2013).

MA is an important chemical intermediate as lubricating oil additives. It is used in gasoline and diesel engine crankcase oil as dispersants and corrosion inhibitors. It is also used in the manufacture of agricultural chemicals such as herbicides, pesticides, plant growth regulators and soil fertilisers (BASF Malaysia, 2013).

2.2.2 Worldwide Demand for Maleic Anhydride

Asia Pacific dominated the maleic anhydride (MA) market in 2012 with 55% of global market shares as shown in Figure 2.4. The increasing infrastructure development coupled with increasing automobile sales in Asia Pacific augmented the growth of its use as unsaturated polyester resins (UPR). It is expected to retain its dominance over the period owing to the increasing demand of automobiles coupled with increasing infrastructural developments in housing sector in Asia Pacific region (Grand View Research, 2013).

Global MA demand in 2013 was 2100.7 kilo tons, where 1034.8 kilo tons accounted for the production of UPR. The demand is expected to grow at a steady rate of 5.6% annually from 2014 to 2020. Increasing demand in end use applications such as marine, automobile and construction industry is expected to surge demand for UPR over the forecast period (Grand View Research, 2013).

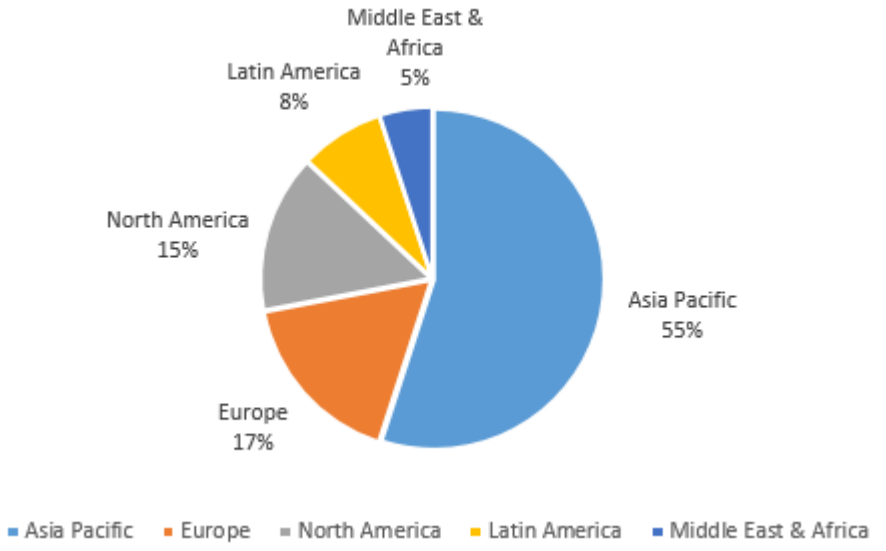

Figure 2.4: Global maleic anhydride production in 2012

2.2.3 Production of Maleic Anhydride from *n*-butane

Butane based catalyst technology can be divided into three categories, namely fixed bed reactor, fluidised bed reactor and transport bed reactor. In the fixed bed route, air and superheated butane are mixed prior being fed to the reactor containing the vanadium-phosphorus oxide (VPO) catalyst and the temperature is controlled with a resistant thermometer connected to a temperature controller. Glass wool is used under the catalyst bed to prevent the sliding of the granular catalyst to the condenser. To obtain a homogeneous flow of air and prevent channelling, glass wool is placed on top of the reactor. Oxidation is carried out at 400°C - 500°C. The reaction gases are cooled and maleic anhydride (MA) is condensed. A schematic drawing of the fixed bed reactor is shown in Figure 2.5 (Fernandez et al., 2010).

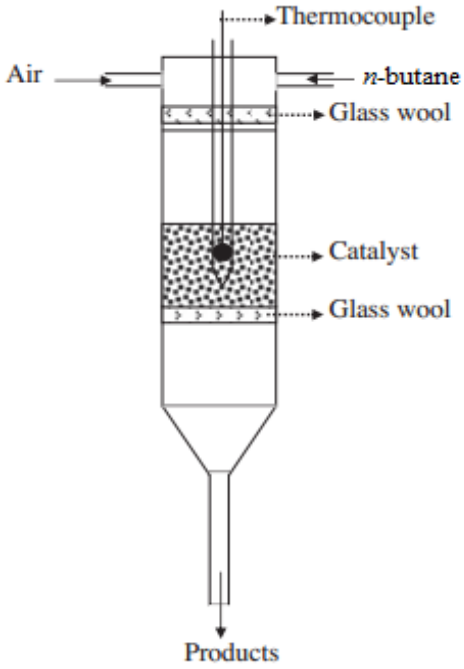

Figure 2.5: Schematic diagram of fixed bed reactor

In fluidised bed reactor an electrical heater is used as the heating element, while glass wool provides insulation for the reactor and the temperature of the reaction is controlled through a temperature controller connected to a thermocouple (Fernandez et al., 2010). The technology to produce MA from butane using transport bed reactor was developed by DuPont and commercialised in 1961. It includes a two-step process whereby *n*-butane is oxidised to MA using abrasion resistant catalyst and recovered in an aqueous system while the catalyst is re-oxidised in a separate reactor. The plant was closed in 2004 and dismantled due to various operational problems (Patience and Bockrath, 2010).

2.3 Vanadium Phosphorus Oxide (VPO)

2.3.1 VPO Phases for Selective Oxidation of *n*-butane

VPO has shown promising results as heterogeneous catalyst in the selective oxidation of propane to acrylic acid, *n*-butane to maleic anhydride and pentane to phthalic anhydride (Lin, 2001; Datta et al., 2002; Zazhigalov et al., 2009). It consists of layered compound that exist in a wide range of structural forms due to the diversity in the bonding of vanadium hexaoxide (VO_6) and phosphate (PO_4) structural units. VPO phases associated with vanadium oxidation states are listed in Table 2.3. These layers are held together by weak Van der Waals forces, therefore amenable for intercalation reaction (Bordes et al., 1984; Johnson et al., 1984; Leonowicz et al., 1985; Bordes, 1987; Sananes et al., 1995).

Table 2.3: VPO phases

Vanadium Oxidation State	Phases
V^{5+}	α_I-$VOPO_4$, α_{II}-$VOPO_4$, β-$VOPO_4$, γ-$VOPO_4$, δ-$VOPO_4$, ε-$VOPO_4$, ω-$VOPO_4$, $VOPO_4 \cdot 2H_2O$
V^{4+}	$(VO)_2P_2O_7$, $VO(PO_3)_2$, $VO(H_2PO_4)_2$, $VOHPO_4 \cdot 0.5H_2O$
V^{3+}	VPO_4 and $V(PO_3)_3$

VPO phases with V^{3+} oxidation states are rarely encountered in *n*-butane oxidation. The common vanadium oxidation phases present would be V^{5+} which accounts for the catalyst selectivity and V^{4+} for its activity, particularly vanadyl pyrophosphate ($(VO)_2P_2O_7$) which is regarded as the catalyst's active phase (Bordes, 1987; Centi, 1993; Dutta, 2005).

2.3.2 Surface Model of Vanadyl Pyrophosphate

Various models of active sites in *n*-butane oxidation to maleic anhydride (MA) have been proposed to date. They are tabulated in Table 2.4.

Table 2.4: Proposed theory in *n*-butane oxidation

	Proposed Theory	References
1)	Coherent interfaces between various vanadyl phosphate ($VOPO_4$) phases and $(VO)_2P_2O_7$	Bordes, 1987
2)	Mixture of well crystallised $(VO)_2P_2O_7$ and an amorphous $VOPO_4$ phase involving corner sharing octahedral	Bergeret et al., 1987; Batis et al., 1991
3)	V^{5+} species in strong interaction with vanadyl phosphite ($VO(PO_3)_2$) structure in VPO catalyst	Sananes et al., 1995
4)	Presence of controlled amount of V^{5+} sites on the (1 0 0) plane of $(VO)_2P_2O_7$	Centi et al., 1988

Studies by Bordes (1987), suggest that the coherent interface between the slabs of (2 0 0) plane of $VOPO_4$ and (1 0 0) plane of $(VO)_2P_2O_7$ are the active site for *n*-butane oxidation to MA. On the contrary, the active sites are believed not to be associated with the interfaces between the crystalline phase but consists of mixture of $(VO)_2P_2O_7$ and amorphous $VOPO_4$ phase involving corner sharing of octahedron (Bergeret et al., 1987; Batis et al., 1991). This amorphous phase was interpreted as β-$VOPO_4$ and γ-$VOPO_4$, and is represented in Figure 2.6 (A) (Volta, 1982). Yamazoe et al., (1988) reported that $VO(H_2PO_4)_2$ as the precursor of the active phase in *n*-butane oxidation and is transformed to an amorphous $VO(PO_3)_2$ catalyst.

According to Cavani and Trifiro (1994) activity of VPO catalyst is attributed to $(VO)_2P_2O_7$ while the selectivity towards MA associated with controlled amount of V^{5+} sites, as shown in Figure 2.6 (C).

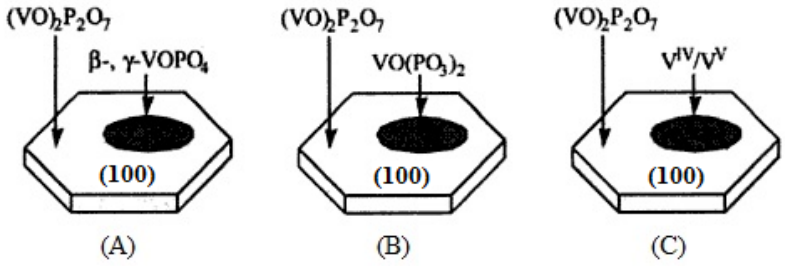

Figure 2.6: Models of active surface of the VPO catalyst according to (A) Volta (1982), (B) Yamazoe et al., (1988) and (C) Cavani and Trifiro (1994)

Based on these suggestions, the best VPO catalyst preferentially expose (1 0 0) planes of $(VO)_2P_2O_7$ and the bulk vanadyl pyrophosphate serves as a support for this active surface. Figure 2.7 shows the selective and non-selective oxidation sites on $(VO)_2P_2O_7$ (Centi et al., 1988; Cavani and Trifiro, 1994). Truncations of the (0 0 1) and (0 2 1) planes are taken as sites for non-selective oxidation of *n*-butane (Volta, 1982; Matsuura and Yamazaki, 1990; Okuhara and Misono, 1993).

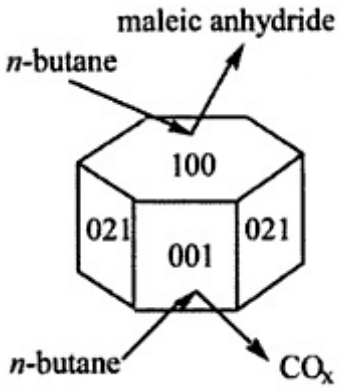

Figure 2.7: Selective and non-selective oxidation sites

2.3.3 Preparation of VPO Catalyst

2.3.3.1 Hemihydrate Route

The preparation of $(VO)_2P_2O_7$ via vanadyl hydrogen phosphate hemihydrate ($VOHPO_4 \cdot 0.5H_2O$) precursor is the most studied route. There are three designated methods in preparing the hemihydrate precursor, namely aqueous method (VPA), organic method (VPO) and dihydrate method (VPD).

Aqueous Method (VPA):

In the aqueous method, V_2O_5 is dissolved in mineral acid such as hydrochloric acid (HCl), followed by the addition of phosphoric acid (H_3PO_4) and refluxed for two hours, as shown in Equation 2.1 (Taufiq Yap et al., 2001).

$$V_2O_5 + HCl + H_3PO_4 \xrightarrow{\Delta\ 2\ hours} VOHPO_4 \cdot 0.5H_2O \quad (2.1)$$

Organic Method (VPO):

As for the organic method, V_2O_5 is reduced using isobutyl alcohol and benzyl alcohol followed by the addition of H_3PO_4 and refluxed for 16 hours, as shown in Equation 2.2 (Taufiq Yap et al., 2001).

$$V_2O_5 + Alcohol + H_3PO_4 \xrightarrow{\Delta\ 16\ hours} VOHPO_4 \cdot 0.5H_2O \quad (2.2)$$

Dihydrate Method (VPD):

V_2O_5 is added to distilled water followed by H_3PO_4 and refluxed for 24 hours to obtain the dihydrate precursor ($VOPO_4 \cdot 2H_2O$), where it is reduced to hemihydrate precursor in a separate step with the addition of alcohol and refluxed for another 24 hours (Taufiq Yap et al., 2004). The reactions are shown in Equation 2.3 and Equation 2.4.

$$V_2O_5 + H_2O + H_3PO_4 \xrightarrow{\Delta\ 24\ hours} VOPO_4 \cdot 2H_2O \quad (2.3)$$

$$VOPO_4 \cdot 2H_2O + Alcohol \xrightarrow{\Delta\ 24\ hours} VOHPO_4 \cdot 0.5H_2O \quad (2.4)$$

The catalyst produced from the precursor obtained through VPA method reported to exhibit lower activity (Taufiq Yap et al., 2006). The usage of alcohol instead of mineral acid to reduce V_2O_5 in the VPO method has produced catalyst with higher specific activity, as the alcohol trapped between the layers during the formation of $VOHPO_4 \cdot 0.5H_2O$ induced more active sites (Busca et al., 1986). The nature of the active sites remained the same for the catalyst prepared via VPD method and VPO method, however the catalyst prepared via VPD method exhibited higher surface area (Kiely et al., 1995).

The catalyst synthesised via VPA method exhibits irregular morphologies, while those obtained via VPO method shows oblong morphology exposing the non-selective (0 0 1) and (0 2 1) active sites in addition to the (1 0 0) plane. $(VO)_2P_2O_7$ prepared via VPD method preferentially expose (1 0 0) plane which contributes to the higher surface area and improved catalytic properties in MA formation (Kiely et al., 1995).

2.3.3.2 Sesquihydrate Route

Matsuura and Yamazaki, (1990) developed an alternate route in preparing $(VO)_2P_2O_7$ via vanadyl hydrogen phosphate sesquihydrate ($VOHPO_4 \cdot 1.5H_2O$) precursor. The synthesis of $VOHPO_4 \cdot 1.5H_2O$ is two step procedure involving formation of $VOPO_4 \cdot 2H_2O$ via VPD method and further reduction of the intermediate using 1-butanol (Taufiq Yap et al., 2004). The reactions are shown in Equation 2.5 and Equation 2.6. Using 1-butanol as a solvent to reduce the intermediate is more environmentally friendly (Matsuura and Yamazaki, 1990).

$$V_2O_5 + H_2O + H_3PO_4 \xrightarrow{\Delta\ 24\ hours} VOPO_4 \cdot 2H_2O \quad (2.5)$$

$$VOPO_4 \cdot 2H_2O + Alcohol \xrightarrow{\Delta\ 24\ hours} VOHPO_4 \cdot 1.5H_2O \quad (2.6)$$

2.3.4 Factors Affecting the Performance of VPO Catalyst

2.3.4.1 Support System

Generally catalyst supports are porous metal oxides with high surface area or activated carbons with high pore volume to produce a well dispersed catalyst, hence improve the catalytic performance. Alumina, silica and carbon are the most common support for VPO catalyst, while magnesia, zirconia, titania and zeolites are used in several applications. Supported catalyst offer several advantages over their unsupported counterparts as shown in Table 2.5 (Zazhigalov et al., 1986; Centi et al., 1988; Harding et al., 1994; Overbeek et al., 1996; Birkeland et al., 1997).

Table 2.5: Advantages of supported catalyst

	Advantages
1)	Increased surface area to volume ratio of the active phase
2)	Higher attrition resistance due to improved mechanical strength
3)	Enhanced lifespan due to improved heat transfer characteristics
4)	Controllable texture leading to higher mass transfer properties

Nakamura et al., (1974) reported the earliest studies on VPO supported catalyst. They investigated alumina-supported VPO catalyst and concluded higher selectivity towards MA were obtained with supported catalyst. Most supported VPO catalyst are reported to consist higher V^{5+} species due to the strong support-oxide interaction that hinders the formation of VPO phases. These catalysts are reported to consist α-$VOPO_4$ or γ-$VOPO_4$ phase and exhibited lower *n*-butane conversion (Bordes, 1987; Hutchings, 1993).

2.3.4.2 Doped System

Addition of dopants or also known as promoters enhance the performance of the VPO catalyst. Dopants by itself are inactive, hence it is added during the preparing of the catalyst to improve the activity, selectivity or the stability of the catalyst (Cheng, 1996; Felthouse et al., 2001). Commonly used promoters in the industrial catalysts include Ba, Bi, Cd, Ce, Cu, Cr, Fe, La, Mg, Mo, Ni, Zn (Cornagalia et al., 2000).

Studies done by Hutchings (1991) pointed out that promoters have a twofold structural role, namely to assist in the formation of the required VPO compound and decrease the formation of the deleterious phases as well as enable the formation of solid solution that regulates the catalytic activity. The types of promoters and their functions are listed in Table 2.6.

Table 2.6: Types of promoters and their functions

Types of Promoters	Function
Textural promoters	Inhibits the growth of small particles in the active phase during usage
Structural promoters	Dissolves in the active phase and alters the electronic character
Poison resistant promoter	Protects the active phase from being poisoned by impurities and products generated by the reaction

Catalyst incorporated with promoters showed improved catalytic properties compared to the bulk catalyst. According to Brutovsky et al., (1997), addition of promoters such as Mg, Ca and Ba showed higher conversion of *n*-butane and greater selectivity towards maleic anhydride. Besides that, the selectivity towards MA increased in the order of Mg, Ca and Ba as the basicity of the promoters increased, suggesting the yield of the catalyst is dependent on the nature of the promoters.

Generally the promoters have a basic nature and can easily donate electrons to the framework of vanadyl phosphate, hence the incorporation of alkali or alkaline earth metal ions would donate electrons to the VPO lattice. This gives rise to the negative charge on the lattice oxygen atoms, increasing the strength of the basic centres at the surface of the VPO catalyst and favours the catalyst to exhibit higher selectivity towards MA formation (Zazhigalov et al., 1996).

Bismuth supported VPO catalyst exhibited enhanced activity as the catalyst possess highly active and labile lattice oxygen originated from the V^{4+} species (Taufiq Yap et al., 2006). Oxygen species associated with V^{4+} played important role in the activity of the catalyst while V^{5+} related oxygen species are linked to the formation of MA. To obtain a catalyst with high *n*-butane oxidation and high formation of maleic anhydride, fine tuning on the amount and type of promoters added need to be done (Goh et al., 2008).

2.3.4.3 Calcination Duration

Calcination duration refers to the time the precursor is activated in the reactor. Catalyst obtained after a prolonged period of time on stream are referred to as "equilibrated catalyst" while a fresh catalyst is termed as "non-equilibrated catalyst". Precursors activated for a period of more than 100 hours will yield "equilibrated catalyst" while those calcined for a duration lesser than 100 hours results in the formation of "non-equilibrated catalyst". The latter is lower in activity due to its lower surface area and higher in selectivity as the V^{4+} phases are easily oxidised to V^{5+} phases (Cavani and Trifiro, 1994; Albonetti et al., 1996).

Figure 2.8 shows the evolution of VPO catalyst as the activation duration is prolonged. Part of the precursor would be topotactically transformed into $(VO)_2P_2O_7$ while the remainder of the catalyst undergoes oxydehydration and forms δ-$VOPO_4$. It then undergoes isovalence transformation to produce α_{II}-$VOPO_4$. Both of these phases undergo reduction to form $(VO)_2P_2O_7$, which corresponds to the change in the vanadium species from the V^{5+} to the V^{4+} state (Abon et al., 1995; Kiely et al., 1996). Increasing the calcination duration would increase the surface area of the catalyst since the precursors are in contact with the flowing gas for a longer duration. In this research all the catalyst are calcined for 24 hours, which is the generally accepted duration for a "non-equilibrated catalyst" (Taufiq Yap et al., 2001).

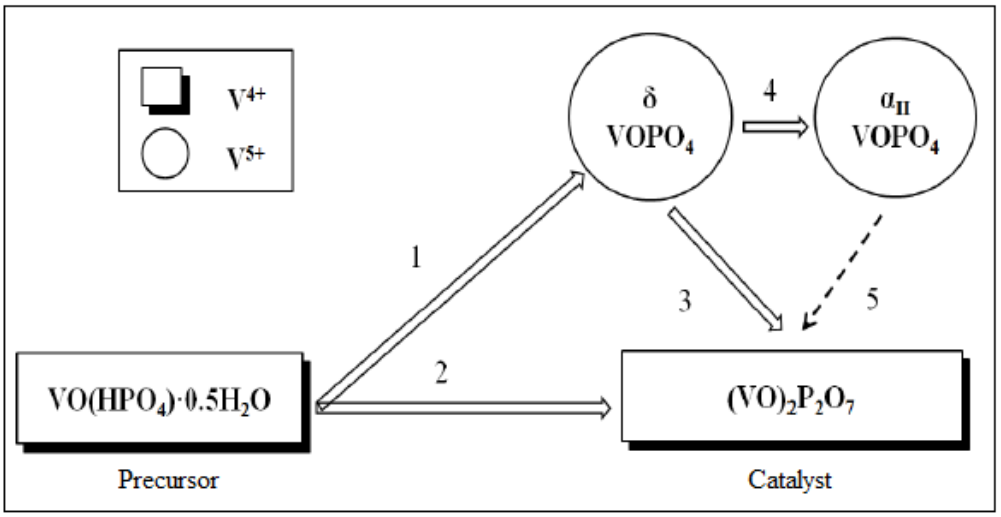

Figure 2.8: Evolution of VPO catalyst with activation time: (1) Oxydehydration, (2) Topotactic transformation, (3) & (5) Reduction and (4) Isovalence transformation

2.3.4.4 Calcination Temperature

Calcination temperature refers to the temperature the precursor is activated in the reactor. The temperature ranges from 400°C to 500°C, with higher calcination temperature often resulting in catalyst with lower surface area and poor conversion as the active sites are decomposed (Irmawati et al., 2004).

The main purpose carrying out calcination is to activate the precursor by removing the excess water content which takes place at the boiling point of water, 100°C. Besides that, various volatile organic compounds formed during the preparation process are also removed when the temperature of the reactor is gradually raised to 200°C. All the catalysts in this research are calcined at 460°C which is accepted as the optimum temperature (Poli et al., 1981).

2.3.4.5 Calcination Environment

Calcination environment refers to the gas used to activate the precursor. Different calcination environment results the catalyst to exhibit different catalytic properties. Studies carried out by Taufiq Yap and Saw (2008) revealed catalyst calcined in the flow of *n*-butane/air mixture showed higher surface area and improved conversion compared to catalyst obtained in flow of propane/air mixture.

According to Cheng and Wang (1997) calcination environment affects the catalyst morphology and vanadium valence. Gas with higher oxidising ability results in higher vanadium valance, higher selectivity towards MA and lower surface area. Hence, *n*-butane/air mixture is chosen as the calcination gas as it has lower oxidising ability and results in catalyst with higher surface area and higher conversion (Taufiq Yap and Saw, 2008)

The concentration of *n*-butane used in industry ranges from 1.5% to 2% in a mixture of air for fixed bed reactor. From an industrial view point, operation under high *n*-butane concentration would result in higher selectivity towards MA. Most laboratory studies involving VPO catalyst are carried out using 0.75% *n*-butane/air mixture with small sample size to maintain the homogeneity of the reaction atmosphere as well as avoid explosion of the fixed bed reactor (Kamiya et al., 2001).

2.3.4.6 P/V Atomic Ratio

Optimal catalyst composition presents a slight excess of phosphorus with respect to the stoichiometric value of the precursor (Okuhara and Misono, 1993; Cornagalia et al., 1999). There is a general agreement that high P/V ratio helps in avoiding the oxidation of V^{4+} phase in $(VO)_2P_2O_7$ (Centi et al., 1988; Stefani et al., 1990; Connor et al., 1990; Guilhoume et al., 1992). Industrial catalyst with P/V ratio between 1.00 - 1.20 have shown optimum performance (Bordes, 1993; Centi, 1993).

According to Cavani and Trifiro (1994) amount of V^{5+} observed in the catalyst is referred as the index of $(VO)_2P_2O_7$ oxidisability while amount of V^{3+} found is referred as index of $(VO)_2P_2O_7$ reducibility. In catalyst with slight defect of phosphorus (P/V = 0.95) the ease of oxidation increases while the reducibility of the catalyst remains high. Catalyst with high phosphorus content (P/V > 1.2) resulted in the reducibility of the catalyst to decrease while the oxidisability to remain high. The low reducibility of the catalyst accounts for its low activity while its high oxidisability can be accounted for the surface enrichment in phosphorus. Catalyst with slight excess of phosphorus (P/V = 1.00 - 1.20) exhibited the right compromise between oxidisability and reducibility, which are necessary to obtain both high activity and high selectivity.

2.4 Research Approach in Enhancing the Catalyst Performance

2.4.1 Exfoliation Reduction Technique

Studies by Okuhara et al., (2002) demonstrated that the (1 0 0) plane of $(VO)_2P_2O_7$ crystallites on which $V^{4+}(=O)\text{-}O\text{-}V^{4+}$ sites are lined up as highly selective while the side planes are non-selective. Koyano et al., (1998) showed that the side planes of the $(VO)_2P_2O_7$ were transformed into the deleterious and non-selective β-$VOPO_4$ phase. Reports by Centi et al., (1988), Bordes (1993) and Agaskar et al., (1993) are consistent with the findings above.

Exfoliation reduction technique implies the usage of layered material and intercalating it in the microstructure of the $(VO)_2P_2O_7$ crystallites (Okuhara et al., 2002). Exposure of the (1 0 0) plane will result in catalyst with high performance (Centi et al., 1988; Cavani and Trifiro, 1994). Since the dihydrate precursor possesses high intercalating capabilities, lamellar compounds formed by the intercalation of alcohols into $VOPO_4{\cdot}2H_2O$ is exfoliated, and then the thin layers of $VOPO_4$ are reduced to form catalyst precursor. Implying this method, $(VO)_2P_2O_7$ crystallites of thin sheets exposing preferentially the (1 0 0) plane can be produced (Kamiya, 2003). Figure 2.9 shows the exfoliation-reduction of $VOPO_4{\cdot}2H_2O$.

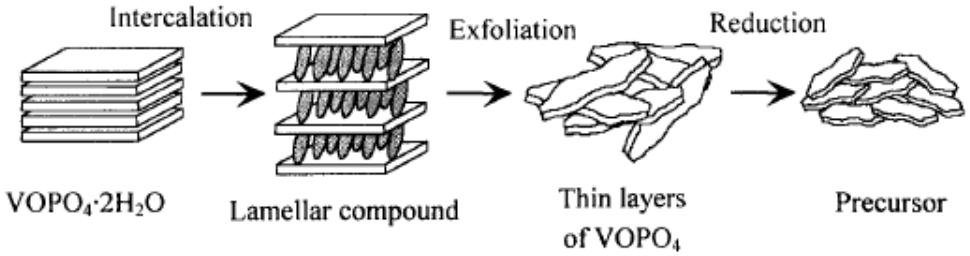

Figure 2.9: Exfoliation-reduction of $VOPO_4{\cdot}2H_2O$

To date various layered materials have been exfoliated in aqueous solution, including chalcogenides (Joensen et al., 1986), zirconium phosphate (Keller et al., 1994), clays (Kleinfeld and Furgson, 1994), niobic acid and titanic acid (Sasaki et al., 1997). Benes et al., (1997) reported that the dihydrate precursor, $VOPO_4 \cdot 2H_2O$ possesses layered structure that can be intercalated with various molecules. The intercalation compounds of $VOPO_4$ could be exfoliated using polar solvents. The above statements are strengthened by the following findings. Yamamoto et al., (2002) intercalated $VOPO_4 \cdot 2H_2O$ with acrylamide in 1-butanol and carried out the exfoliation of $VOPO_4 \cdot 2H_2O$ in mixtures of alcohols.

The reduction of the layered $VOPO_4 \cdot 2H_2O$ in mixtures of alcohol resulted in the formation of $VOHPO_4 \cdot 0.5H_2O$ with various morphologies depending on the type of alcohols used (Johnson et al., 1984; Ellison et al., 1994; Sananes et al., 1995; Hutchings et al., 1997; Bartley et al., 2001). Okuhara et al., (2002) studied the effect of exfoliating $VOPO_4 \cdot 2H_2O$ in various alcohols such as 1-butanol, 2-butanol and iso-butanol, followed by the reduction in ethanol. Exfoliation-reduction in a mixture of 2-butanol-ethanol resulted in catalyst with high selectivity towards maleic anhydride. Hiyoshi et al., (2004) deduced that the exfoliated catalyst showed higher selectivity and activity by comparing the catalyst synthesised by exfoliating $VOPO_4 \cdot 2H_2O$ in 2-butanol and direct reduction of the $VOPO_4 \cdot 2H_2O$. Similar finding was obtained by Imai et al., (2007) when the catalyst was exfoliated in 2-butanol followed by subsequent reduction in various volumes of ethanol showed increased surface area.

Most of the research have been revolving around reducing the exfoliated precursor from the organic method in ethanol as it improves the catalyst properties, however these research did not cap the maximum volume of reducing agents used (Okuhara et al., 2002; Hiyoshi et al., 2004; Imai et al., 2007). In the present research, $VOPO_4 \cdot 2H_2O$ is synthesised implying VPD method followed by exfoliation-reduction of the precursor via hemihydrate method using various volume combinations of 1-butanol and ethanol, where the total volume of reducing agents capped at 150 ml. VPD method was chosen as it preferentially exposes the (1 0 0) plane which is the selective phase for *n*-butane oxidation (Kiely et al., 1995). Implying hemihydrate method results the exfoliated precursor with wide spacing capabilities for intercalation, hence improving the catalytic properties (Taufiq Yap et al., 2004; Leong et al., 2011).

2.4.2 Strength of Reducing Agents

Common perception of determining the strength of reducing agents would be by measuring the percentage of hydrogen atoms (H) present in a molecule, as shown in Equation 2.7. Higher percentage of hydrogen atoms indicates the solvent has higher reducing capabilities (Tsuchiya et al., 2006). Stronger reducing agents would avoid the formation of the unwanted V^{5+} phases which lower the catalytic properties as they are reduced to the more desirable V^{4+} phase (Kamiya, 2003).

$$\%\ of\ H = \frac{(Number\ of\ H)\ x\ (Relative\ Atomic\ Mass\ of\ H)}{Relative\ Molecular\ Mass\ of\ the\ compound}\ x\ 100\% \qquad (2.7)$$

Ethanol, C_2H_5OH and 1-butanol, C_4H_9OH have different numbers of hydrogen atoms present in their structure, hence their strength as reducing agents differs. This would affect the properties of the synthesised catalyst. The relative strength of ethanol and 1-butanol as reducing agents are shown below based on the method in equation 2.7.

$$Strength\ of\ Ethanol\ = \frac{(6)\ x\ (1)}{2(12) + 5(1) + 1(16) + 1(1)}\ x\ 100\%$$

$$= 13.04\% \qquad (2.8)$$

$$Strength\ of\ 1 - butanol\ = \frac{(10)\ x\ (1)}{4(12) + 9(1) + 1(16) + 1(1)}\ x\ 100\%$$

$$= 13.51\% \qquad (2.9)$$

Implying hemihydrate method to obtain the precursor, the total volume of reducing agent used would be 150 ml for 10g of $VOPO_4 \cdot 2H_2O$ (Leong et al., 2011). Various volume combinations of 1-butanol to ethanol can be established within the limits of 150 ml of reducing agents, either by having higher volume ratio for 1-butanol to ethanol or lower volume ratio for 1-butanol to ethanol. When the volume combinations of the reducing agents are altered, its reducing capabilities are affected and the resulting catalyst would exhibit various properties for each volume combination of reducing agents, as it reduces the catalyst to different extents.

Following are the proposed outcomes of this research by varying the volume combinations of reducing agents. Since 1-butanol is a stronger reducing agent compared to ethanol, higher volume of 1-butanol in the mixture of reducing agents are expected to reduce the V^{5+} phase to V^{4+} phase more effectively. More V^{5+} phase related species would be produced when the volume of ethanol is higher than 1-butanol. Poor catalytic properties for the synthesised catalyst with higher volume of ethanol to 1-butanol, as more V^{5+} phase tend be more selective and lower the activity of the catalyst.

2.4.3 Application of Ultrasonic Technology

2.4.3.1 Origins of Sonochemistry

The chemical application of ultrasound, also known as sonochemistry was observed by Thornycroft and Barnaby (1895), when they discovered large bubbles formed due to the severe vibration from the ship propellers. These bubbles caused rapid erosion to the ship propellers and were minimised by increasing the size of the propellers and reducing its rate of rotation. Richard and Loomis (1927) were the first to discover the chemical effect of ultrasound using high intensity ultrasound irradiation, however the field gained substantial interest only in 1980's. The chemical effect of ultrasound is diverse and can produce improvement in both stoichiometric and catalytic chemical reactions, hence the application of ultrasound became increasingly important in analytical chemistry. Table 2.7 shows the industrial applications involving ultrasound treatment (Mason et al., 1996; Pena-Farfal et al., 2004).

Table 2.7: Common industrial application of ultrasound

Field	Application
Biology	Power ultrasound used for homogenisation and cell disruption
Engineering	Used to assist cutting, drilling, grinding and welding of both plastics and metals
Geology	Sound Navigation and Ranging (SONAR), Radio Detection and Ranging (RADAR)
Medicine	To observe foetus and perform subcutaneous surgery

2.4.3.2 Acoustic Cavitation

Studies on the chemical effect of ultrasound is rapidly growing as high intensity ultrasound can induce a wide range of chemical effect, which arises due to the acoustic cavitation (Suslick, 1988; Suslick and Crum 1997). The formation, growth and collapse of the bubbles provides the primary mechanism for sonocatalysis. As ultrasound crosses a medium, the average distance between the molecules of liquid will vary as they oscillate about their mean position. When the distance between the liquid molecules increases, the liquid breaks down and cavitation bubbles are created. These bubbles behave in two ways when the liquid is compressed (C) and stretched (R). Stable cavitation refers to bubbles formed at fairly low ultrasonic intensities and will continue to oscillate about their equilibrium size. Transient cavitation corresponds to bubbles formed at higher intensities which expands through several acoustic cycles before collapsing violently on compression. Figure 2.10 shows types of cavitation bubbles through its acoustic cycle (Suslick, 1986; Suslick, 1997; Mason and Tiehm, 2001).

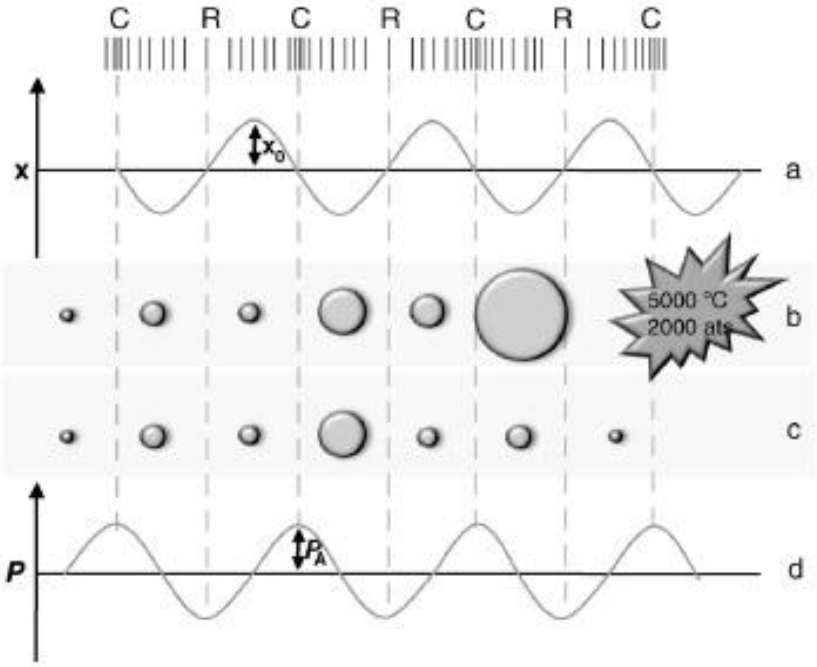

Figure 2.10: Cavitation bubbles: (a) Displacement graph, (b) Transient cavitation bubble, (c) Stable cavitation bubble and (d) Pressure graph

Transient bubbles collapsing is considered the main source of chemical and mechanical effects of ultrasonic energy. Each collapsing bubble produces intense local heating and high pressure over a very short lifetime that drives the high energy chemical reaction. Thus, cavitation concentrates the diffused sound energy to carry out high energy chemical reaction (Suslick, 1986; Wibetoe et al., 1999). Implying ultrasonication aids in shortening the duration of a required reaction as high energy is released by the collapsing bubbles. The product of ultrasound reactions usually possesses enhanced mass transport efficiency due to turbulent mixing and acoustic streaming. Moreover, the product have high surface area as a result of high velocity interparticle collision in the solution (Ensminger and Bond, 2012).

2.4.3.3 Types of Ultrasonic Application

Ultrasonication can be carried out using either direct probe sonication or indirect probe sonication. Direct sonication is achieved through immersing ultrasonic probes into the sample and performing ultrasonication directly over the solution without any barrier, as shown in Figure 2.11. This ensures the entire solution is exposed to the radiation generated which is dispersed to the other part of the mixture from the centre of the probe (Santos and Capelo, 2009).

Advantages of using direct probe sonication are its ability to generate high power ultrasound radiation and the performance of the probe can be controlled by adjusting the probe's power. The major drawback of this technique would be sample contamination with metals detaching from the probe (Vale et al., 2008). Although high purity titanium probe are used, contamination by metal such as Cr and Al have been reported (Wibetoe et al., 1999).

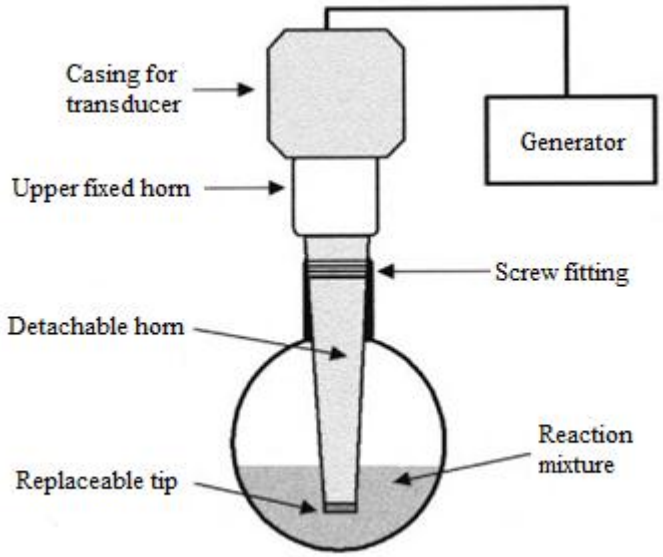

Figure 2.11: Direct probe sonication

Indirect probe sonication is also known as water bath sonication. In this method, the probe is not directly in contact with the sample as shown in Figure 2.12. Ultrasonic waves need to cross the liquid in the ultrasonic device and then cross the wall of the sample container before the ultrasonication could take place. This results in the intensity of the ultrasonication inside the reaction vessel lower than direct probe sonication and limiting its application (Santos and Capelo, 2009).

To overcome this drawback, water bath sonication is coupled with heaters to generate additional heat energy and transmit it to the samples. This results in the water molecules to oscillate at a higher energy as the reduced kinetic energy from the poor sound waves are compensated by additional heat energy, resulting in transient cavitation. Moreover, this method does not require special consideration in selecting the intermediate liquid, as sample contamination will not take place since the intermediate liquid is not in contact with the sample (Mason and Tiehm, 2001; Vale et al., 2008).

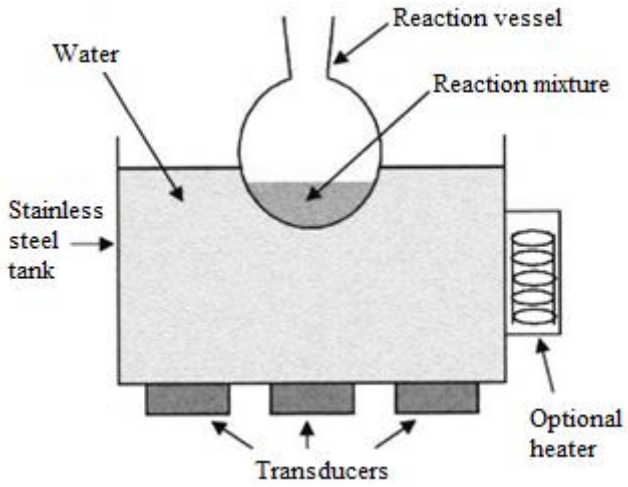

Figure 2.12: Indirect probe sonication

2.4.3.4 Effect of Ultrasound on Heterogeneous Catalyst

Ultrasonic irradiation can alter the reactivity of heterogeneous catalyst, especially those involving the solid-liquid interface. Cavitation in pure liquids involves the mixing of the liquids to produce a homogeneous solution which is different from the cavitation near a liquid-solid interface (Suslick et al., 1999).

Near a solid interface, the direct collapse of transient bubbles becomes non-spherical, driving high speed jets of liquid into the surface of the solid particles. The formation of liquid micro-jets is shown in Figure 2.13. These jets can reach very high speed and result in high velocity interparticle collision in the solution, which produces fragmented particles of the bulk material. In addition, shockwaves created by the cavity collapse in the liquid also induce fragmentation, hence contributing to higher total surface area. The impingements of micro-jets and shockwaves on the surface results in the sonochemical effects such as changes in surface morphology, composition and reactivity of heterogeneous catalyst (Suslick and Doktycz, 1990).

Figure 2.13: Formation of liquid micro-jets

A few studies on ultrasound treated VPO catalyst which have been reported are summarised in the following section. Unnikrishnan et al., (2003) compared the phase composition and reactivity of the catalyst prepared via conventional method and ultrasonic irradiation. He concluded ultrasonic irradiated catalyst prepared in shorter duration (6 hour) possesses similar surface composition to catalyst prepared via conventional heating method (24 hours). As the duration of ultrasound irradiation was increased (8 hours), the surface area, activity and selectivity of the VPO catalyst increased.

Taufiq Yap et al., (2011) studied the effect of sonochemical treatment in synthesising nanostructured VPO with the addition of mineralisers. Samples of V_2O_5 prepared with the addition of KNO_3 and KCl as mineralisers are treated implying ultrasound route for various durations. The incorporation of the mineralisers into the structure of the catalyst was observed as the duration of sonochemical treatment was prolonged. This resulted in catalyst with higher amount of reactive oxygen species removed (V^{4+}-O^-), hence contributing to its higher activity.

In the present research, the dihydrate precursor ($VOPO_4 \cdot 2H_2O$) is synthesised using ultrasound irradiation technique while past studies have synthesised the precursor implying conventional reflux method and treated it in ultrasound irradiation. This research also focuses on shorter synthesis duration, namely from one hour to three hours as compared to previous findings where the precursors were treated up to six hours to improve its physical properties (Unnikrishnan et al., 2003; Wong and Taufiq Yap, 2011).

2.4.4 Activated Carbon Catalyst Support

2.4.4.1 Activated Carbon

Activated carbon (AC) is the generic term used to describe a family of carbonaceous adsorbents with a highly crystalline form and extensively developed internal pore structure. It is extremely porous with very large surface area, which makes it an effective adsorbent material. Activated carbon can be produced by either chemical activation or physical activation. Chemical activation involves the degradation of the raw material structure using phosphoric acid as the activating agent and heating the carbon to high temperatures where it will be oxidised by the acid. Corrosion, water pollution and higher production cost inhibited the chemical activation from being developed further (Tan et al., 2008; Sodeinde, 2012).

Another method to activate carbon is known as steam activation, which does not involve chemicals. In steam activation, the volatile compounds are removed in kilns and furnaces at temperatures about 400°C - 500°C, followed by activation with steam at temperature ranging from 800°C - 1000°C. Both technique require the use of elevated temperature, however this method is preferred over the former as it does not cause changes to the surface of the support. Physical activation which implies the use of air is simple process, does not produce pollution and economically more attractive to carry out. (Tan et al., 2008; Sodeinde, 2012).

Generally, there are two major classification for activated carbon, powdered activated carbon (PAC) and granular activated carbon (GAC). The former is made in particulate form of fine granules between 1μm - 150μm. They present a very large surface to volume ratio as the diffusion distance is very small. PAC generally possesses micropores due to its finer structure. GAC has a relatively larger particle size, hence its represents a smaller surface area and its pore structure would be either mesopores or macropores. Pore size distribution plays an important part when comes to the application. Micropores generally contribute to the major part of the internal surface area while mesopores and macropores can generally be regarded as the highways into the carbon particle (Olivares-Marin et al., 2006).

Several studies on activated carbon are summarised in the following section. Martinez et al., (2003) compared the physical and morphological characteristics of AC obtained from walnut shell and peach stone. The AC obtained from walnut shell showed higher adsorption capacity due to its heterogeneous carbonaceous structure. Hence, the structure of the AC contributes to its adsorption capacity.

Huang and Cheng (2007) studied the effect of wood based activated carbon in the adsorption-reduction of bromate (BrO_3^-) ions. The maximum adsorption capacity was calculated as a function of the effect of mesopore volume and it was revealed that the characteristic of the AC determines the adsorption capacity. Higher adsorption capacity resulted in removal of more BrO_3^- ions.

2.4.4.2 Coconut Shell Activated Carbon

Coconut shell based activated carbon (CSAC) is generally micro porous, which contribute to the major part of the internal surface area and is well suited for organic chemical adsorption. Coconut shell based carbon is least dusty and has the most hardness compared to other type of activated carbon which makes it ideal for many applications. Its high purity enables it to be widely used in water purification and hazardous heavy metal removal (Parsons and Jefferson, 2006). A sample of coconut shell activated carbon is shown in Figure 2.14.

Figure 2.14: Coconut shell activated carbon

Activated carbon is produced from coconut shell using a two-step process, whereby the first step is carbonise the shells to drive out volatile compounds such as oxygen, hydrogen and nitrogen. As for the second step, the carbonised shell are activated at high temperature, about 1100°C in steam. Advantages of using coconut shell activated carbon are listed in Table 2.8 (Mohd Iqbaldin et al., 2013)

Table 2.8: Advantages of using coconut shell activated carbon

Advantages
1. It is inert, hence it does not take part in the chemical reaction
2. Provides exceptionally high surface area to volume ratio due to its large proportion of micropores
3. It has improved mechanical property and heat transfer property as it is harder than other activated carbon materials.
4. Excellent purity and low dust generation due to its low ash content
5. Balanced pore structure which provides a better adsorption range
6. Lower cost due to easy availability in many regions

Application of CSAC which have been reported are summarised in the following section. Tan et al., (2008) studied the effect of preparation variable such as activation temperature, activation time and impregnation ratio of CSAC on its selectivity towards 2,4,6-trichlorophenol and activated carbon yield. The impregnation ratio greatly affected the selectivity while the activation temperature played an important role in determining the carbon yield.

According to Sodeinde, (2012), the reduction of hexamine cobalt (III) is affected by the mass of CSAC. The pH of the solution did not affect the conversion, but increasing the mass of CSAC increased the conversion by several folds. Chali and Yakub (2013), used CSAC to treat drinking water and found that increasing the amount of CSAC reduced the metal content in the water as it provided greater total surface area for the support. Increasing the carbon dosage improved the water quality due to its increased ability of reducing metal contents.

2.4.4.3 Incipient Wetness Impregnation Method

Impregnation is a preparation technique where a solution of the precursor of the active phase is brought into contact with the support, and is widely used in preparing supported VPO catalyst. Generally there are two methods in impregnating a catalyst. In wetness impregnation method the active phase of the precursor is dissolved in excess solution before the support system is introduced. Deposition of the active phase on the support depends on the solid/liquid ratio, and the process occurs very slowly which usually takes several hours or even days as the excess liquid is eliminated by evaporation or drying. Due to the prolonged duration in obtaining the supported catalyst, extensive restructuring of the surface occurs which leads to lower surface area. This is considered the major drawback of this technique (Haber et al., 1995; Van Dillen et al., 2003).

Dry impregnation which is also referred to as incipient wetness impregnation, uses sufficient solution of the precursor to fill the pore volume of the support. The solubility of the catalyst precursor and the pore volume of the support determines the maximum loading achievable in each impregnation. If higher loadings are required, successive impregnations are needed, which is the major drawback of this technique. However, implying incipient wetness impregnation, more precise control over vanadium oxide loading can be achieved (Haber, 1994; Haber et al., 1995; Van Dillen et al., 2003).

In incipient wetness impregnation, the capillary action draws the solution containing the active sites into the pores, as shown in Figure 2.15. When the volume of the solution is greater than the pore volume as in the case of wetness impregnation, the solution transport changes from capillary action to diffusion which occurs at a slower rate. This explains why it takes a longer duration to dry the catalyst prepared via wetness impregnation method. Incipient wetness impregnation technique does not form very strong catalyst-support interaction that hinders the formation of the desired VPO phases (Haber, 1994; Haber et al., 1995; Van Dillen et al., 2003).

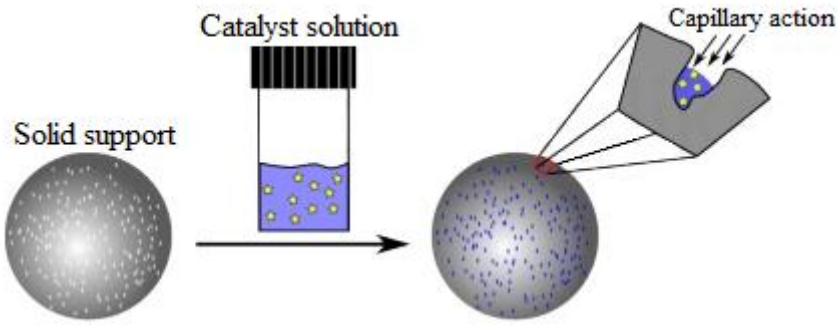

Figure 2.15: Capillary action

In this research, both the exfoliated-reduced precursor and ultrasound irradiated precursor are impregnated with coconut shell activated carbon (CSAC) by varying the weight percentage of VPO loading implying the usage of incipient wetness impregnation technique. This method was chosen as it favours the formation of desired VPO phases. Past studies have focused on the application of zirconia and silica derived supports such as MCM-41 and SBA-15 using liquid crystal templating (LCT) mechanism which results the catalyst to exhibit high selectivity but poor conversion (Nakamura et al., 1974; Van Dillen et al., 2003; Li et al., 2006b).

CHAPTER THREE

MATERIALS AND METHODOLOGY

3.1 Chemicals and Gases

List of reagents that were used to synthesise and characterise the catalyst are listed in Table 3.1.

Table 3.1: List of reagents used in synthesising and characterising VPO Catalyst

Reagent	Brand	Purity
Vanadium (V) Pentoxide, V_2O_5	Merck	≥ 99.0%
Ortho-Phosphoric Acid, *o*-H_3PO_4	Merck	≥ 85.0%
1-Butanol, $CH_3(CH_2)_3OH$	Merck	≥ 99.5%
Ethanol, C_2H_5OH	Merck	≥ 99.9%
Sulphuric Acid, H_2SO_4	Merck	≥ 95.0%
Nitric Acid, HNO_3	Merck	≥ 65.0%
Ammonium Iron (II) Sulphate Hexahydrate, $(NH_4)_2Fe(SO_4)_2•6H_2O$	Merck	≥ 99.0%
Potassium Permanganate, $KMnO_4$	Fisher Scientific	≥ 99.0%
Diphenylamine, $(C_6H_5)_2NH$	Acros Organic	≥ 99.0%
Ammonium Metavanadate, NH_4VO_3	BDH Chemicals	≥ 99.0%
Ammonium Dihydrogen Phosphate, $NH_4H_2PO_4$	AJAX Chemicals	≥ 99.0%
Liquid Nitrogen	MOX	≥ 99.0%
Coconut Shell Activated Carbon	Kekwa Indah Sdn. Bhd.	≥ 99.0%

List of gases used in the activation and characterisation of the catalyst are listed in Table 3.2.

Table 3.2: List of gases used in activating and characterising VPO catalyst

Gases	Brand	Purity
n-Butane in Air	MOX	0.75%
Hydrogen in Nitrogen, H_2/N_2	MOX	5.55%
Purified Argon, Ar	MOX	≥ 99.99%
Purified Helium, He	MOX	≥ 99.99%
Purified Hydrogen, H_2	MOX	≥ 99.99%
Purified Nitrogen, N_2	MOX	≥ 99.99%

3.2 Research Outline

Four series of catalyst were synthesised in this research. 1st series involves the formation of bulk catalyst, which serves as a preliminary study to evaluate the effect of various volume combination of environmentally friendly reducing agents. Based on the optimal volume combination determined, the remaining series were synthesised. 2nd series involves the formation of dihydrate precursor by varying the duration of ultrasonic irradiation. The effect of various weight percentages of VPO loading on support system were investigated through the 3rd and 4th series, respectively. In the 3rd series, VPO catalyst which exhibited the optimum volume combination of reducing agents was impregnated on the support system. As for the 4th series, ultrasound irradiated catalyst which exhibited superior catalytic performances was impregnated on the support system. Figure 3.1 shows the above mentioned research outline.

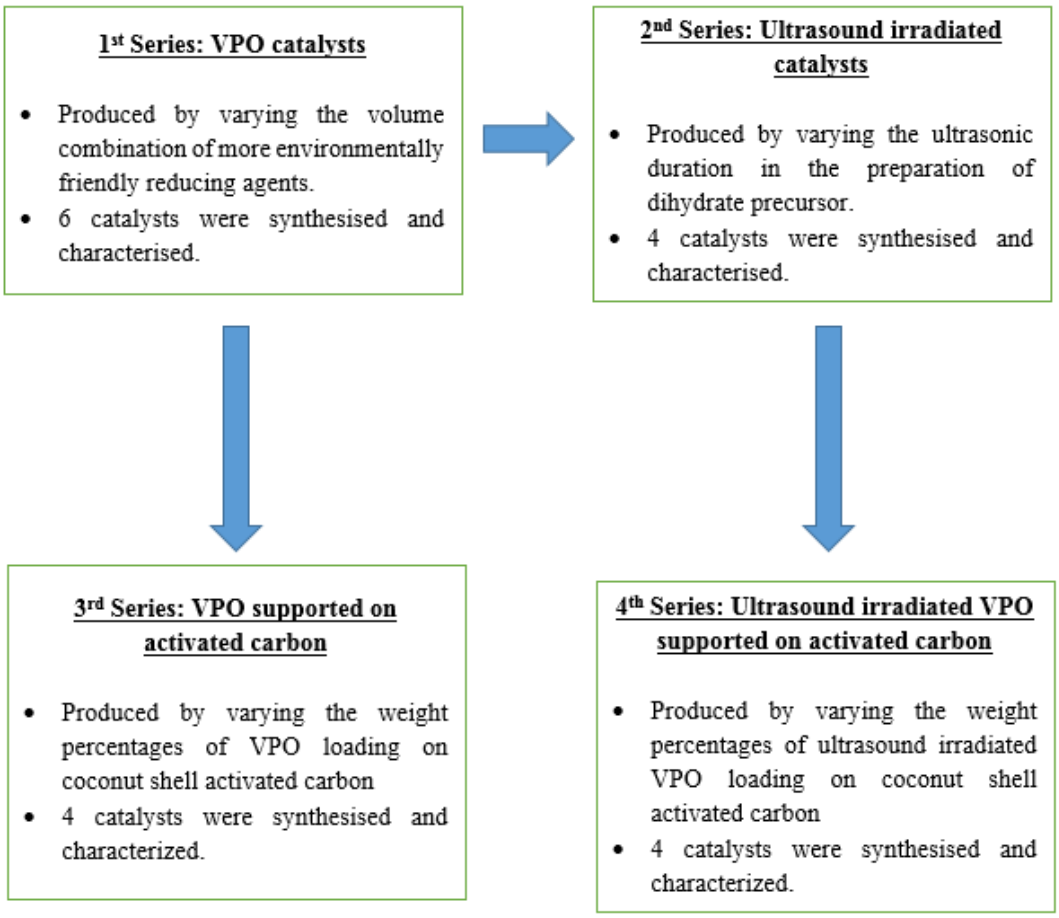

Figure 3.1: Research outline

3.3 Synthesising VPO Catalyst

3.3.1 Preparation of Bulk VPO Catalyst

Synthesis of VPO catalyst involves three stages. In the first stage (Figure 3.2), 15.0 g of vanadium pentoxide (V_2O_5) was refluxed with 360 ml of distilled water (H_2O) and 90 ml of ortho-phosphoric acid (*o*-H_3PO_4) at 393 K for 24 hours. The resulting mixture was cooled to room temperature, centrifuged and the yellow slurry ($VOPO_4 \cdot 2H_2O$) obtained was oven dried at 353 K for 24 hours.

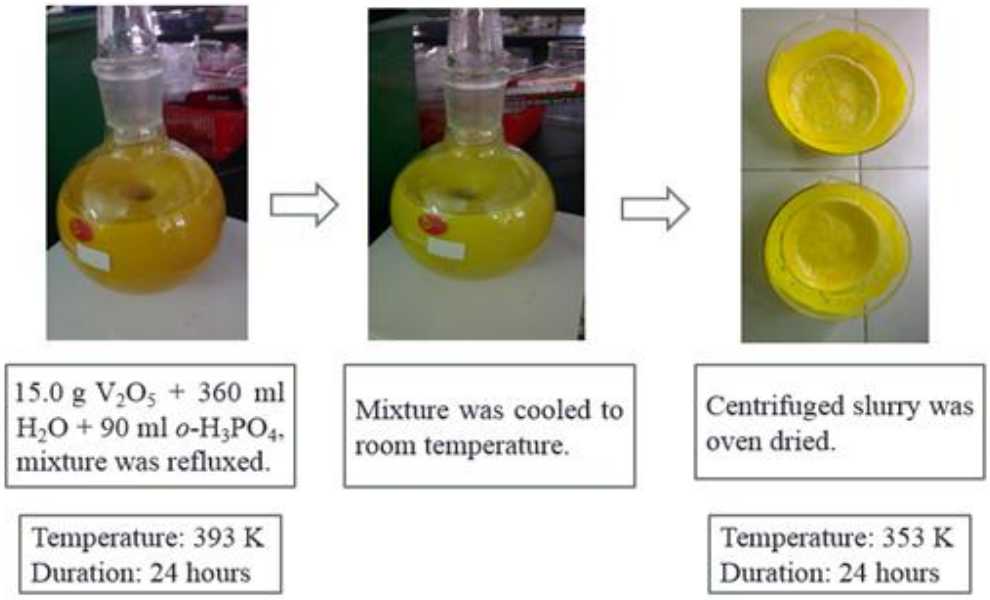

Figure 3.2: Preparation of dihydrate precursor

In the second stage (Figure 3.3), 10.0 g of $VOPO_4 \cdot 2H_2O$ was refluxed with 150 ml of 1-butanol at 393 K for 24 hours based on the ratio 1 g of dihydrate precursor: 15 ml of reducing agents. The resulting mixture was cooled to room temperature, centrifuged and the blue slurry obtained was oven dried at 353 K for 24 hours. Similar sets were carried by reducing the volume of 1-butanol by 30 ml and increasing the volume of ethanol by 30 ml, hence maintaining the total volume of the reducing agents at 150 ml.

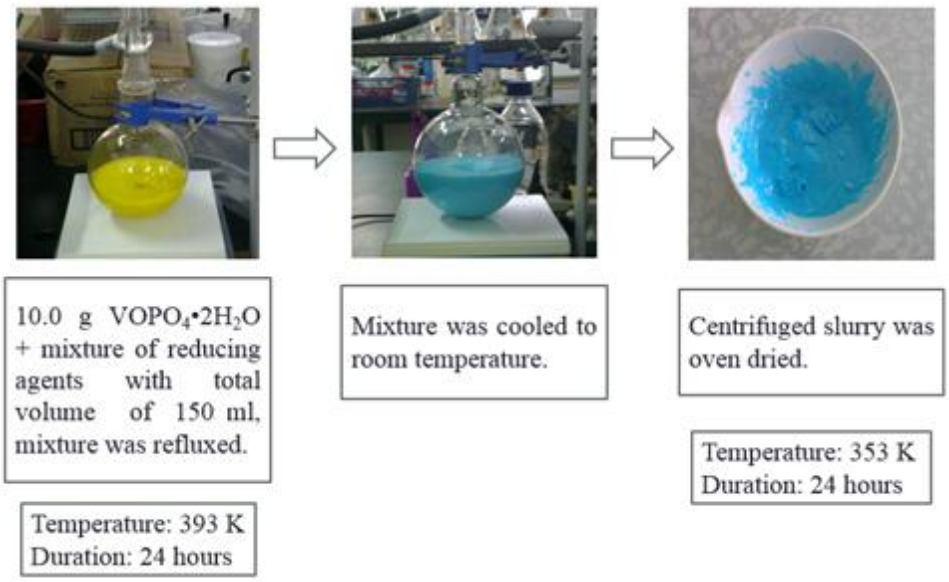

Figure 3.3: Preparation of hemihydrate precursor

The whitish blue precursor obtained from the second stage was calcined in a reaction flow of 0.75% *n*-butane/air at 733 K for 24 hours (Figure 3.4). The activated catalysts were cooled to room temperature, collected and stored. The synthesised catalysts were denoted as VPO-*X*B*Y*E, where *X* represents the volume of 1-butanol while *Y* represents the volume of ethanol (Table 3.3).

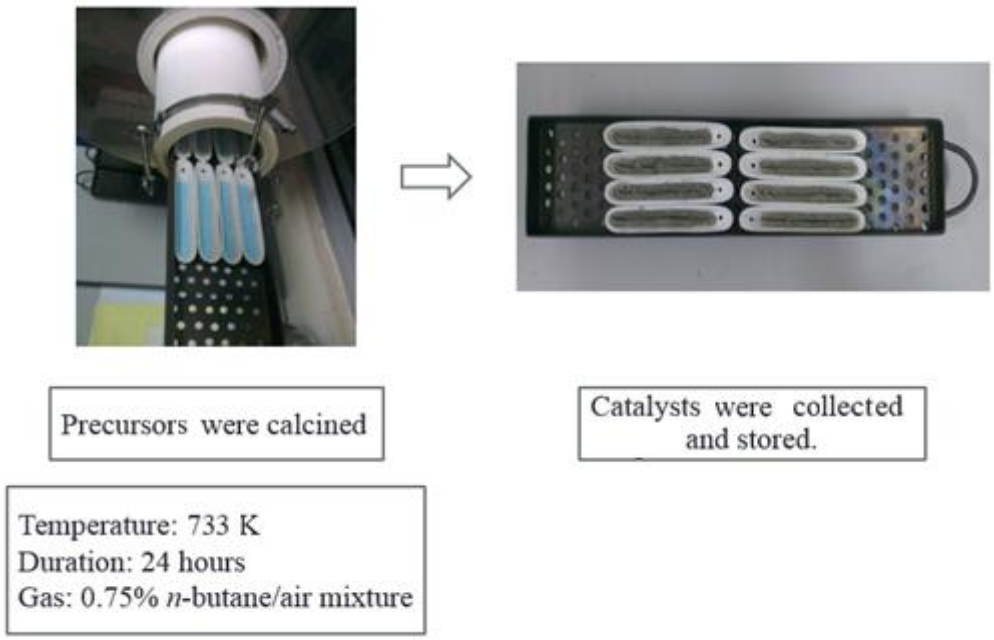

Figure 3.4: Catalyst activation

Table 3.3: Denotations for the catalysts synthesised in the 1st Series

Denotations	Volume of 1-butanol (ml)	Volume of Ethanol (ml)
VPO-150B0E	150	0
VPO-120B30E	120	30
VPO-90B60E	90	60
VPO-60B90E	60	90
VPO-30B120E	30	120
VPO-0B150E	0	150

3.3.2 Preparation of Ultrasound Irradiated Catalyst

In the first stage (Figure 3.5), 15.0 g of V_2O_5 was transferred into 1000 ml beaker and mixed with 360 ml of H_2O followed by 90 ml of *o*-H_3PO_4. The mixture was stirred to produce a well-mixed solution. It was placed in an ultrasound machine, which had been filled with 4 litres of water. The beaker was placed at the centre of the heating space. Frequency of the ultrasound machine was 5 kHz.

Ultrasonication was carried out for 1 hour at 353 K. The resulting mixture was cooled to room temperature, centrifuged and the yellow slurry ($VOPO_4 \cdot 2H_2O$) obtained was oven dried at 353 K for 24 hours. Similar sets were carried out by increasing the ultrasound duration to 2 and 3 hours, respectively. A control catalyst sample was synthesised using conventional reflux method and heating the mixture for 24 hours to form the dihydrate precursor. Application of ultrasound irradiation in synthesising the dihydrate precursor produces better physical characteristic such as smaller sized particles which increases the specific surface area of the catalyst as well as shorter

synthesis duration compared to the conventional reflux method allows the preparation to be accomplished faster.

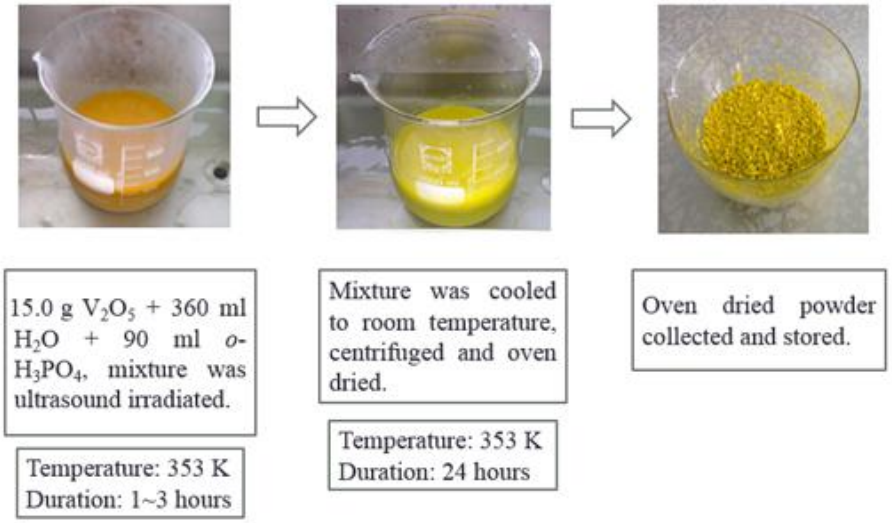

Figure 3.5: Preparation of dihydrate precursor via ultrasound irradiation

Formation of hemihydrate precursor in the second stage follows the steps outlined for the bulk catalyst. 10.0 g of ultrasound irradiated $VOPO_4 \cdot 2H_2O$ precursor was refluxed with the optimal volume combination of reducing agents determined from the 1st series. The precursors obtained were calcined in a reaction flow of 0.75% *n*-butane/air at 733 K for 24 hours to generate the active phase of the catalysts. The denotations used for the synthesised catalysts are shown in Table 3.4.

Table 3.4: Denotations for the catalysts synthesised in the 2nd Series

Denotations	Reflux Duration Stage 1 (hours)	Ultrasound Duration Stage 1 (hours)	Reflux Duration Stage 2 (hours)
VPO-R24R24	24	-	24
VPO-U1R24	-	1	24
VPO-U2R24	-	2	24
VPO-U3R24	-	3	24

3.3.3 Preparation of Coconut Shell Activated Carbon Supported Catalyst

In the 3rd Series, the dihydrate precursor was produced implying the steps outlined in the 1st Series. 10.0 g of synthesised dihydrate precursor was refluxed with the optimal volume combination of reducing agents at 393 K for 24 hours. Required mass of coconut shell activated carbon (CSAC) was weighed in a glass bowl and the blue solid solution ($VOHPO_4 \cdot 0.5H_2O$) formed was mixed homogeneously with CSAC implying incipient wetness impregnation method (Figure 3.6). The mixture was oven dried at 353 K for 24 hours to produce the supported precursor.

Similar sets were carried by varying the amount of CSAC to produce a variation on the catalyst loading. The supported precursors were calcined in a reaction flow of 0.75% *n*-butane/air at 733 K for 24 hours. Table 3.5 shows the denotations of the synthesised catalysts.

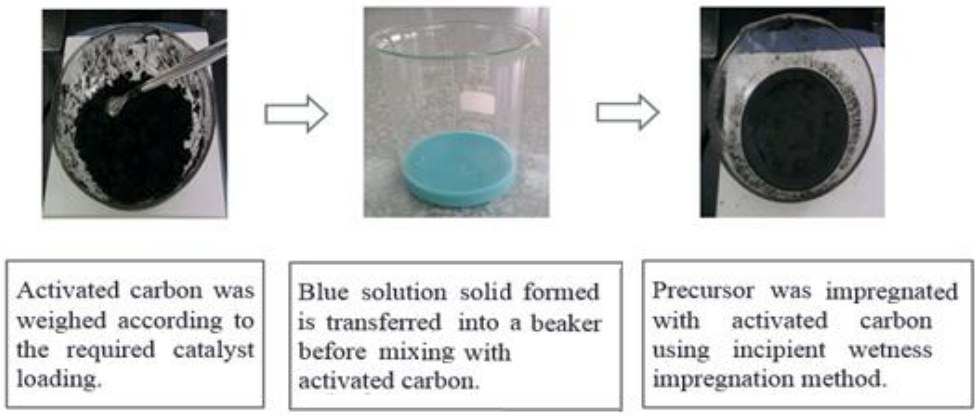

Figure 3.6: Preparation of coconut shell activated carbon supported precursor

Table 3.5: Denotations for the catalysts synthesised in the 3rd Series

Denotations	Mass of $VOPO_4 \cdot 2H_2O$ used in first stage (grams)	Mass of CSAC (grams)
10 wt% VPO/AC	10.0	90.0
20 wt% VPO/AC	10.0	40.0
30 wt% VPO/AC	10.0	23.3
40 wt% VPO/AC	10.0	15.0

Similar synthesising condition to the ultrasound irradiated catalyst, which exhibited superior catalytic properties was used to synthesise the dihydrate precursor in the 4th series. 10.0 g of ultrasound irradiated dihydrate precursor was refluxed with the optimal volume combination of reducing agents determined from the 1st series to produce the blue solid solution.

Coconut shell activated carbon (CSAC) was impregnated on the VPO following similar steps outlined in the 3rd series. Mass of CSAC was reduced according to the required VPO loading to vary the weight percentages of VPO supported on the CSAC. The supported precursors were calcined in a reaction flow of 0.75% *n*-butane/air at 733 K for 24 hours. Table 3.6 shows the denotations of the synthesised catalysts.

Table 3.6: Denotations for the catalysts synthesised in the 4th Series

Denotations	Mass of $VOPO_4 \cdot 2H_2O$ used in second stage (grams)	Mass of CSAC (grams)
10 wt% UVPO/AC	10.0	90.0
20 wt% UVPO/AC	10.0	40.0
30 wt% UVPO/AC	10.0	23.3
40 wt% UVPO/AC	10.0	15.0

3.4 Catalyst Characterisation

3.4.1 X-ray Diffraction (XRD) Analysis

The x-ray diffraction (XRD) analysis was carried out using Shimadzu XRD-6000 diffractometer, manufactured by Shimadzu Corporation, Japan (Figure 3.7). Catalyst placed on the aluminium sample holder was mounted on the diffractometer. CuKα radiation was generated by a glass diffraction x-ray tube and it scanned the sample in the range between 2θ = 2.00° - 60.00° at a rate of 1.20° min^{-1}. Basal spacing was determined via powder technique.

The x-ray produced was focused on the sample mounted on the diffractometer. Changes in the diffracted x-ray intensities was measured, recorded and plotted against the rotation angle of the sample. The diffractogram obtained was compared with Joint Committee on Powder Diffraction Standard (JCPDS) and the active phase present in the catalyst was determined.

Figure 3.7: Shimadzu XRD-6000

The crystallite size was calculated using the Debye-Scherrer method, as shown in Equation 3.1.

$$t = \frac{0.89\lambda}{\beta_{hkl}\theta_{hkl}} \quad (3.1)$$

Where: t = crystallite size for (h k l) plane
λ = x-ray wavelength for CuKα radiation
$\beta_{h\,k\,l}$ = full width at half maximum (FWHM) (h k l) plane
$\theta_{h\,k\,l}$ = diffraction angle of (h k l) plane

3.4.2 Scanning Electron Microscopy (SEM) Analysis

Hitachi S-3400N, manufactured by Hitachi Science Systems Ltd., Japan (Figure 3.8) was used to examine the surface morphologies of the catalysts. A small amount of fresh catalyst was placed on the surface of the carbon tape which had been fixed on an aluminium stub. It was coated with gold using Sputter Coater (Figure 3.9).

An electron beam was focused into the fine probe and scanned over the catalyst. As the beam interacted with the sample, various signals were emitted which was detected by secondary electron detector. These signals were used to modulate the brightness of the cathode ray tube and the sample images were produced.

Figure 3.8: Hitachi S-3400

Figure 3.9: Sputter coater

3.4.3 Brunauer-Emmett-Teller (BET) Surface Area Measurement

Thermo Finnigan Sorptomatic 1990, manufactured by Thermo Fisher Scientific Inc., USA (Figure 3.10) was used to analyse the multi-point surface area of the catalysts. 0.5 g of fresh catalyst was degassed at 393 K overnight to remove the water vapour and impurities.

Figure 3.10: Thermo finnigan sorptomatic 1990

Adsorption and desorption of nitrogen gas over the sample's exposed surface was used to determine the surface area of the catalyst. Surface area of the catalyst was calculated based on Langmuir theory as shown in Equation 3.2.

$$\frac{1}{v\left(\frac{P_0}{P}-1\right)} = \frac{c-1}{V_M c}\left(\frac{P_0}{P}\right) + \frac{1}{V_M c} \qquad (3.2)$$

Where: P = equilibrium pressure at measurement temperature

P_0 = saturation pressure at measurement temperature

v = adsorbed gas quantity

V_M = monolayer gas adsorbed quantity

c = BET constant

$$= \exp\left(\frac{E_1 - E_L}{RT}\right)$$

Where: E_1 = heat of adsorption in the first layer

E_L = heat of liquefaction

R = gas constant

T = absolute temperature in Kelvin

3.4.4 Redox Titration

Redox titration method was used to determine the average vanadium oxidation state according to the procedure developed by Niwa and Murakami, (1982). In the first stage of the procedure, 0.10 g of fresh catalyst was dissolved in 2M sulphuric acid (H_2SO_4). 20 ml of the solution was then titrated with 0.01M potassium permanganate solution ($KMnO_4$).

The end point was determined when the greenish blue solution turned pink, the volume used was recorded as V_1. All the V^{3+} and V^{4+} were converted to V^{5+}. The solution was titrated with 0.01M ammonium iron (II) sulphate solution ($(NH_4)Fe(SO_4)_2$) with few drops of diphenylamine ($(C_6H_5)_2NH$) as an indicator. The end point was determined when the purple solution turned back to greenish blue and the volume used was recorded as V_2. All the V^{5+} was converted to V^{4+}. (Niwa and Murakami, 1982).

Another 20 ml of the solution was added with a few drops of $(C_6H_5)_2NH$ and directly titrated with $(NH_4)Fe(SO_4)_2$ The end point was determined when the purple solution turned back to greenish blue and the volume used was recorded as V_3. In this step only the V^{5+} present in the original solution was reduced to V^{4+} (Niwa and Murakami, 1982).

Niwa and Murakami (1982) developed the Equation 3.3, 3.4 and 3.5, respectively, which was used to determine the relative amount of V^{3+}, V^{4+} and V^{5+}.

$$(2V^{3+} + V^{4+})(V_a) = (MnO_4^-)(V_1) \quad (3.3)$$

$$(V^{3+} + V^{4+} + V^{5+})(V_b) = (Fe^{2+})(V_2) \quad (3.4)$$

$$(V^{5+})(V_c) = (Fe^{2+})(V_3) \quad (3.5)$$

Where: V^{3+}, V^{4+} and V^{5+} = concentration of vanadium species
MnO_4^- = concentration of potassium permanganate solution
Fe^{2+} = concentration of ammonium iron (II) sulphate solution
V_1 = volume of potassium permanganate solution

V_2 and V_3 = volume of ammonium iron (II) sulphate solution

V_a, V_b and V_c = volume of catalyst solution

The average vanadium oxidation state (AV) obtained using the Equation 3.6:

$$V_{AV} = \frac{3V^{3+} + 4V^{4+} + 5V^{5+}}{V^{3+} + V^{4+} + V^{5+}} \quad (3.6)$$

3.4.5 Energy Dispersive X-ray (EDX) Analysis

Energy dispersive x-ray (EDX), analysis was carried out to determine the elemental composition of the catalyst. The EDX instrument was manufactured by EDAX, USA and it is attached together with Hitachi S-3400N (Figure 3.11). A small amount of fresh catalyst was placed on the surface of the carbon tape, which had been fixed on an aluminium stub. X-ray beam was focused on the sample, resulting it to emit an electron from its inner shell. This produced an electron hole, which was filled by electrons from the outer surface. The difference in energy between the higher energy shell and lower energy shell was emitted as x-ray. The intensities of the x-ray emitted was measured by energy dispersive spectrometer and the difference in energy level was used to determine the elemental composition.

Figure 3.11: Edax-Ametex-Apollo X

3.4.6 Inductively Coupled Plasma – Optical Emission Spectrometry (ICP-OES) Analysis

Sequential scanning Perkin Elmer Optima 2000 DV optical emission spectrometer manufactured by PerkinElmer Inc., USA was used to analyse the bulk chemical composition of the catalyst (Figure 3.12). 0.010 g of fresh catalyst was dissolved in 10 ml of 8M nitric acid (HNO_3). The solution was diluted with deionised water and a concentration of 100ppm was produced.

Standard solution of vanadium and phosphorus were prepared in concentrations of 10 ppm, 20 ppm and 30 ppm, respectively. Deionised water was used as a control solution.

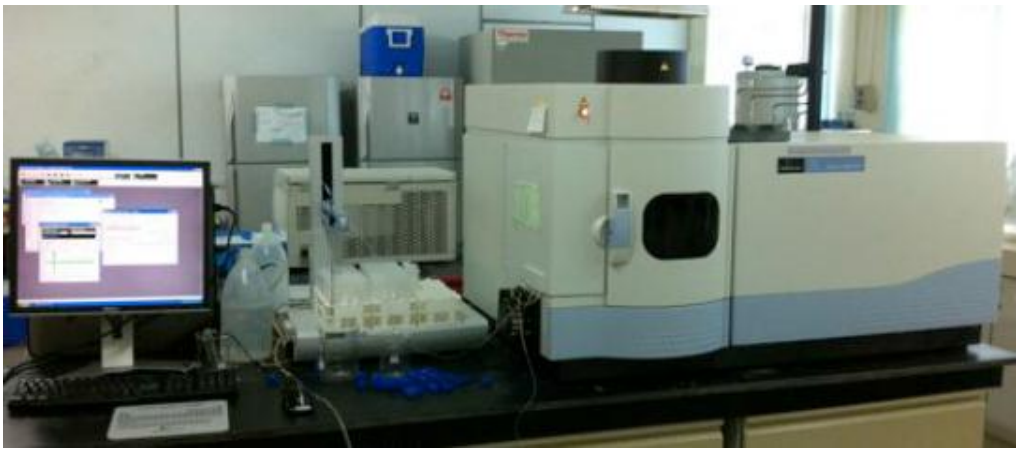

Figure 3.12: Perkin Elmer Optima 2000 DV Optical Emission Spectrometer

3.4.7 Temperature Programmed Reduction (TPR) Analysis

Reactivity analysis was carried out using TPD/R/O 1100, manufactured by Thermo Fisher Scientific Inc., USA (Figure 3.13). 0.02 g of fresh catalyst was weighed and placed into the reactor. It was pre-treated with a flow of purified nitrogen gas (N_2) at a rate of 20 cm^3 min^{-1} for 5 minutes without increasing the temperature. Next, the sample's temperature was increased from room temperature to 473 K at 10 K min^{-1}, and was held for 10 minutes. Contaminants and moisture from the catalyst were removed by the pre-treatment process.

After completion of pre-treatment, the sample was cooled to room condition and the reactor's connection was switched to analysis port. 5.55% of H_2/N_2 was flown through the catalyst from room temperature to 1273 K at 5 K min^{-1}. Consumption of hydrogen against time was measured by the thermal conductivity detector (TCD) and plotted as a graph. The plot was converted as a function of temperature and the number of peaks present, types of oxygen species removed, amount of oxygen species removed and the reduction temperature were obtained from the generated report.

Figure 3.13: TPD/R/O 1100 Instrument

The values of reduction activation energy was obtained from modified Redhead equation (Equation 3.7), where E_r represents the reduction activation energy (kJ mol^{-1}), A_r represent the reduction pre-exponential term (cm^3 mol^{-1} s^{-1}) which was given the value of standard collision number of 10^{13} cm^3 mol^{-1} s^{-1}, R represents the gas constant (J K^{-1} mol^{-1}), β represents the heating rate (K s^{-1}), T_m (K) represents the temperature of maximum peak and $[H_2]_m$ represents the gas phase concentration of hydrogen (mol cm^3) at maximum peak (Redhead, 1962).

$$\frac{E_r}{R(T_m)^2} = \left(\frac{A_r}{\beta}\right)[H_2]_m exp\left(\frac{-E_r}{RT_m}\right) \quad (3.7)$$

3.4.8 Catalytic Analysis

Oxidation of *n*-butane was carried out using a fixed bed reactor coupled with Trace GC Ultra, manufactured by Thermo Fisher Scientific Inc., USA (Figure 3.14). 0.25 g of fresh catalyst was placed in the reactor and held using quartz wool. The reaction was carried out at 673 K with gas hourly space velocity (GHSV) of 2400 h^{-1}. A thermocouple was placed at the centre of the fixed bed stainless steel tube to control the reaction temperature at 673±1 K. A mixture of 1% *n*-butane in air was fed to the reactor via calibrated mass flow meter. The sample was vaporised and fed into the Trace GC Ultra via heated lines for an online gas chromatography analysis. Carbon mass balance ≥ 95% was observed.

Figure 3.14: Fixed bed reactor coupled with Trace GC Ultra

CHAPTER FOUR

RESULTS AND DISCUSSIONS

4.1 Effect of Varying Reducing Agent Mixtures on VPO Catalyst

4.1.1 X-ray Diffraction (XRD) Analysis

XRD pattern of the synthesised catalysts obtained via variable volume combination of reducing agents are shown in Figure 4.1. Main characteristic peaks of $(VO)_2P_2O_7$ were observed at 2θ = 22.9°, 28.4° and 29.9° (JCPDS File No. 34-1381), which were corresponded to the reflection of (0 2 0), (2 0 4) and (2 2 1) planes, respectively. Studies on these planes were conducted as it was more important in determining the active phase for *n*-butane oxidation (Taufiq Yap et al., 2004).

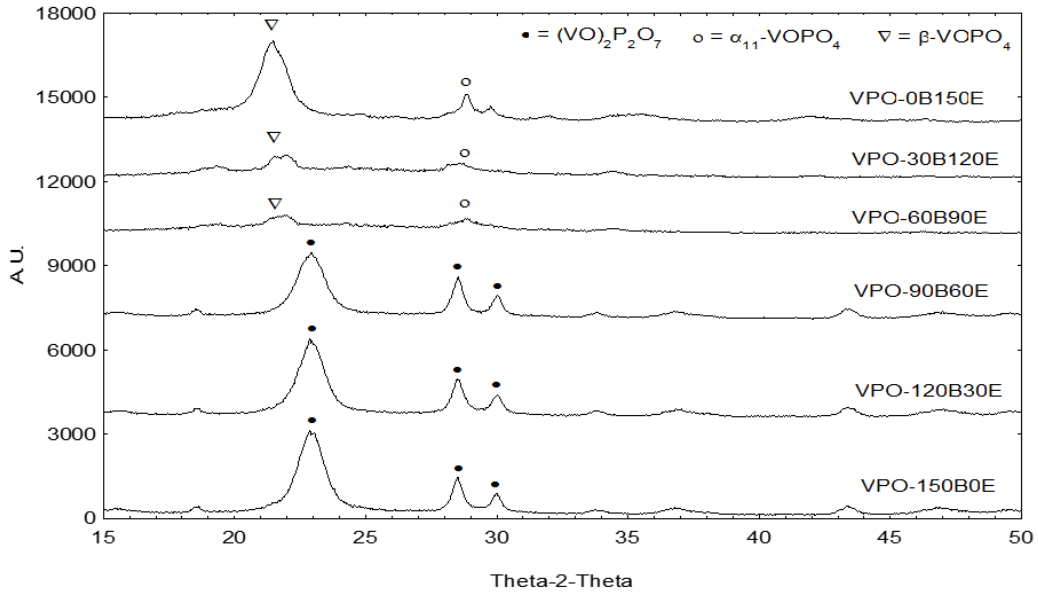

Figure 4.1: XRD profile of the catalysts synthesised via variable volume combination of environmentally friendly reducing agents

The diffractogram of VPO-150B0E, VPO-120B30E and VPO-90B60E showed similar diffraction pattern of a well crystallised $(VO)_2P_2O_7$ phase. However, VPO-60B90E, VPO-30B120E and VPO-0B150E showed no diffraction lines corresponding to $(VO)_2P_2O_7$ main characteristic peaks. Peaks which belong to the V^{5+} phases were detected in VPO-60B90E, VPO-30B120E and VPO-0B150E, respectively., i.e. α_{11}-$VOPO_4$ observed at $2\theta = 29.3°$ (JCPDS File No. 34-1247) and β-$VOPO_4$ observed at $2\theta = 21.5°$ (JCPDS File No. 27-0948).

As the volume of ethanol was increased from 0 ml to 60 ml, the intensity of all the main characteristic peaks assigned to (0 2 0), (2 0 4) and (2 2 1) planes were found to be less intense. When the volume of ethanol was further increased i.e. from 90 ml - 150 ml, and volume of 1-butanol was decreased from 60 ml to 0 ml, the main characteristic peaks of VPO were diminished. The crystalline V^{4+} phase could be too small to be detected or it existed as amorphous phase, explaining why it was not observed in the XRD analysis. VPO-0B150E showed drastic increase in the intensity of β-$VOPO_4$ phase.

The FWHM of (0 2 0) and (2 0 4) planes were used to calculate the crystallite size of the catalysts (Table 4.1). The addition of ethanol from 0 ml to 60 ml increased the line width of (0 2 0) plane, which decreased the crystallite size of the particle. Exfoliation-reduction of the precursor using mixtures of 1-butanol and ethanol produced smaller crystallite size catalyst.

Taufiq Yap et al., (2007) reported that the thickness of the (2 0 4) plane is only an indicative mean length of the (2 0 4) phase, while the thickness of the (0 2 0) plane represents the actual thickness of the particle. Haber et al., (1997) proposed the relative exposure of (0 2 0) plane could improve the catalytic performance of the VPO catalyst, since this plane is directly involved in the partial oxidation of *n*-butane to maleic anhydride. Hence, more emphasis was placed on the exposure of the (0 2 0) plane.

Table 4.1: XRD data of the catalysts synthesised via variable volume combination of environmentally friendly reducing agents

Catalyst	Line width [a] (0 2 0) / °	Line width [b] (2 0 4) / °	Crystallite size [c] (0 2 0) / Å	Crystallite size [c] (2 0 4) / Å
VPO-150B0E	1.1895	0.6102	67.3593	132.7746
VPO-120B30E	1.2016	0.6696	66.6822	121.0007
VPO-90B60E	1.2819	0.6386	62.5031	126.8725
VPO-60B90E	-	-	-	-
VPO-30B120E	-	-	-	-
VPO-0B150E	-	-	-	-

[a] FWHM of (0 2 0) reflection
[b] FWHM of (2 0 4) reflection
[c] Crystallite size calculated using Debye Scherrer equation

4.1.2 Scanning Electron Microscopy (SEM) Analysis

The surface morphologies of all the VPO catalyst retrieved by SEM analysis are shown in Figure 4.2 (a) – (f). Shapes of the catalyst were significantly different and varied depending on the volume combination of 1-butanol and ethanol. The catalyst prepared in 1-butanol alone (Figure 4.2(a)) showed principle secondary structure of platelet like crystals, which were agglomerated (Leong et al., 2011;

Leong et al., 2012). As the volume of ethanol was increased i.e. 30 ml - 60 ml, the synthesised catalysts (Figure 4.2 (b) and (c)) showed leaf like platelets that are layered supporting the idea that ethanol had intercalated into the exfoliated sheets of $VOPO_4$ and provided it with sufficient shear force to slide away from one another (Kiely et al., 1995; Okuhara et al., 2002).

Blocky type of rectangular shaped crystallites which were assigned to the presence of β-$VOPO_4$ was observed as the volume of ethanol was increased from 90 ml - 150 ml (Kiely et al., 1995; Imai et al., 2007). The micrograph results confirmed the presence of this V^{5+} phase in the catalyst which was also observed in the XRD analysis. Studies done by Kiely et al., (1995) showed that the presence of deleterious β-$VOPO_4$ phases were related to lower surface area. Increasing intensity of β-$VOPO_4$ phase observed in the XRD diffractogram (Figure 4.1) as the volume of ethanol was increased from 90 ml to 150 ml suggests VPO-60B90E, VPO-30B120E and VPO-0B150E have lower surface area.

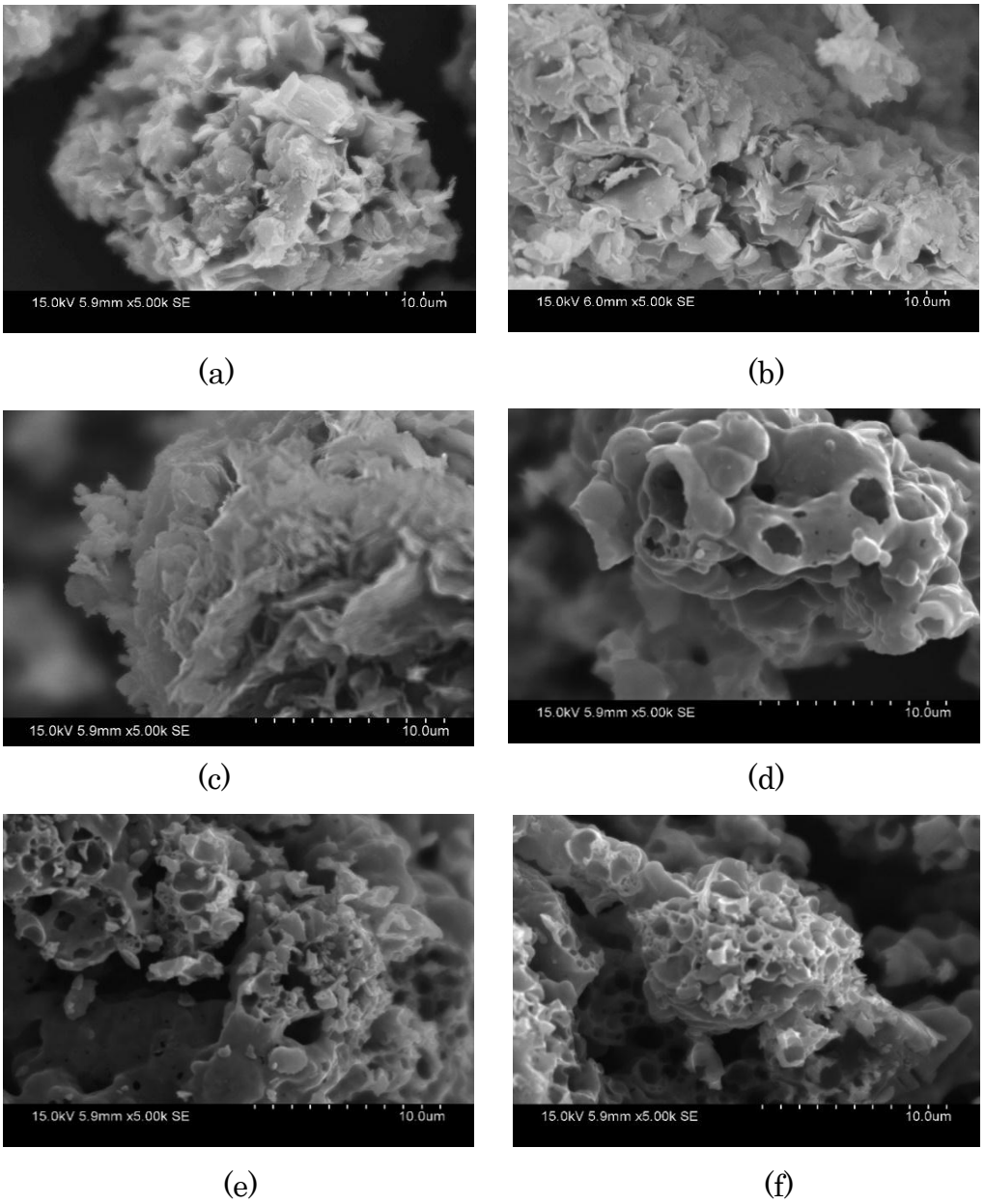

Figure 4.2: SEM micrograph for (a) VPO-150B0E, (b) VPO-120B30E, (c) VPO-90B60E, (d) VPO-60B90E, (e) VPO-30B120E and (f) VPO-0B150E

4.1.3 Brunauer-Emmett-Teller (BET) Surface Area Measurement and Chemical Analyses

Table 4.2 shows the specific surface area, P/V atomic ratio, average oxidation state of vanadium and percentage of V^{4+} and V^{5+} phases present in the synthesised catalyst. A sample of Adsorption Desorption Isotherm is shown in Appendix F. The surface area of the catalyst increased with the addition of ethanol from 0 ml to 60 ml. VPO-90B60E exhibited the highest surface area which was 29.02 m^2 g^{-1}. This was in agreement with the earlier XRD data analysis. As the crystallite size in the (0 2 0) plane decreased, catalyst with higher surface area were produced. Hence, addition of small volume of ethanol had led to the formation of smaller crystallite size particles by intercalating into the crystal platelets of $VOPO_4$ (Okuhara et al., 2002). When volume of ethanol was higher than 1-butanol, the surface area of the catalyst was found to decrease drastically, explaining why it was not detected in the XRD analysis.

Table 4.2: Surface area and chemical compositions of the catalysts synthesised via variable volume combination of environmentally friendly reducing agents

Catalyst	BET Surface Area (m^2 g^{-1})	EDX	ICP	V_{AV}	V^{4+} (%)	V^{5+} (%)
VPO-150B0E	17.02	1.15	1.16	4.273	72.73	27.27
VPO-120B30E	22.03	1.11	1.08	4.165	83.54	16.46
VPO-90B60E	29.02	1.05	1.04	4.135	86.47	13.53
VPO-60B90E	7.15	1.48	1.30	4.808	19.16	80.84
VPO-30B120E	4.07	1.54	1.39	4.848	15.22	84.78
VPO-0B150E	4.04	1.57	1.44	4.852	14.84	85.16

V_{AV} Average oxidation state of vanadium

When the volume of ethanol was increased from 90 ml to 150 ml, the catalyst was oxidised to a higher extent as higher ratio of weaker reducing agents were present in the solution. Hence, greater amount of V^{4+} phases were oxidised to the undesirable V^{5+} phase such as β-$VOPO_4$, which are deemed to exhibit lower surface area as it forms a series of square and rectangular like particles which has high tendency to agglomerate and stack on each other. Thus, the catalyst produced from higher volume of ethanol than 1 butanol would promote the formation of V^{5+} phases, which accounts for its lower surface area.

As the volume ratio of ethanol was higher compared to 1-butanol, the catalyst was further oxidised to form more V^{5+} phases which decreased its surface area. Increasing intensities of V^{5+} phases observed from the XRD analysis supports this claim. Higher volume of 1-butanol reduced the catalyst to greater extent resulting it to exhibit higher V^{4+} phases which corresponded to higher surface area.

Imai et al. (2007) reported that as the volume of ethanol was increased, the surface area of the catalyst increased, which contradicts with the current findings due to the different volume of reducing agents used. The present study conducted capped the total volume of reducing agents at 150 ml and varied the volume ratio of 1-butanol and ethanol while the reported finding was based on increasing the total volume of reducing agents used in the synthesis stage.

EDX and ICP analyses showed that the P/V atomic ratio were in between the range of 1.05 - 1.57 and 1.04 - 1.44 respectively. Studies by Bordes (1993) and Centi (1993) showed that catalysts with P/V atomic ratio between the range 1.00 - 1.20 exhibited the desired property to enhance the catalyst performance. Both EDX and ICP analyses showed good agreement with the optimal P/V atomic ratio as the volume of ethanol was increased from 0 ml to 60 ml.

As the volume of ethanol was further increased from 90 ml to 150 ml, it resulted the P/V atomic ratio to deviate from the optimal range. The presence of β-$VOPO_4$ was linked to higher amount of phosphorus present in the catalyst which was due to surface phosphorus enrichment. The presence of this deleterious phase have been reported to exhibit catalysts with lower surface area and poor catalytic properties (Cornagalia et al., 2000).

The oxidation number of vanadium exceeded 4.0 for all the catalysts, indicating presence of both V^{4+} and V^{5+} phases. The percentage of V^{4+} increased from 72.73% to 86.47% as the volume of ethanol was increased from 0 ml to 60 ml. Higher volume of ethanol compared to 1-butanol decreased the percentage of V^{4+} from 19.16% to 14.84% and increased the percentage of V^{5+} from 80.84% to 85.16%. The percentages of V^{4+} and V^{5+} obtained support the BET results, as the surface area of the catalyst increased with addition of ethanol from 0 ml to 60 ml and drastic fall was observed when volume of ethanol was higher due to the presence of minute V^{4+} phase.

The average oxidation number of vanadium lies within the range of 4.8, as the percentage of V^{5+} were higher than the corresponding percentage of V^{4+} as the volume of ethanol was increased from 90 ml to 150 ml (Kiely et al., 1995; Imai et al., 2007). These finding supports the claim that higher volume of ethanol compared to 1-butanol oxidises the V^{4+} phases to V^{5+} phases.

4.1.4 Temperature Programmed Reduction (TPR) Analysis

Figure 4.3 shows the TPR profile of the VPO catalysts in a stream of 5.55% H_2/N_2. Table 4.3 lists the peaks maxima temperature, total amount of oxygen atoms removed, reduction activation energies, ratio of V^{4+} to V^{5+} oxygen species and ratio of V^{5+} to V^{4+} oxygen species removed. All the catalysts showed two peaks maxima, whereby the first peak corresponds to the reduction of V^{5+}-O^{2-} species while the second peak corresponds to the reduction of V^{4+}-O^{-} species (Abon et al., 2001). Reduction of V^{4+} species appeared to be the major peak for VPO-150B0E, VPO-120B30E and VPO-90B60E, while reduction of V^{5+} peak appeared as the major peak for VPO-60B90E, VPO-30B120E and VPO-0B150E. This was in agreement with the percentages of V^{4+} and V^{5+} obtained via redox titration and XRD analyses.

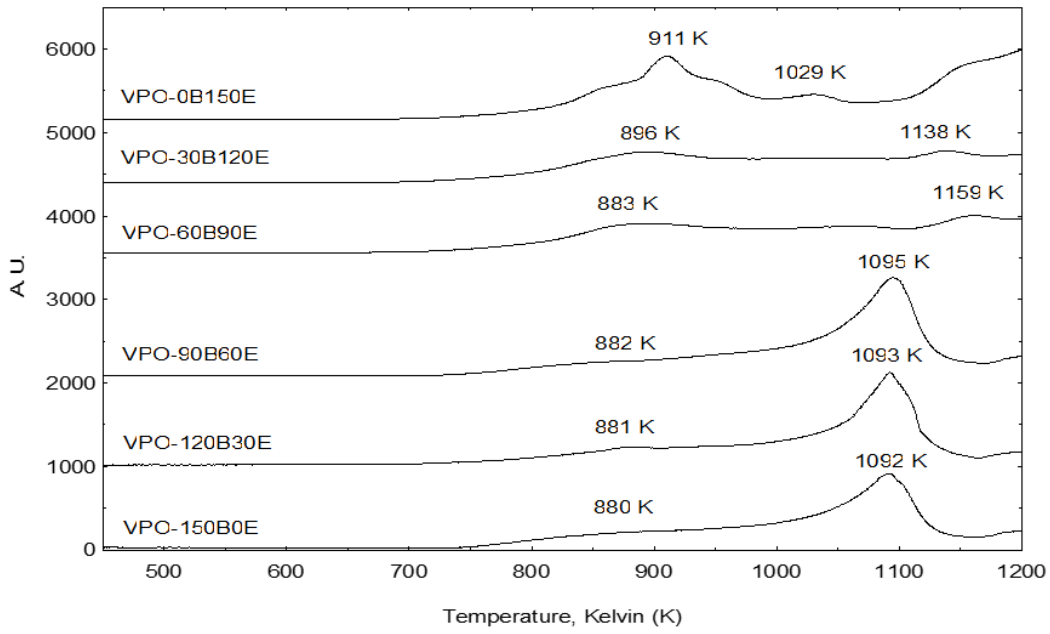

Figure 4.3: TPR profile of the catalysts synthesised via variable volume combinations of 1-butanol and ethanol

Total amount of oxygen removed from the catalyst increased from 1.209 x 10^{21} atom g^{-1} for VPO-150B0E to 1.513 x 10^{21} atom g^{-1} for VPO-90B60E. As the volume of ethanol was increased from 90 ml to 150 ml, total amount of oxygen removed decreased from 1.308 x 10^{21} atom g^{-1} for VPO-60B90E to 1.047 x 10^{21} atom g^{-1} for VPO-0B150E. Data in Table 4.3 indicate more oxygen was removed from the V^{4+} peak as the addition of ethanol was increased from 0 ml to 60 ml, while further increasing the volume of ethanol from 90 ml to 150 ml favoured the removal of oxygen species from V^{5+} peak.

Table 4.3: Reactivity analysis of the catalysts synthesised via variable volume combinatios of 1-butanol and ethanol

Catalyst	Peak	T (°C)	T_m (K)	Reduction Activation Energy, E_r (KJ mol^{-1})	Amount Oxygen Removed (mol g^{-1})	Amount Oxygen Removed (atom g^{-1})	Ratio for Oxygen Removal of V^{4+}/V^{5+}	Ratio for Oxygen Removal of V^{5+}/V^{4+}
VPO-150B0E	1	607	880	135.295	4.140×10^{-4}	2.494×10^{20}	3.85	0.26
	2	819	1092	167.889	1.595×10^{-3}	9.607×10^{20}		
	Total amount of oxygen removed				2.009×10^{-3}	1.209×10^{21}		
VPO-120B30E	1	608	881	135.449	4.020×10^{-4}	2.421×10^{20}	4.50	0.22
	2	820	1093	168.043	1.809×10^{-3}	1.089×10^{21}		
	Total amount of oxygen removed				2.211×10^{-3}	1.331×10^{21}		
VPO-90B60E	1	609	882	135.603	3.910×10^{-4}	2.353×10^{20}	5.43	0.18
	2	822	1095	168.350	2.124×10^{-3}	1.278×10^{21}		
	Total amount of oxygen removed				2.514×10^{-3}	1.513×10^{21}		
VPO-60B90E	1	610	883	135.756	1.624×10^{-3}	9.779×10^{20}	0.34	2.95
	2	886	1159	178.190	5.500×10^{-4}	3.312×10^{20}		
	Total amount of oxygen removed				2.174×10^{-3}	1.308×10^{21}		
VPO-30B120E	1	623	896	137.755	1.642×10^{-3}	9.885×10^{20}	0.29	3.40
	2	865	1138	174.961	4.830×10^{-4}	2.910×10^{20}		
	Total amount of oxygen removed				2.125×10^{-3}	1.279×10^{21}		
VPO-0B150E	1	638	911	140.061	1.413×10^{-3}	8.507×10^{20}	0.23	4.31
	2	756	1029	158.203	3.280×10^{-4}	1.972×10^{20}		
	Total amount of oxygen removed				1.740×10^{-3}	1.047×10^{21}		

The amount of oxygen removed are directly related to the surface area of the catalyst. Higher surface area resulted in the exposure of more crystallites exposing the V^{4+}-O^{-} oxygen species. Hence more V^{4+}-O^{-} species were removed (Hutchings and Higgins, 1996). According to Rownaghi et al., (2010), the rise of phosphorus concentration on the surface accompanied by simultaneous enrichment of the surface in oxygen basicity favours the removal of O^{2-} oxygen species.

Ratio of oxygen species removed from V^{4+} phase relative to V^{5+} phase increased from 3.85 to 5.43 as the volume of ethanol was increased from 0 ml to 60 ml. This result was in agreement with increasing percentage of V^{4+} obtained from redox analysis as well as increasing surface area obtained from BET analysis. Drastic fall in the ratio of oxygen species removed from V^{4+} phase relative to V^{5+} phase (Table 4.3) as volume of ethanol was increased from 90 ml to 150 ml, suggests higher volume of ethanol favours the formation of more V^{5+} related species (Pierini and Lombardo, 2005). Increasing percentage of V^{5+} and higher P/V atomic ratio observed in EDX and ICP analyses supports the obtained result.

Reduction activation energy gradually increased as the volume of ethanol was increased from 0 ml to 60 ml. The layered leaf like structure observed from the SEM analysis stacks on one another, resulting in higher energy required to overcome the additional bonds formed, consequently reduced the mobility of the oxygen (V^{4+}-O^{-}) removed and increased the temperature at which it was reduced (Pierini and Lombardo, 2005).

4.1.5 *n*-Butane Oxidation to Maleic Anhydride

The catalytic performance of *n*-butane oxidation to maleic anhydride (Table 4.4) was analysed at 673 K (GSHV = 2400 h^{-1}), a typical reaction temperature for VPO catalyst (Leong et al., 2011).

Table 4.4: Catalytic performance of the catalysts synthesised via variable volume combinations of 1-butanol and ethanol

Catalyst	*n*-butane conversion (%)	Product selectivity (%)		
		MA	CO_2	CO
VPO-150B0E	21	84	15	1
VPO-120B30E	24	85	14	1
VPO-90B60E	30	86	13	1
VPO-60B90E	17	87	12	1
VPO-30B120E	14	88	11	1
VPO-0B150E	12	89	10	1

The addition of ethanol from 0 ml to 60 ml had increased the activity and selectivity of *n*-butane oxidation to MA, however, further addition of ethanol from 90 ml to 150 ml decreased the activity of the catalyst. According to Rownaghi et al., (2010) V^{4+}-O^- acts as a centre for *n*-butane activation, hence removal of more O^- oxygen species with higher amount of active sites (V^{4+}) results in the enhancement of the catalytic activity. This was observed for VPO-120B30E and VPO-90B60E, where the addition of ethanol has led to the exposure of (0 2 0) plane by producing catalyst with smaller crystallite size, higher surface area which contributed to the removal of more O^- oxygen species and higher amount of active site due to its higher percentage of V^{4+} present in the catalyst.

As for VPO-60B90E, VPO-30B120E and VPO-0B150E, higher volume of ethanol had oxidised the V^{4+} phases to V^{5+} phases as observed in the XRD analysis. This explains the lower *n*-butane conversion obtained when volume of ethanol was increased from 90ml to 150ml. Higher volume of ethanol favours the formation of V^{5+} phase, contributing to more O^{2-} oxygen species. This phenomenon would enhance the selectivity of the VPO catalyst system (Rownaghi et al., 2010).

Similarities of the present findings with that of reported by Imai et al. (2007) are increasing conversion towards maleic anhydride (MA) as the volume of ethanol was increased and remarkably high selectivity to MA despite low conversion as the volume of ethanol was further increased. These results demonstrate that the exfoliation reduction of $VOPO_4 \cdot 2H_2O$ in mixture of reducing agents produces a highly active and selective catalyst for the oxidation of *n*-butane to MA.

When the volume of ethanol was increased from 0 ml to 60 ml, the synthesised catalyst showed slight increase in selectivity despite lower percentage of V^{5+} observed from Redox analysis. This indicates minute amount of V^{5+} phases were sufficient to exhibit high selectivity (Bordes, 1993). As for the catalyst with higher volume combination of ethanol compared 1-butanol, further increase in selectivity is attributed to the development of α_{11}-$VOPO_4$.

Studies by Bordes, (1993) had indicated that presence of α_{11}-$VOPO_4$ is dominated by large and flat plates with small particles on the surface which exposes the desired plane for selective oxidation sites on $(VO)_2P_2O_7$. Hence, increasing amount of α_{11}-$VOPO_4$ phase as the volume of ethanol was increased from 90 ml to 150 ml results in higher selectivity of Maleic anhydride. Increasing intensity of the α_{11}-$VOPO_4$ peak observed from the XRD analysis support these findings.

4.1.6 Series Findings

VPO catalyst was successfully synthesised implying exfoliation reduction technique using various volume combinations of environmental friendly reducing agents (1-butanol and ethanol). Based on the outcome of this series, higher volume of weaker reducing agents (ethanol) favoured the development of V^{5+} phases which result the synthesised catalysts to exhibit poorer physico-chemical, reactivity and catalytic properties.

Catalyst synthesised with higher volume combination of 1-butanol to ethanol prevents the oxidation of V^{4+} phase to V^{5+} phase, which resulted the synthesised catalysts to exhibit higher amount of active sites. Exfoliating the dihydrate precursor in ethanol produced catalysts that were layered, which increased the surface area and led to removal of more V^{4+}-O^- oxygen species. These factors aided the synthesised catalyst to exhibit improved activity and selectivity.

From the range of catalyst synthesised and analysed, VPO-90B60E showed enhanced catalytic properties with highest surface area (29.02 m^2 g^{-1}), highest amount of oxygen species removed (1.513 x 10^{21} atom g^{-1}) where 1.278 x 10^{21} atom g^{-1} corresponded to the removal of V^{4+}-O^- oxygen species. It also showed highest *n*-butane conversion (30%) and product selectivity towards MA was 86%. Hence, 90 ml of 1-butanol and 60 ml of ethanol were determined as the optimal volume combination of environmentally friendly reducing agents within the range of catalysts analysed in this series. By comparison to the bulk catalyst used in the industry, the synthesised catalyst is lower in *n*-butane conversion to maleic anhydride by 35%, but higher in terms of selectivity by 4%.

4.2 Effect of Ultrasound Duration on VPO Catalyst

4.2.1 X-ray Diffraction (XRD) Analysis

XRD pattern of the synthesised catalyst obtained by varying the ultrasound duration are shown in Figure 4.4. Focus was the main characteristic peaks of $(VO)_2P_2O_7$ observed at $2\theta = 22.9°$, 28.4° and 29.9° (JCPDS File No. 34-1381) which corresponded to the reflection of (0 2 0), (2 0 4) and (2 2 1) planes respectively. All the catalysts showed similar diffraction pattern of a well crystallised $(VO)_2P_2O_7$ phase corresponding to the main characteristic peaks. Emphasis was given to the exposure of (0 2 0) plane as it was more important in enhancing the catalytic property (Haber et al., 1997; Taufiq Yap et al., 2007).

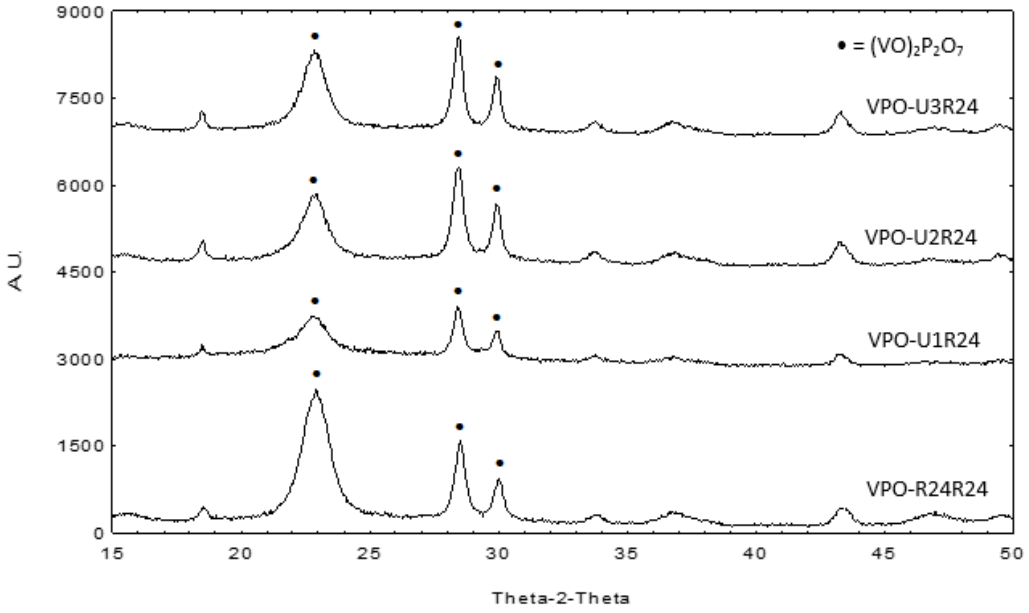

Figure 4.4: XRD profile of the catalysts synthesised by varying the ultrasound duration

Catalyst prepared via conventional reflux method (VPO-R24R24) showed higher degree of crystallinity as compared to the ultrasound irradiated catalysts (VPO-U1R24, VPO-U2R24 and VPO-U3R24). XRD profiles of the VPO catalyst prepared by varying the ultrasound duration showed a more amorphous nature, hence the intensity of the peaks observed was lower. As the ultrasound duration increased, the catalyst showed higher degree of crystallinity and sharper peaks were observed, which can be attributed to the enhancement of the molecular motion caused by prolonged acoustic streaming.

The similarity in the pattern of diffractogram between the catalyst prepared via reflux (VPO-R24R24) and ultrasound irradiated catalyst (VPO-U1R24, VPO-U2R24 and VPO-U3R24) suggest that there were no changes to the basic matrix of the $VOPO_4 \cdot 2H_2O$ precursor. This suggests that the catalyst preparation can be accomplished much faster using ultrasound irradiation technique at 5 kHz and 353 K, i.e. 1 hour - 3 hours, compared to the conventional reflux method, i.e. heating at 393 K for 24 hours. Moreover, no additional peak besides the main characteristic peaks were observed for ultrasound irradiated catalyst indicating that high purity catalyst consisting predominantly of V^{4+} phase with trace amount of V^{5+} phase can be produced through ultrasound irradiation technique (Unnikrishnan et al., 2003).

Based on the Debye Scherrer equation, the crystallite size of the catalysts were calculated using the full width at half maximum (FWHM) of (0 2 0) and (2 0 4) planes. The line width and crystallite size of (0 2 0) and (2 0 4) plane were tabulated in Table 4.5.

Table 4.5: XRD data of the catalysts synthesised via varying ultrasound duration

Catalyst	Line width [a] (0 2 0) / °	Line width [b] (2 0 4) / °	Crystallite size [c] (0 2 0) / Å	Crystallite size [c] (2 0 4) / Å
VPO-R24R24	1.2819	0.6386	62.5031	126.8725
VPO-U1R24	1.3375	0.5468	59.8954	148.1470
VPO-U2R24	1.3869	0.6264	57.7638	129.3225
VPO-U3R24	1.4543	0.6319	55.0878	128.1958

[a] FWHM of (0 2 0) reflection
[b] FWHM of (2 0 4) reflection
[c] Crystallite size calculated using Debye Scherrer equation

As the ultrasound duration was increased from one hour to three hours, the line width of (0 2 0) plane increased, which decreased the crystallite size of the particle. Cornagalia et al., (2003) stated as the line width of a plane increased, the crystallite size corresponding to that plane will decrease. Prolonged ultrasonication would lead to the collapse of more transient bubbles, hence resulting in high velocity interparticle collision which produced smaller crystallites of the bulk material (Suslick et al., 1999).

4.2.2 Scanning Electron Microscopy (SEM) Analysis

The surface morphologies of the VPO catalysts obtained from SEM analysis are shown in Figure 4.5 (a) (i) – (d) (ii). The catalyst prepared via conventional reflux method (VPO-R24R24) using mixtures of 1-butanol and ethanol as reducing agents showed leaf like structures that were layered as observed in Figure 4.5 (a) (i) and (ii). Similar findings were obtained by Okuhara et al., (2002) and Imai et al., (2007).

As ultrasound duration was increased from one hour to three hours, the catalysts showed smaller platelets under similar magnification conditions. This can be attributed to the fragmentation of the solid as the duration of ultrasonic irradiation was increased. According to Suslick et al., (1999), ultrasound irradiation smoothes the crystalline surface and causes agglomeration of small particles under prolonged ultrasound duration. This was observed for VPO-U3R24 (Figure 4.5 (a) (i) and (ii)) as it formed smaller particles which were layered and agglomerated.

Studies done by Cavani and Trifiro (1994) reported that these aggregates preferentially expose (1 0 0) crystal plane and therefore were less oxidisable. Fragmentation of particles produced smaller crystallites, while smoothing the crystal surface prevented the oxidation of the catalyst, as a result of interparticle collision owing to cavitation induced shockwaves. Hence, decreasing the thickness of the particles and enhancing the catalytic performances (Suslick et al., 1999; Chen and Munson, 2002).

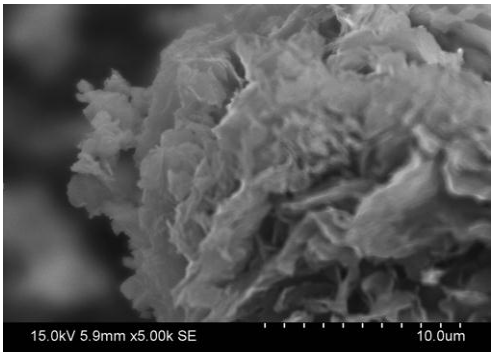

(a) (i)

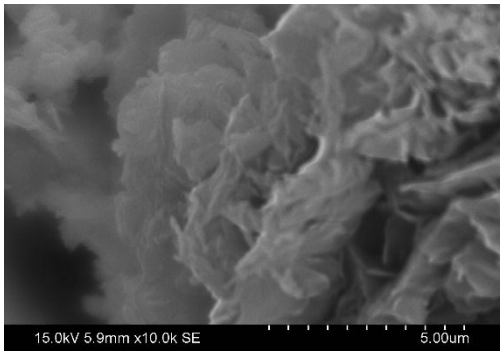

(a) (ii)

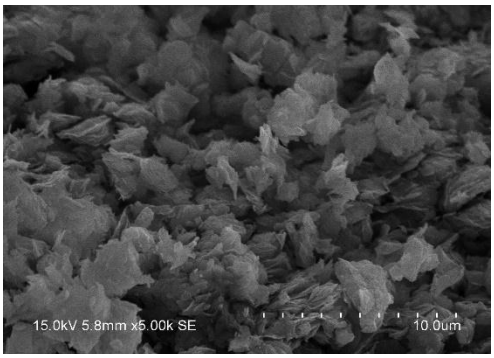

(b) (i)

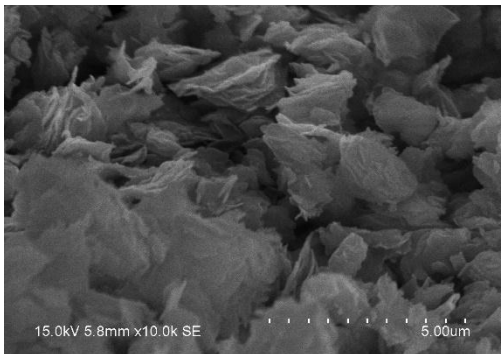

(b) (ii)

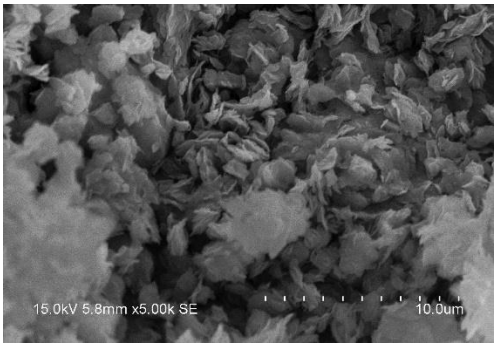

(c) (i)

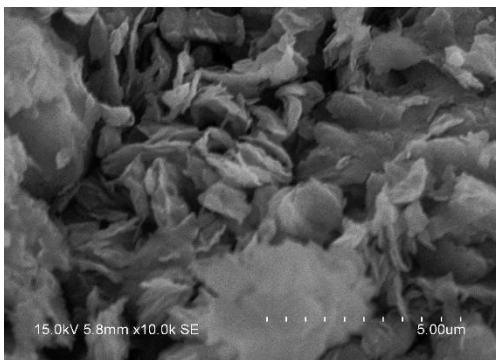

(c) (ii)

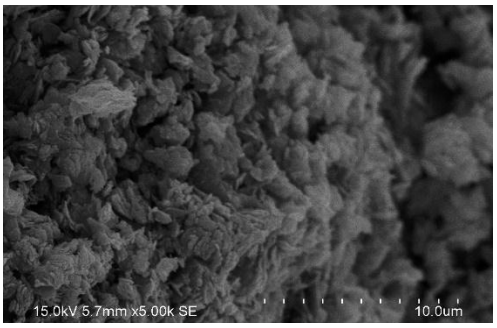

(d) (i)

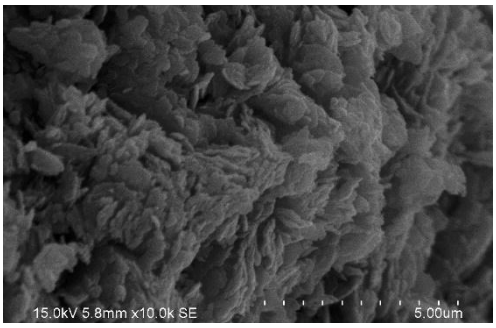

(d) (ii)

Figure 4.5: SEM micrograph for (a) VPO-R24R24: (i) x 5000, (ii) x 10000, (b) VPO-U1R24: (i) x 5000, (ii) x 10000, (c) VPO-U2R24: (i) x 5000, (ii) x 10000, (d) VPO-U3R24: (i) x 5000, (ii) x 10000

4.2.3 Brunauer-Emmett-Teller (BET) Surface Area Measurement and Chemical Analyses

The surface area of ultrasound irradiated catalysts were discerned to be higher than catalyst prepared via conventional reflux method. As ultrasound duration was increased from one hour to three hours, surface area of the catalyst increased. VPO-U3R24 showed the highest surface area of 39.15 $m^2 g^{-1}$ (Table 4.6) within the range of catalysts synthesized in this series. Prolonged ultrasonication led to the collapse of more transient bubbles, which resulted in high velocity interparticle collision. The crystallite produced were smaller, hence it increased the specific surface area (Ensminger and Bond, 2012).

Table 4.6: Surface area and chemical compositions of the catalysts synthesised by varying the ultrasound duration

Catalyst	BET Surface Area ($m^2 g^{-1}$)	EDX	ICP	V_{AV}	V^{4+} (%)	V^{5+} (%)
VPO-R24R24	29.02	1.05	1.04	4.135	86.47	13.53
VPO-U1R24	31.29	1.10	1.08	4.197	80.35	19.65
VPO-U2R24	34.00	1.07	1.05	4.160	84.02	15.98
VPO-U3R24	39.15	1.04	1.03	4.111	88.89	11.11

V_{AV} Average oxidation state of vanadium

Studies by Unnikrishnan et al. (2003) showed similar trend in surface area as ultrasound duration was increased, however, the highest surface area reported was 10.3 $m^2 g^{-1}$ for six hours of sonication implying organic method. Present findings derived from dihydrate method yields higher surface area in shorter ultrasound duration, indicating that environmental friendly reducing agents coupled with ultrasonication improves the physical properties of the catalyst.

EDX and ICP analyses showed the P/V atomic ratio of ultrasound irradiated catalyst were in the optimal range as suggested by Bordes (1993) and Centi (1993). High purity of VPO catalyst could be obtained via ultrasound irradiation, which inhibited the oxidation of the V^{4+} phase to V^{5+} phase.

The oxidation number of vanadium exceeded 4.0 for all the catalysts, indicating the presence of both V^{4+} and V^{5+} phases (Centi, 1993). Slight increase in the average vanadium oxidation state was observed when ultrasound technique was introduced (VPO-U1R24). A possible suggestion for this might be its amorphous nature, which prevented it from being detected. Lower intensity of VPO-U1R24 observed in the XRD diffractogram supports this suggestion.

As ultrasound duration was increased from one hour to three hours, the percentage of V^{4+} increased as it was less oxidisable due to the exposure of (1 0 0) plane (Cavani and Trifiro, 1994). Increasing the ultrasound duration drastically has decreased the formation of V^{5+} phase from 19.65% to 11.11%. Prolonged ultrasound irradiation, favoured the formation of more V^{4+} phase, which is deemed to be responsible for the partial oxidation of *n*-butane to maleic anhydride (Wong and Taufiq Yap, 2011).

4.2.4 Temperature Programmed Reduction (TPR) Analysis

Figure 4.6 shows the TPR profile of the VPO catalyst in a stream of 5.55% H_2/N_2. Table 4.7 lists the peaks maxima temperature, total amount of oxygen atoms removed, reduction activation energies, ratio of V^{4+} to V^{5+} oxygen species and ratio of $V^{5+}$to V^{4+} oxygen species removed. All the catalysts gave two reduction peaks, where the first peak corresponded to the removal of V^{5+}-O^{2-} species, while second peak corresponded to the removal of V^{4+}-O^{-} species.

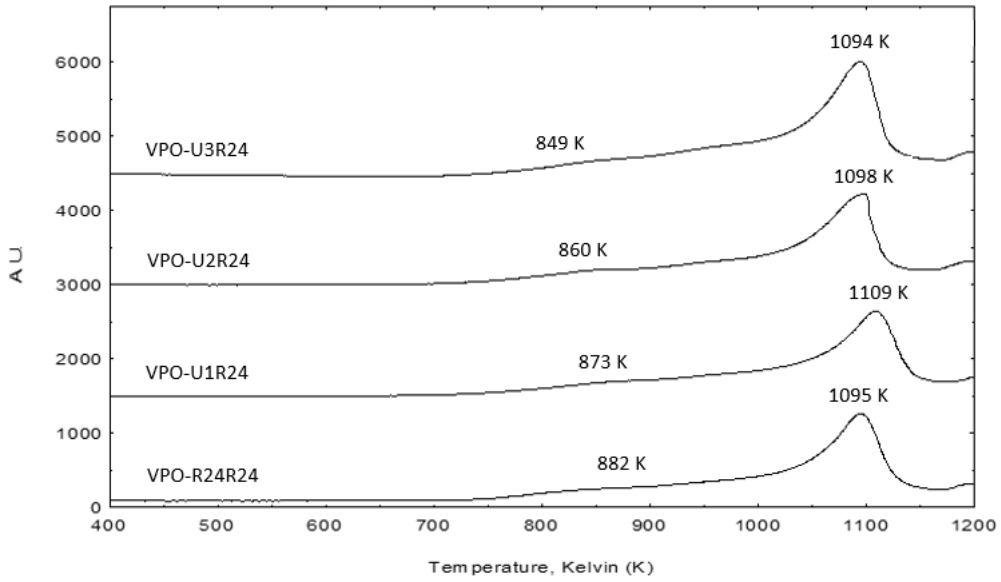

Figure 4.6: TPR profile of the catalysts synthesised by varying the ultrasound duration

The total amount of oxygen removed from the catalyst increased from 1.513 x 10^{21} atom g^{-1} for VPO-R24R24 to 1.787 x 10^{21} atom g^{-1} for VPO-U3R24. As the ultrasound duration was increased from one hour to three hours, more oxygen species were removed as the catalyst exhibited higher exposed surface area. Higher reducible V^{4+}-O^{-} oxygen species was removed as ultrasound duration was prolonged, indicating that the catalyst were less oxidisable, hence supporting the findings by Cavani and Trifiro (1994).

Peak assigned to the removal of V^{4+}-O^{-} species showed a declining trend in the reduction activation temperature as the duration of ultrasound irradiation was increased from one hour to three hours. This suggests that the lattice oxygen species in ultrasound irradiated catalyst were easily accessible as the crystallite size was smaller than conventionally produced catalyst (Wong and Taufiq Yap, 2011).

Table 4.7: Reactivity analysis of the catalysts synthesised by varying the ultrasound duration

Catalyst	Peak	T (^{o}C)	T_m (K)	Reduction Activation Energy, E_r (KJ mol^{-1})	Amount Oxygen Removed (mol g^{-1})	Amount Oxygen Removed (atom g^{-1})	Ratio for Oxygen Removal of V^{4+}/V^{5+}	Ratio for Oxygen Removal of V^{5+}/V^{4+}
VPO-R24R24	1	609	882	135.603	3.910×10^{-4}	2.353×10^{20}	5.43	0.18
	2	822	1095	168.350	2.124×10^{-3}	1.279×10^{21}		
	Total amount of oxygen removed				2.514×10^{-3}	1.513×10^{21}		
VPO-U1R24	1	600	873	134.219	4.710×10^{-4}	2.833×10^{20}	4.55	0.22
	2	836	1109	170.503	2.140×10^{-3}	1.288×10^{21}		
	Total amount of oxygen removed				2.611×10^{-3}	1.571×10^{21}		
VPO-U2R24	1	587	860	132.220	4.490×10^{-4}	2.703×10^{20}	4.89	0.20
	2	825	1098	168.811	2.192×10^{-3}	1.319×10^{21}		
	Total amount of oxygen removed				2.641×10^{-3}	1.589×10^{21}		
VPO-U3R24	1	576	849	130.529	3.510×10^{-4}	2.114×10^{20}	7.46	0.13
	2	821	1094	168.196	2.618×10^{-3}	1.576×10^{21}		
	Total amount of oxygen removed				2.969×10^{-3}	1.787×10^{21}		

4.2.5 *n*-Butane Oxidation to Maleic Anhydride

The catalytic performance of *n*-butane oxidation to maleic anhydride (Table 4.8) was analysed at 673 K (GSHV = 2400 h^{-1}), a typical reaction temperature for VPO catalyst (Leong et al., 2011).

Table 4.8: Catalytic performance of the catalysts synthesised by varying the ultrasound duration

Catalyst	*n*-butane conversion (%)	Product selectivity (%)		
		MA	CO_2	CO
VPO-R24R24	30	86	13	1
VPO-U1R24	32	87	12	1
VPO-U2R24	35	88	11	1
VPO-U3R24	39	89	10	1

From the catalytic evaluation, ultrasound irradiated catalysts showed an improvement in *n*-butane conversion. Highest conversion obtained was 39% from VPO-U3R24, indicating prolonged ultrasound irradiation increased the activity of the catalyst. As the ultrasound irradiation was increased from one hour to three hours, catalytic activity increased owing to the prolonged duration available for acoustic cavitation to take place (Suslick et al., 1999; Chen and Munson, 2002).

Prolonged ultrasound irradiation led to the collapse of more transient bubbles which induced higher interparticle collision and produced smaller crystallite size. More V^{4+}-O^{-} oxygen species were reduced, as the smoothing of the crystallite edges preferentially expose (1 0 0) plane. This prevented the oxidation of V^{4+} phase (Suslick et al., 1999; Chen and Munson, 2002).

An overall 3% increase in the selectivity was observed as ultrasound duration was prolonged. Bordes (1993) showed that only a small amount of V^{5+} phase were required to achieve high selectivity. Minute amount of V^{5+} phase present in the catalyst coupled with its increasing degree of crystallinity as ultrasound duration was increased resulted the synthesised catalyst to exhibit higher selectivity (Imai et al., 2007).

Ultrasound irradiated catalyst exhibited improved catalytic activity and selectivity as compared to the bulk catalyst. Studies by Unnikrishnan et al., (2003) pointed out that strong convective current formed as the transient bubbles collapsed, which reduced the thickness of the diffusing layer thereby enhancing the diffusion controlled process. Reduction in the thickness of the particle, particularly the thickness of (0 2 0) plane improved the catalytic performances of the catalyst. These results were in agreement with the decreasing crystallite size observed for (0 2 0) plane as ultrasound irradiation was increased.

4.2.6 Series Findings

VPO catalyst was successfully synthesised implying ultrasound irradiation technique. Minimum one hour ultrasound irradiation was carried out as indirect probe sonication at 5 kHz and 353 K required more than 27 minutes for V_2O_5 to begin transformation into $VOPO_4 \cdot 2H_2O$ precursor. Based on the XRD diffractogram observed for VPO-U1R24, all the V_2O_5 were transformed into the dihydrate precursor as no additional peaks were observed.

SEM analysis indicated prolonged ultrasound irradiation result in the agglomeration of crystallites, hence increasing the ultrasound duration more than three hours might produce more bulky structure which reduces the surface area of the catalyst. Lower surface area reduced the mobility of O^- oxygen species and increased the temperature at which it was removed, hence the reduction activation energy was higher.

Implying ultrasound irradiation can significantly shorten the process of synthesising VPO catalyst, as the formation of dihydrate precursor can be achieved in less than three hours as compared to the conventional reflux method which takes up to 24 hours. Ultrasound irradiated catalyst also showed better physical properties. The ability of ultrasound irradiation to expedite the catalyst preparation and enhance its activity and selectivity are attributed to its acoustic cavitation.

Collapse of transient bubbles induces shockwaves and results in high velocity interparticle collision which produced smaller crystallite size particles. The synthesised catalyst exhibited higher specific surface area and was more reducible as the lattice oxygen were more labile. Higher amount of V^{4+} related oxygen species were reduced and this increased the ratio of V^{4+}/V^{5+} oxygen species removed.

From the range of catalysts synthesised and analysed, VPO-U3R24 showed enhanced catalytic properties with highest surface area (39.15 m^2 g^{-1}) and highest amount of V^{4+} related oxygen species removed (1.576 x 10^{21} atom g^{-1}). It also showed highest *n*-butane conversion (39%) and highest product selectivity (89%) towards MA. Hence, three hours of ultrasound irradiated VPO catalyst exhibited superior physico-chemical, reactivity and catalytic performances, as compared to those lower duration sonicated VPO catalysts analysed within this series implying ultrasonication at 5 kHz and 353 K.

4.3 Effect of VPO Loading on Coconut Shell Activated Carbon Supported Catalyst

4.3.1 X-ray Diffraction (XRD) Analysis

XRD pattern of the synthesised catalyst obtained by varying the bulk VPO loading and ultrasound irradiated VPO loading on coconut shell activated carbon (CSAC) were shown in Figure 4.7 and Figure 4.8, respectively. Main characteristic peaks of $(VO)_2P_2O_7$ observed at 2θ = 22.9°, 28.4° and 29.9° (JCPDS File No. 34-1381) were corresponded to the reflection of (0 2 0), (2 0 4) and (2 2 1) planes respectively.

Besides the main characteristic peaks additional peaks, which belong to the activated carbon were observed for both the diffractogram (Figure 4.7 and Figure 4.8) at 2θ = 20.9° and 26.6° (JCPDS File No. 46-1045). The intensities of these peaks were discerned to decrease as VPO loadings was increased from 10 wt% to 40 wt%, due to the partial blocking of the micropores by the VPOs (Li et al., 2006b).

The main characteristic peaks of the VPO catalyst with low loading, i.e. 10 wt% VPO/CSAC and 20 wt% VPO/CSAC, were not discernible mainly due to its relatively low percentage of loading (APPENDIX E). These characteristic peaks appeared more intense as the loading was increased, i.e. 30 wt% VPO/CSAC and 40 wt% VPO/CSAC. Studies by Nie et al. (2003), using Al-containing MCM-41 support indicated a strong bond between the VPOs and the support system at high VPO loading.

As the VPO loading was increased from 10 wt% to 40 wt%, more active phase were available to agglomerate. Bigger structures were formed, which improved the XRD detection and a detectable diffraction was observed, i.e. 30 wt% VPO/CSAC and 40 wt% VPO/CSAC. As for the ultrasound irradiated catalyst, these characteristic peaks were hardly observable even at high loadings as the individual diffractogram did not give a very high detection (APPENDIX E). Ultrasound irradiated catalyst consists of amorphous crystals compared to the bulk catalyst, hence it was well dispersed on the surface of the support (Nie et al., 2001).

Both diffractogram (Figure 4.7 and Figure 4.8) showed no peaks attributed to the V^{5+} phase. According to Li et al. (2006b), the crystalline phase could be too small to be detected or it existed as amorphous phase. The half width of the (0 2 0) and (2 0 4) plane was used to determine the crystallite size of the catalyst according to the Debye Scherrer equation. Table 4.9 summarises the line width and crystallite size obtained for the reflection of (0 2 0) and (2 0 4) plane.

The VPO species had notable effect on the line width of the (0 2 0) plane, as it became broader on higher loading suggesting that the long range order of CSAC decreased due the presence of more VPO species (Nie et al., 2001). Both the bulk VPO and ultrasound irradiated VPO supported catalyst showed smaller crystallite size as VPO loading was increased from 10 to 40 wt%. This was in agreement with Nie et al. (2001) findings indicating the active phase was well dispersed, producing a broader line width and smaller crystallite structure.

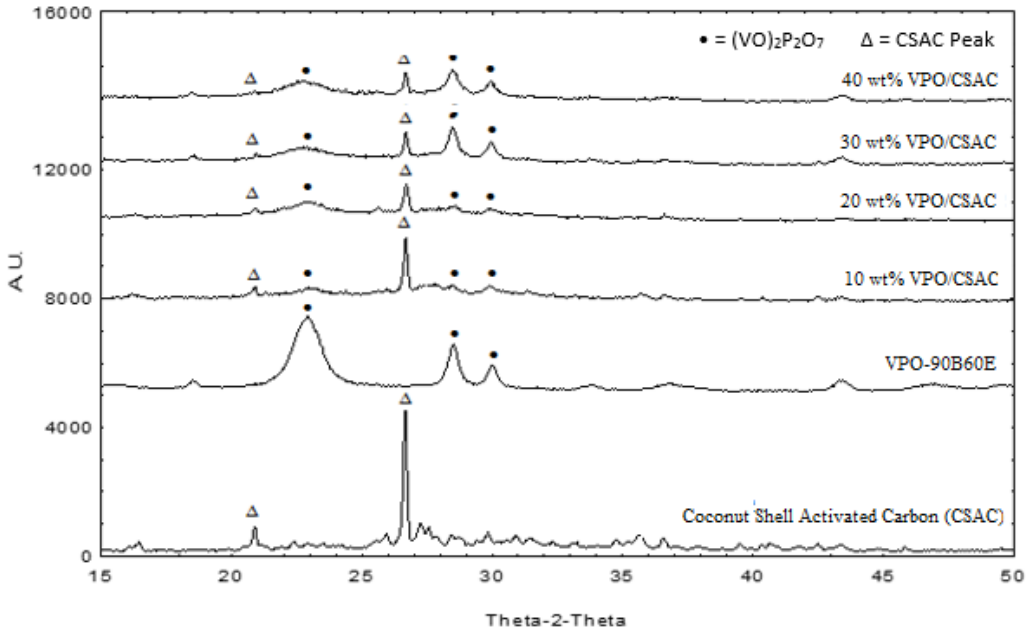

Figure 4.7: XRD profile of the catalysts synthesised via varying the weight percentages of VPO loading on CSAC

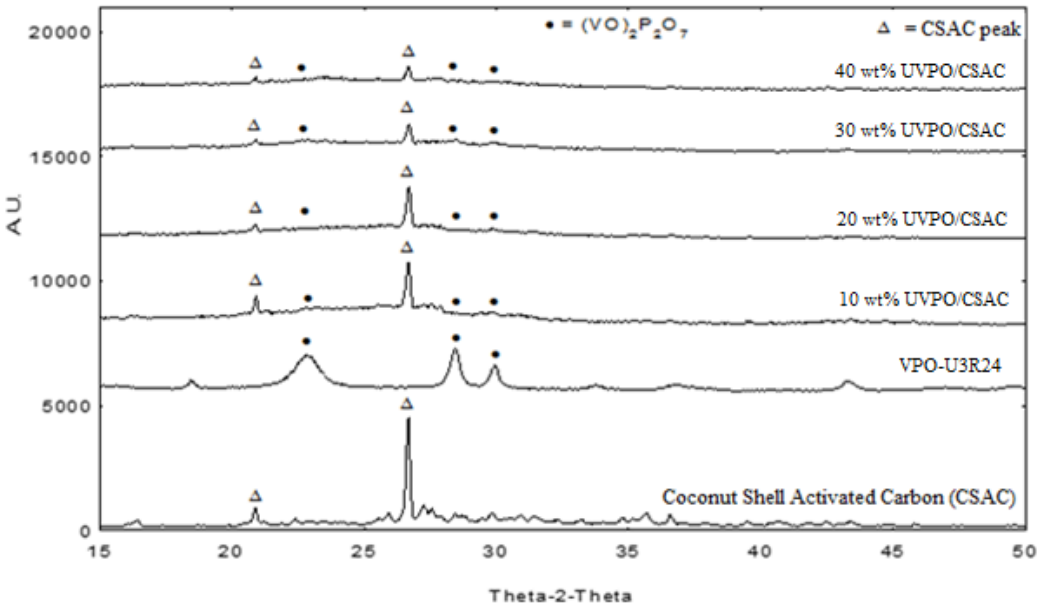

Figure 4.8: XRD profile of the catalysts synthesised via varying the weight percentages of ultrasound irradiated VPO loading on CSAC

Table 4.9: XRD data of the catalysts synthesised by varying the weight percentages of VPO and ultrasound irradiated VPO loading on CSAC

Catalyst	Line width [a] (0 2 0) / °	Line width [b] (2 0 4) / °	Crystallite size [c] (0 2 0) / Å	Crystallite size [c] (2 0 4) / Å
VPO-90B60E	1.2819	0.6386	62.5031	126.8725
10 wt% VPO/CSAC	1.2936	0.6112	61.9401	132.5455
20 wt% VPO/CSAC	1.3198	0.6266	60.7099	129.2822
30 wt% VPO/CSAC	1.3344	0.6465	60.0432	125.3154
40 wt% VPO/CSAC	1.3524	0.6579	59.2417	123.1448
VPO-U3R24	1.4543	0.6319	55.0878	128.1958
10 wt% UVPO/CSAC	1.4865	0.6625	53.8955	122.2798
20 wt% UVPO/CSAC	1.5241	0.6798	52.5696	119.1622
30 wt% UVPO/CSAC	1.5667	0.6934	51.1366	116.8327
40 wt% UVPO/CSAC	1.5967	0.6996	50.1794	115.7922

[a] FWHM of (0 2 0) reflection
[b] FWHM of (2 0 4) reflection
[c] Crystallite size calculated using Debye Scherrer equation

4.3.2 Scanning Electron Microscopy (SEM) Analysis

The surface morphologies of bare coconut shell activated carbon (CSAC) is shown in Figure 4.9 (a) which exist as stone like clusters made up of irregular shape and different sizes of crystals. These irregular shape crystals were stacked up in layers when observed under higher magnification (Figure 4.9 (a) (ii)). SEM images of VPO supported on CSAC and ultrasound irradiated VPO supported on CSAC were shown in Figure 4.10 (a) (i) - (d) (ii) and Figure 4.11 (a) (i) - (d) (ii), respectively.

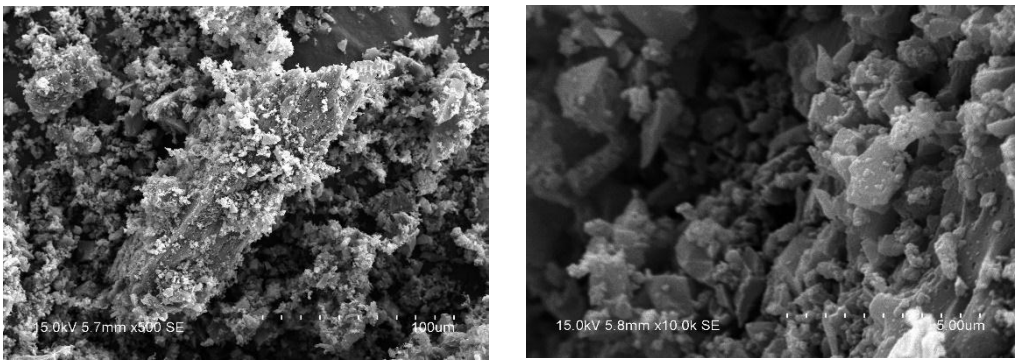

(a) (i) (ii)

Figure 4.9: SEM micrograph for CSAC: (a) (i) x 500, (ii) x 10000

The micrographs obtained for variable loading of VPO catalyst supported on CSAC and ultrasound irradiated VPO catalyst supported on CSAC showed the active component fairly dispersed on the surface of CSAC (APPENDIX G). Tiny leaf like structures were observed at 10 wt% VPO loading from (Figure 4.10 (a) (ii)). These leaf like structure became more prominent at higher loading, i.e. 30 wt% VPO/CSAC and 40 wt% VPO/CSAC. Based on the obtained results, higher loadings of VPO were believed to form agglomerated structures which stacked together.

Similar surface morphologies were observed for the ultrasound irradiated VPO catalyst supported on CSAC at higher magnifications. Ultrasonication flatten the crystal edges, which preferentially exposed the (1 0 0) crystal lattice and formed layered leaf like structures, which contributed to the enhanced surface area and catalytic activity (Suslick et al., 1999; Chen and Munson, 2002). The exposed crystal edges were observed for 40 wt% UVPO/CSAC, where the SEM images showed crystallite consisting of many layers of platelets.

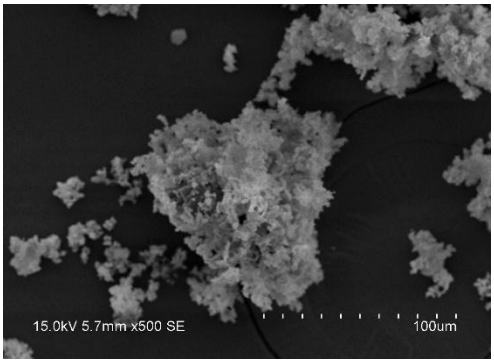

(a) (i)

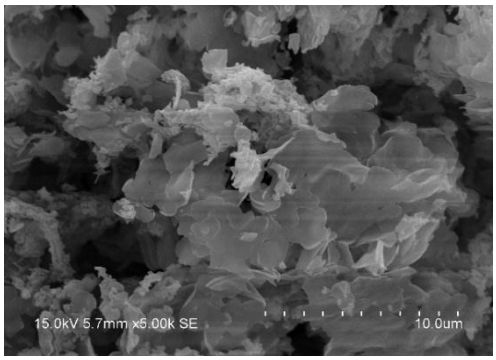

(a) (ii)

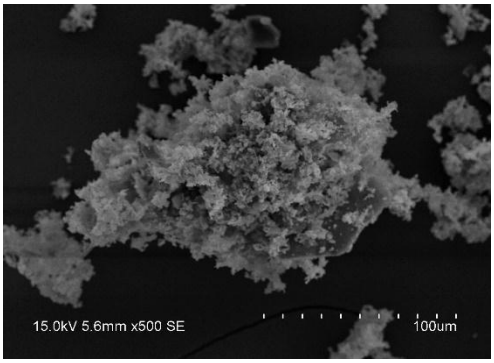

(b) (i)

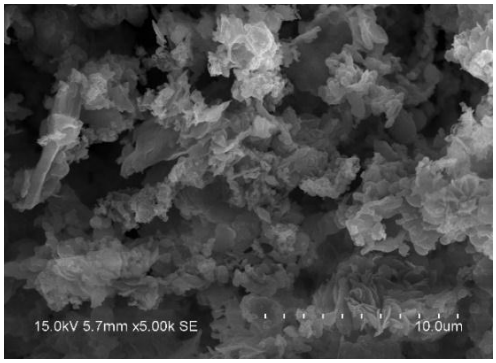

(b) (ii)

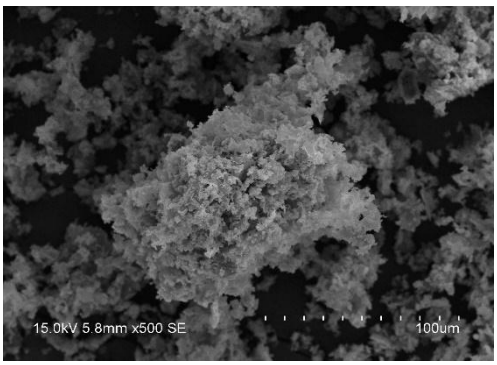

(c) (i)

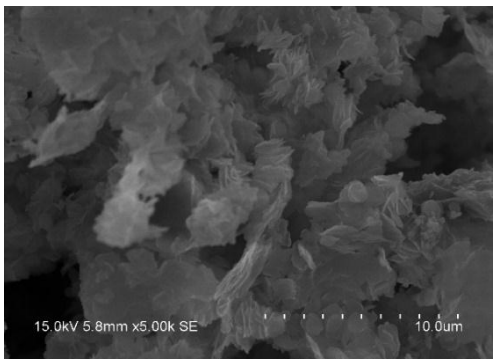

(c) (ii)

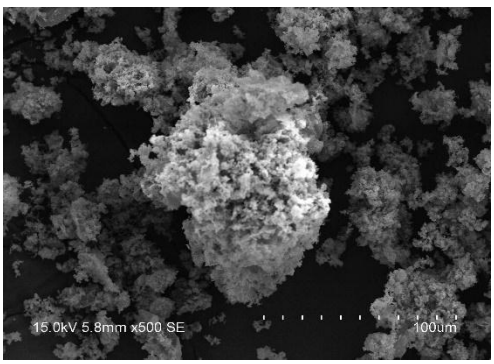

(d) (i)

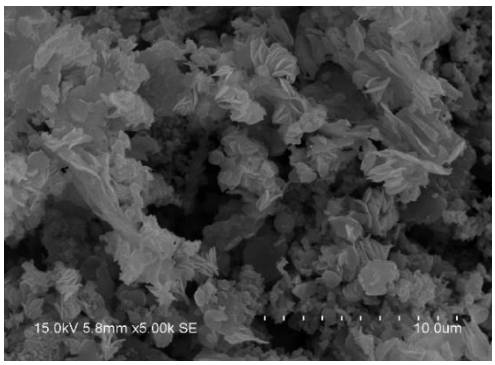

(d) (ii)

Figure 4.10: SEM micrograph for (a) 10 wt% VPO/CSAC: (i) x 500, (ii) x 5000, (b) 20 wt% VPO/CSAC: (i) x 500, (ii) x 5000, (c) 30 wt% VPO/CSAC: (i) x 500, (ii) x 5000, (d) 40 wt% VPO/CSAC: (i) x 500, (ii) x 5000

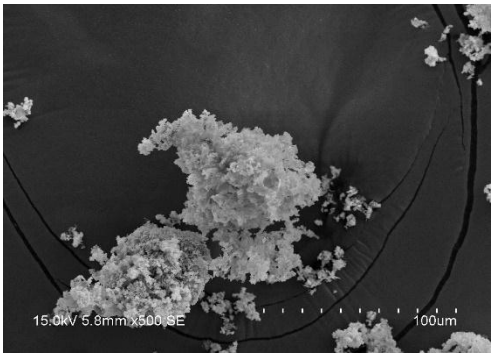

(a) (i)

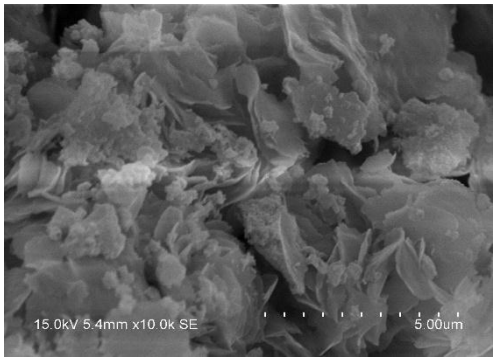

(a) (ii)

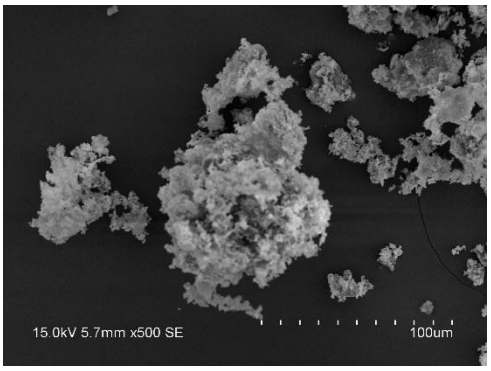

(b) (i)

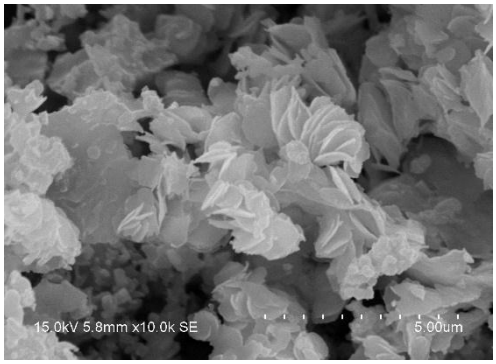

(b) (ii)

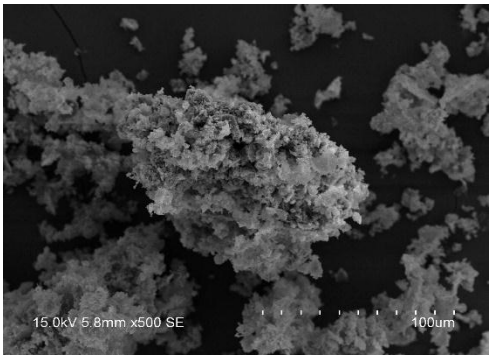

(c) (i)

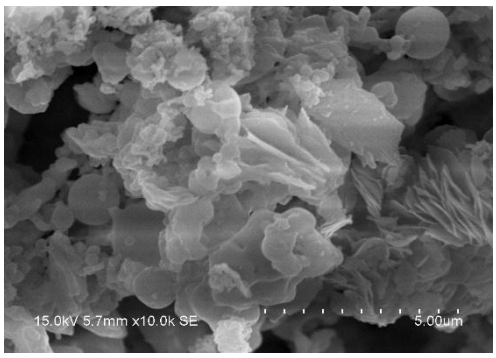

(c) (ii)

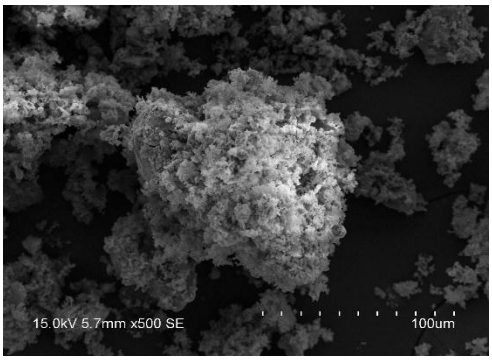

(d) (i)

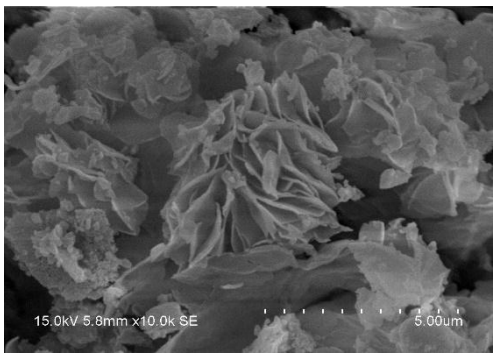

(d) (ii)

Figure 4.11: SEM micrograph for (a) 10 wt% UVPO/CSAC: (i) x 500, (ii) x 10000, (b) 20 wt% UVPO/CSAC: (i) x 500, (ii) x 10000, (c) 30 wt% UVPO/CSAC: (i) x 500, (ii) x 10000, (d) 40 wt% UVPO/CSAC: (i) x 500, (ii) x 10000

4.3.3 Brunauer-Emmett-Teller (BET) Surface Area Measurement and Chemical Analyses

Surface area and chemical composition of VPO supported on CSAC and ultrasound irradiated VPO supported on CSAC are shown in Table 4.10. Coconut shell activated carbon (CSAC) exhibited exceptionally high surface area (811.65 $m^2 g^{-1}$) mainly due to its greater volume of micropores. As the VPO loading was increased from 10 wt% to 40 wt%, the surface area of the supported catalyst decreased to 85 $m^2 g^{-1}$. Similar trend was observed when the loading of ultrasound irradiated VPO catalyst was increased from 10 wt% to 40 wt%. However, 40 wt% UVPO/CSAC gave a higher surface area (98.51 $m^2 g^{-1}$) as compared to the VPO supported on CSAC.

On higher loading samples, most of the CSAC pores were covered by the VPO component around the pore mouth, resulting in those pores no longer accessible for nitrogen adsorption and consequently decreasing the specific surface area. Thus, presumably the VPO species were well dispersed on the support surface (Overbeek et al., 1996a; Nie et al., 2001; Nie et al., 2003). Ultrasound irradiated catalyst exhibited smaller size of VPO crystal platelets as compared to the VPO catalyst supported on CSAC. Hence, the dispersion of these smaller particles on the surface of the support created more active sites (V^{4+} phase). As a result, the active sites must be further apart owing to the lower surface density which reduces the formation of long chain branching. This in return reduces the stacking of particles which leads to its higher surface area (Nie et al., 2003; Wong and Taufiq Yap, 2011).

Table 4.10: Surface area and chemical compositions of the catalysts synthesised by varying the weight percentages of VPO and ultrasound irradiated VPO on CSAC

Catalyst	BET Surface Area (m^2 g^{-1})	EDX	ICP	V_{AV}	V^{4+} (%)	V^{5+} (%)
CSAC	811.65	-	-	-	-	-
VPO-90B60E	29.02	1.05	1.04	4.135	86.47	13.53
10 wt% VPO/CSAC	409.99	1.08	1.05	4.343	65.68	34.32
20 wt% VPO/CSAC	305.62	1.11	1.06	4.282	71.78	28.22
30 wt% VPO/CSAC	121.84	1.16	1.11	4.218	78.21	21.79
40 wt% VPO/CSAC	85.00	1.20	1.16	4.195	80.50	19.50
VPO-U3R24	39.15	1.04	1.03	4.111	88.89	11.11
10 wt% UVPO/CSAC	425.34	1.06	1.04	4.166	83.41	16.59
20 wt% UVPO/CSAC	315.73	1.09	1.07	4.146	85.42	14.58
30 wt% UVPO/CSAC	142.20	1.14	1.12	4.127	87.25	12.75
40 wt% UVPO/CSAC	98.51	1.19	1.16	4.114	88.59	11.41

V_{AV} Average oxidation state of vanadium

As VPO loading was increased from 10 wt% to 40 wt%, P/V atomic ratio obtained via EDX analysis for the VPO supported catalyst and ultrasound irradiated VPO supported catalyst increased from 1.08 to 1.20 and 1.06 to 1.19, respectively. ICP analysis showed an increment from 1.05 to 1.16 and 1.04 to 1.16. Since vanadium (V) and phosphorus (P) signals were detected in all cases, it has reflected that the active phase was well dispersed on the surface of the support (Feng et al., 2007; Frey et al., 2009).

The degree of surface phosphorus enrichment became more pronounced on higher VPO loading, i.e. 40 wt% VPO/CSAC and 40 wt% UVPO/CSAC. This could be realised at the expense of CSAC support, by forming phosphorus-carbon (P-C) bond. Despite the increase in P/V atomic ratio as the VPO loading was increased from 10 wt% to 40 wt%, the synthesised catalysts showed good agreement with the optimal P/V atomic ratio suggested by Bordes (1993) and Centi (1993), i.e. 1.0 - 1.2.

The average oxidation state of vanadium (V_{AV}) both the VPO and ultrasound irradiated VPO supported catalysts decreased as the VPO loadings were increased from 10 wt% to 40 wt%. At low VPO loadings, the stronger CSAC-VPO interaction hindered the formation of crystalline $(VO)_2P_2O_7$ phase, and favoured the formation of amorphous V^{5+} phase (Nie et al., 2001, Li et al., 2006b). As the VPO loading was increased from 10 wt% to 40 wt%, V_{AV} decreased closer to 4.00 indicating stronger phosphorus-carbon bond was formed, which prevented the oxidation of V^{4+} phase to V^{5+} phase. Higher percentage of V^{4+} was observed as the VPO loading and ultrasound irradiated VPO loading was increased from 10 wt% to 40 wt%.

4.3.4 Temperature Programmed Reduction (TPR) Analysis

TPR profile of the catalyst obtained by varying the VPO loading and ultrasound irradiated VPO loading on coconut shell activated carbon (CSAC) are shown in Figure 4.12 and Figure 4.13, respectively. Peaks maximum temperature, total amount of oxygen atoms removed, reduction activation energies, ratio of V^{4+} to V^{5+} oxygen species and ratio of V^{5+} to V^{4+} oxygen species removed are shown in Table 4.11 and Table 4.12, respectively. All catalysts gave two reduction peaks, where the first peak corresponded to the removal of V^{5+}-O^{2-} oxygen species, while second peak corresponded to the removal of V^{4+}-O^{-} oxygen species (Abon et al., 2001).

As the VPO loading was increased from 10 wt% to 40 wt%, the total amount of oxygen species removed increased from 5.189 x 10^{20} atom g^{-1} to 9.383 x 10^{20} atom g^{-1}, respectively. Similar trend was observed when ultrasound irradiated catalyst loading was increased from 10 wt% to 40 wt%. The total amount of oxygen species removed increased from 4.640 x 10^{20} atom g^{-1} to 1.230 x 10^{21} atom g^{-1}, respectively. Although all these catalysts showed lower amount of oxygen species removed as compared to its respective unsupported counterpart, the ratio of V^{4+} to V^{5+} oxygen species removed were higher. Higher amount of V^{4+}-O^{-} oxygen species removed suggested that the VPO catalyst supported on CSAC would tend to exhibit higher activity.

As the VPO loading was increased from 10 wt% to 40 wt%, the reduction activation energy for V^{4+} associated peak increased, resulting in the catalyst to exhibit higher reduction activation energy (Figure 4.12). Studies by Baldychev et al., (2010) showed that lower reducibility of a supported catalyst was due its stronger interaction with the catalyst support's surface. The interaction of the VPO species and the CSAC surface resulted in the sharing of oxygen atom between the surface of vanadium (V) and CSAC. The stability of O^- oxygen species was enhanced, as more energy required to break the additional bond formed. Higher loading of VPO on CSAC also tends to form agglomerated structure, decreasing the mobility of O^- oxygen species.

The reduction activation energy for V^{4+}-O^- and V^{5+}-O^{2-} oxygen species decreased as the ultrasound irradiated catalyst loading was increased from 10 wt% to 40 wt% (Figure 4.13). Oxygen species removed from the ultrasound irradiated VPO supported on CSAC were more mobile and were removed easily. As the ultrasound irradiated VPO loading was increased from 10 wt% to 40 wt%, the leaf like platelet formed layered structure and reduced its contact with the CSAC surface. Hence, lower reduction activation energy were obtained. The nature of the interaction between the VPO species and the catalyst support system varied with VPO loading and likewise affected the reduction behaviour of the lattice oxygen. This was in agreement with the findings obtained for other catalyst supports (Overbeek et al., 1996; Nie et al., 2001; Li et al., 2006; Feng et al., 2007).

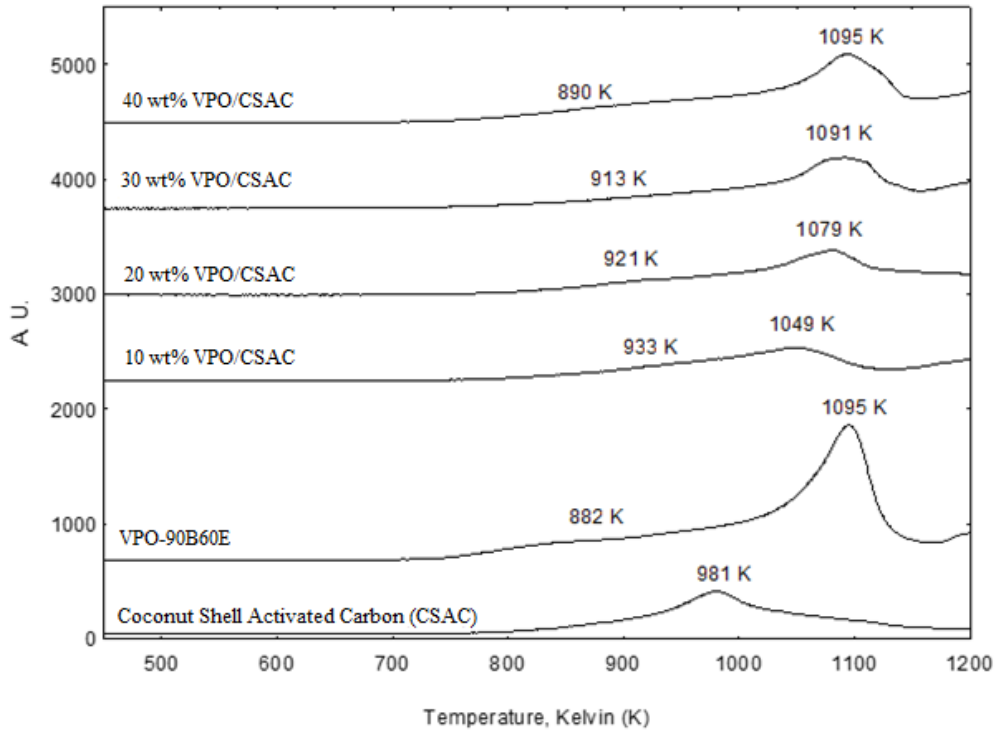

Figure 4.12: TPR profile of the catalysts synthesised via varying the weight percentages of VPO loading on CSAC

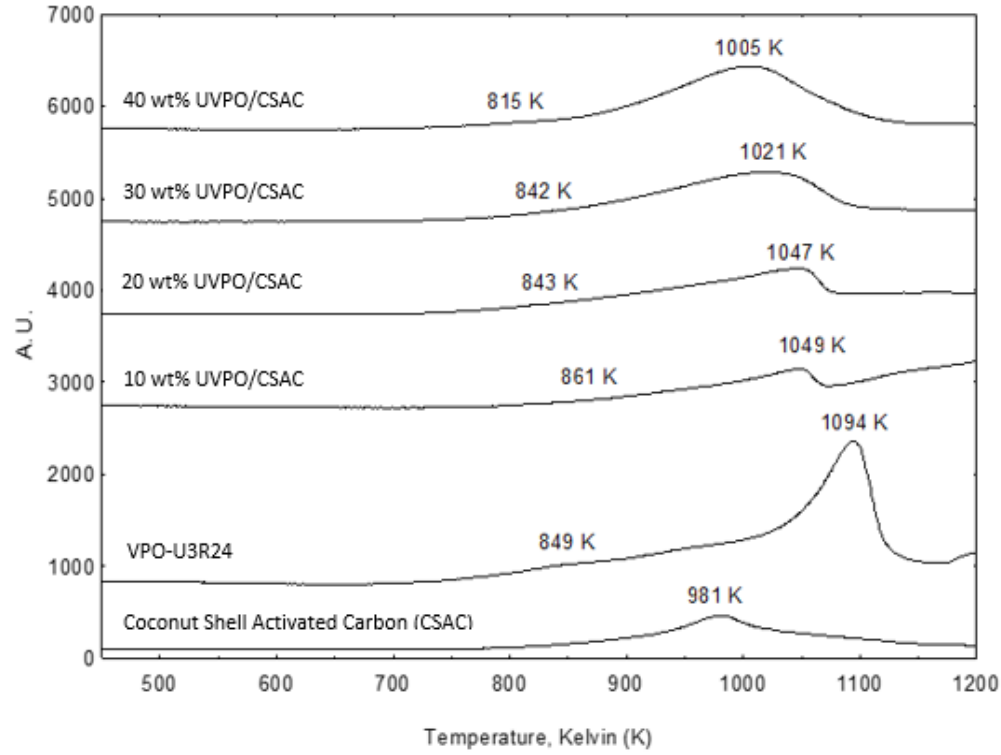

Figure 4.13: TPR profile of the catalysts synthesised by varying the weight percentages of ultrasound irradiated VPO loading on CSAC

Table 4.11: Reactivity analysis of the catalysts synthesised by varying the weight percentages of VPO loading on CSAC

Catalyst	Peak	T (^{o}C)	T_m (K)	Reduction Activation Energy, E_r (KJ mol^{-1})	Amount Oxygen Removed (mol g^{-1})	Amount Oxygen Removed (atom g^{-1})	Ratio for Oxygen Removal of V^{4+}/V^{5+}	Ratio for Oxygen Removal of V^{5+}/V^{4+}
VPO-90B60E	1	609	882	135.603	3.910×10^{-4}	2.353×10^{20}	5.43	0.18
	2	822	1095	168.350	2.124×10^{-3}	1.279×10^{21}		
	Total amount of oxygen removed				2.514×10^{-3}	1.513×10^{21}		
10 wt% VPO/CSAC	1	660	933	143.444	2.060×10^{-4}	1.242×10^{20}	3.18	0.31
	2	776	1049	161.278	6.560×10^{-4}	3.948×10^{20}		
	Total amount of oxygen removed				8.620×10^{-4}	5.189×10^{20}		
20 wt% VPO/CSAC	1	648	921	141.599	2.190×10^{-4}	1.321×10^{20}	4.05	0.25
	2	806	1079	165.890	8.880×10^{-4}	5.347×10^{20}		
	Total amount of oxygen removed				1.117×10^{-3}	6.668×10^{20}		
30 wt% VPO/CSAC	1	640	913	140.369	2.230×10^{-4}	1.341×10^{20}	4.27	0.23
	2	818	1091	167.735	9.510×10^{-4}	5.725×10^{20}		
	Total amount of oxygen removed				1.174×10^{-3}	7.067×10^{20}		
40 wt% VPO/CSAC	3	617	890	136.833	2.360×10^{-4}	1.421×10^{20}	5.60	0.18
	4	822	1095	168.350	1.323×10^{-3}	7.962×10^{20}		
	Total amount of oxygen removed				1.569×10^{-3}	9.383×10^{20}		

Table 4.12: Reactivity analysis of the catalysts synthesised by varying the weight percentages of ultrasound irradiated VPO loading on CSAC

Catalyst	Peak	T (^{o}C)	T_m (K)	Reduction Activation Energy, E_r (KJ mol^{-1})	Amount Oxygen Removed (mol g^{-1})	Amount Oxygen Removed (atom g^{-1})	Ratio for Oxygen Removal of V^{4+}/V^{5+}	Ratio for Oxygen Removal of V^{5+}/V^{4+}
VPO-U3R24	1	576	849	130.529	3.510×10^{-4}	2.114×10^{20}	7.46	0.13
	2	821	1094	168.196	2.618×10^{-3}	1.576×10^{21}		
	Total amount of oxygen removed				2.969×10^{-3}	1.787×10^{21}		
10 wt% UVPO/CSAC	1	588	861	132.374	7.956×10^{-5}	4.784×10^{19}	8.70	0.11
	2	776	1049	161.278	6.920×10^{-4}	4.163×10^{20}		
	Total amount of oxygen removed				7.710×10^{-4}	4.640×10^{20}		
20 wt% UVPO/CSAC	1	570	843	129.607	1.410×10^{-4}	8.488×10^{19}	9.04	0.11
	2	774	1047	160.970	1.276×10^{-3}	7.669×10^{20}		
	Total amount of oxygen removed				1.416×10^{-3}	8.520×10^{20}		
30 wt% UVPO/CSAC	1	569	842	129.453	1.790×10^{-4}	1.080×10^{20}	9.24	0.11
	2	748	1021	156.973	1.666×10^{-3}	9.979×10^{20}		
	Total amount of oxygen removed				1.846×10^{-3}	1.110×10^{21}		
40 wt% UVPO/CSAC	3	542	815	125.302	1.940×10^{-4}	1.169×10^{20}	9.52	0.11
	4	732	1005	154.513	1.856×10^{-3}	1.112×10^{21}		
	Total amount of oxygen removed				2.046×10^{-3}	1.230×10^{21}		

4.3.5 *n*-Butane Oxidation to Maleic Anhydride

Catalytic performance of *n*-butane oxidation to maleic anhydride (Table 4.13) were analysed at 673 K (GSHV = 2400 h^{-1}), a typical reaction temperature for VPO catalyst (Leong et al., 2011).

Table 4.13: Catalytic performance of the catalysts synthesised by varying the weight percentages of VPO and ultrasound irradiated VPO loading on CSAC

Catalyst	*n*-butane conversion (%)	Product selectivity (%)		
		MA	CO_2	CO
VPO-90B603	30	86	13	1
10 wt% VPO/CSAC	31	83	16	1
20 wt% VPO/CSAC	32	85	14	1
30 wt% VPO/CSAC	34	87	12	1
40 wt% VPO/CSAC	36	88	11	1
VPO-U3R24	39	89	10	1
10 wt% UVPO/CSAC	40	90	9	1
20 wt% UVPO/CSAC	42	91	8	1
30 wt% UVPO/CSAC	45	92	7	1
40 wt% UVPO/CSAC	50	93	6	1

Based on the results obtained, an improved *n*-butane conversion was observed for catalyst with higher VPO loading. The highest conversion exhibited by the VPO supported on CSAC was 36%, while the highest conversion exhibited by ultrasound irradiated catalyst supported on CSAC was 50%. Small increase in the MA selectivity was observed as the VPO loading was increased in both VPO supported CSAC catalysts.

The increase in *n*-butane conversion at higher VPO loading can be related to its higher number of active sites (V^{4+} phase). All the ultrasound irradiated VPO supported on CSAC showed higher conversion as compared to the VPO supported on CSAC. The agglomeration of the leaf like structures for the VPO on higher CSAC loading could have reduced the mobility of V^{4+}-O^- oxygen species as the bulkier structure preferentially shared the oxygen atom with the surface of the support and decreased the reducibility of the O^- oxygen species (Baldychev et al., 2010). As for the ultrasound irradiated catalyst, the layered structures formed preferentially exposed (1 0 0) plane, which increased the reducibility of O^- oxygen species (Suslick et al., 1999; Chen and Munson, 2002). The removal of more O^- oxygen species could enhance the catalytic activity as V^{4+}-O^- acts as a centre for *n*-butane activation (Rownaghi et al., 2010).

Maleic anhydride (MA) selectivity increased with increasing VPO loading. At low VPO loading, the support surface are not fully covered by VPO, hence responsible for the higher percentage of carbon dioxide (CO_2) formed (Li et al., 2006; Feng et al., 2007). As the VPO loading was increased the additional active phase covered the CSAC pores and the resulted an increment in the yield of MA. Studies done by Bordes (1993) showed that minute V^{5+} phase present in the catalyst were sufficient to produce high selectivity towards MA.

4.3.6 Series Findings

Two series of VPO catalyst supported on coconut shell activated carbon (CSAC) were successfully synthesised implementing incipient wetness impregnation method. As the percentages of VPO loading on CSAC was increased from 10 wt% to 40 wt%, the supported catalysts showed improved catalytic properties. It exhibited higher amount of active sites and greater ratio of V^{4+} to V^{5+} oxygen species removed, hence contributing to its higher activity.

Similar trend was observed for ultrasound irradiated VPO supported on CSAC as the VPO loading was increased from 10 wt% to 40 wt%. However, due to the ultrasonication effect, the ultrasound irradiated VPO supported catalyst exhibited better catalytic properties as compared to its counterpart. It exhibited layered leaf like structure which contributed to its higher surface area and lower reduction activation energy. Hence, higher amount of lattice oxygen associated with V^{4+}-O^{-} oxygen species were more easily removed.

Generally as the VPO loading was increased from 10 wt% to 40 wt%, the supported catalyst exhibited overall improved catalytic properties. Based on the range of catalysts analysed within these series, 40 wt% VPO loading exhibited better physico-chemical, reactivity and catalytic performance, as compared to those lower percentage VPO supported on activated carbon catalyst support. By comparison to 40 wt% VPO/CSAC, 40 wt% UVPO/CSAC showed higher *n*-butane conversion (50%) and product selectivity to maleic anhydride (93%).

CHAPTER FIVE

CONCLUSION

This research involved four series of VPO catalysts, where the first and second series studied the effect of preparation methodology of the catalysts. This was achieved by varying the volume combination of reducing agents and varying ultrasound irradiation duration in synthesising the dihydrate precursor. Third and fourth series focused on the effect of catalyst support in enhancing the catalytic performances of the synthesised catalyst. Various weight percentage of VPO loadings supported on CSAC were synthesised and analysed.

Six catalysts were synthesised with variable volume combinations of 1-butanol and ethanol as reducing agents in the first series. Increasing the volume of ethanol from 0 ml to 60 ml, resulted in the synthesised catalyst to exhibit enhanced physical properties such as smaller crystallite size particles and layered structure which are responsible for the higher surface area exhibited by the catalysts. Its chemical property, such as P/V atomic ratio were in good agreement with the optimal P/V atomic ratio suggested by Bordes (1993) and Centi (1993), while its chemical composition showed the presence of more V^{4+} phases, which are vital for the enhancement of catalytic activity. From the reactivity analysis, more V^{4+}-O^{-} oxygen species were removed as the oxygen species were more mobile, as a result increasing the catalyst activity as observed from the catalytic performance of *n*-butane oxidation to maleic anhydride.

Further increasing the volume of ethanol from 90 ml to 150 ml, culminated the catalyst in exhibiting impoverished physico-chemical properties. Higher ratio of weaker reducing agents oxidised the desired V^{4+} phases to the development of deleterious V^{5+} phase (β-$VOPO_4$) that stacked together and lowered the surface area of the catalyst. Smaller surface area resulted the catalyst with higher surface density as the active sites are concentrated which in return formed agglomerated structures and reduced the mobility of the V^{4+}-O^- oxygen species. As a result, the catalytic conversion decreased with when the volume of ethanol was increased further from 90 ml to 150 ml. Among the synthesised VPO catalysts, 90 ml of 1-butanol and 60 ml of ethanol was determined as the optimal volume combination of reducing agents within the range of studies conducted in this series as it exhibited highest surface area 29.02 $m^2\ g^{-1}$ and highest V^{4+}-O^- oxygen species (1.278×10^{21} atom g^{-1}) removed, which accounted for its highest activity (30%) and selectivity (86%).

Based on the outcome of the second series, as the duration of ultrasound irradiation was increased from one hour to three hours, the synthesised ultrasound irradiated VPO catalysts exhibited improved catalytic properties. Collapse of more transient bubbles as the ultrasound duration was prolonged induced high velocity interparticle collision and produced smaller crystallites which accounted for its higher surface area compared to the catalyst synthesised via conventional reflux method. Ultrasound irradiation also produced high purity VPO catalysts consisting predominantly V^{4+} phase, which was in agreement with the Redox analysis as all the ultrasound irradiated catalysts

showed more than 80% presence of V^{4+} phase. Prolonged ultrasonication reduced the activation temperature at which the oxygen species (V^{4+}-O^{-}) was removed as the fragmentation of the solid produced more labile oxygen species. Highest conversion and selectivity obtained in this series are 39% and 89%, respectively. Hence, three hours of ultrasound irradiation in synthesising the dihydrate precursor resulted in the activated catalyst to exhibit superior physico-chemical, reactivity and catalytic performances.

Coconut shell activated carbon's large pore volume dispersed the active sites of VPO catalyst and produced supported catalyst with improved properties as compared to the unsupported catalyst. The production cost of VPO catalysts are also reduced with the usage of CSAC as lower weight percentage of VPO supported on the catalyst support yields better catalytic performance as compared to the VPO catalyst itself. As the percentage of VPO loading was increased from 10 wt% to 40 wt%, the catalysts showed an improved catalytic properties as more dispersed active phase was available to catalyse the reaction. Ultrasound irradiated VPO supported on CSAC exhibited an enhanced catalytic properties as compared to the corresponding VPO supported on CSAC due to the lower reduction activation temperature at which the desired V^{4+}-O^{-} oxygen species was removed. The highest conversion and selectivity obtained in this research from 40%UVPO/CSAC were 50% and 93%, respectively, which is 15% lower in conversion but 11% higher in selectivity compared to the catalyst synthesised in the industry.

In conclusion, the research aims were achieved as VPO catalysts were synthesised using more environmental friendly reducing agents (1-butanol and ethanol) where the optimum volume combination were determined as 90 ml 1-butanol and 60 ml ethanol. The synthesis duration of dihydrate precursor was shorten to less than three hours implying ultrasound irradiation as compared to the conventional 24 hours methodology. The physico-chemical, reactivity and catalytic performances were improved utilising CSAC as support with 40%UVPO/CSAC yielding the highest improvements.

REFERENCES

Abon, M. et al., 1995. Evolution of a VPO catalyst in *n*-butane oxidation reaction during the activation time. *Journal of Catalysis*, 156, pp. 28 – 36.

Abon, M., Herrmann, J. M. and Volta, J. C., 2001. Correlation with the redox V^{5+} /V^{4+} ratio in vanadium phosphorus oxide catalysts for mild oxidation of *n*-butane to maleic anhydride. *Catalysis Today*, 71(1–2), pp. 121 – 128.

Agaskar, P. A., DeCaul, L., and Grasselli, R. K., 1993. A molecular level mechanism of *n*-butane oxidation to maleic anhydride over vanadyl pyrophosphate. *Catalysis Letter*, 23 (3–4), pp. 339 – 351.

Albonetti, S. et al., 1996. A comparison of the reactivity of "nonequilibrated" and "equilibrated" VPO catalysts: structural evolution, surface characterisation, and reactivity in the selective oxidation of *n*-butane and *n*-pentane. *Journal of Catalysis*, 160, pp. 52 – 64.

Baldychev, I., Vohs, J. M. and Gorte, R. J., 2010. The impact of redox properties on the reactivity of V_2O_5/Al_2O_3 catalyst. *Journal of Catalysis*, 269(2), pp. 397 – 403.

Bartley, J. K., Kiely, C. J. Wells, P. K. and Hutchings, G. J., 2001. Vanadium (v) phosphate prepared using solvent free method. *Catalysis Letters*, 72(1-2), pp. 99 – 105.

BASF., 2013. *Economic, Environmental and Social Performance* [Online]. Available at: http://www.basf.com/group/corporate/en/function/conversions:/publish/content/about-basf/facts-reports/reports/2013/BASF_Report_2013.pdf [Accessed: 11st February 2014].

Batis, N. H., Batis, H., Ghorbel, A., Vedrine, J. C. and Volta, J. C., 1991. Synthesis and characterisation of new VPO catalysts for partial *n*-butane oxidation to maleic anhydride. *Journal of Catalysis*, 128(1), pp. 248 – 263.

Benes, L., Melanova, K., Zima, V., Kalousova, J. and Votinsky, J., 1997. *Inorg. Chem*., 36, pp. 2850 – 2854.

Bergeret, G., David, M., Broyer, J. P., Volta, J. C. and Hecquer, G., 1987. A contribution to the knowledge of the active sites of VPO catalysts for *n*-butane oxidation to maleic anhydride. *Catalysis Today*, 1(1), pp. 37 – 47.

Berzelius, J. J, 1836. Copal varnish. *Journal of Franklin Institute*, 10(1). pp. 146 – 151.

Birkeland K. E., Babitz, S. M., Bethke, G. K. and Kung, H. H., 1997. Supported VPO catalyst for selective oxidation of *n*-butane. *Journal of Physical Chemistry*, 101, pp. 6895 – 6902.

Bordes, E., Courtine, P. and Johnson, J. W., 1984. On the topotactic dehydration of $VOHPO_4 \cdot 0.5H_2O$ into vanadyl pyrophosphate. *Journal of Solid State Chemistry*, 55(3), pp. 270 – 279.

Bordes, E., 1987. Crystallochemistry of VPO phases and application to catalysis. *Catalysis Today*, 1(5), pp. 499 – 526.

Bordes, E., 1993. Nature of the active and selective sites in vanadyl pyrophosphate catalyst oxidation of *n*-butane, butene and pentane to maleic anhydride. *Catalysis Today*, 16(1), pp. 27 – 38.

Brutovsky, M., Kladekova, D., Reiffova, K. and Kosturiak, A., 1997. Vanadium phosphorus catalysts modified with magnesium, calcium and barium. *Collection of Czechoslovak Chemical Communications*, 62(3), pp. 392 – 396.

Busca, G., Cavani, F., Centi, G. and Trifiro, F., 1986. Nature and mechanism of formation of vanadyl pyrophosphate: active phase in *n*-butane selective oxidation. *Journal of Catalysis*, 99(2), pp. 400 – 414.

Cavani, F. and Trifiro, F., 1994. Catalysing butane oxidation to make maleic anhydride. *Chemtech*, 25(34), pp. 18 – 25.

Centi, G., Trifiro, F., Ebner, J. R. and Franchetti, V. M., 1988. Mechanistic aspects of maleic anhydride synthesis from C4 hydrocarbons over phosphorus vanadium oxide. *Chemical Reviews*, 88(1), pp. 55 – 80.

Centi, G., 1993. Vanadyl pyrophosphate – A critical overview. *Catalysis Today*, 24(16), pp. 5 – 26.

Chali, W. and Yakub, I., 2013. The performance of coconut shell based activated carbon in treating drinking water. *Journal of Civil Engineering*, 4(3), pp. 1 – 6.

Chen, B. and Munson, E. J., 2002. Investigation of the mechanism of *n*-butane oxidation on vanadium phosphorus oxide catalysts: evidence from isotopic labelling studies. *Journal of the American Chemical Society*, 124(8), pp. 1638 – 1652.

Cheng, W. H., 1996. Effect of composition of promoted VPO catalyst on selectivity oxidation of *n*-butane to maleic anhydride. *Applied Catalysis A: General*, 147(1), pp. 55 – 57.

Cheng, W. and Wang, W., 1997. Effect of calcination environment on the selective oxidation of *n*-butane to maleic anhydride over promoted and unpromoted VPO catalyst. *Applied Catalysis A: General*, 156(1), pp. 57 – 69.

Clark, J., 2012. *Types of catalysis* [Online]. Available at: http://www.chemguide.co.uk/physical/catalysis/introduction.html [Accessed: 1st February 2014]

Connor, M. O., Dason, F. and Hodnett, B. K., 1990. Preparation of vanadium phosphorus oxide catalyst: Influence of macroscopic P:V ratio in determining phase composition after calcination. *Applied Catalysis*, 64(12), pp. 161 – 171.

Cornagalia, L. M., Carrare, C., Petunchi, J. O. and Lombardo, E. A., 1999. The role of cobalt as promoter of equilibrated vanadium phosphorus oxygen catalysts. *Applied catalysis A: General*, 183(1), pp. 177 – 187.

Cornagalia, L. M. et al., 2000. Characterisation of cobalt impregnated VPO Catalysts. *Catalysis Today*, 57, pp. 313 – 322.

Cornagalia, L., Irusta, S., Lombardo, E. A., Durupty, M. C. and Volta, J. C., 2003. The beneficial effect of cobalt on VPO catalysts. *Catalysis Today*, 78(1), pp. 291 – 301.

Datta, A., Agarwal, M. and Dasgupta, S., 2002. Novel vanadium phosphate phases as catalyst for selective oxidation. *Proc. Indian Acad. Sci*., 114(4), pp. 379 – 390.

Dutta, A., 2005. *Selective oxidation of hydrocarbons using vanadium phosphates*, 1st ed. New Delhi: Narosa Publishing House.

Ellison, I. J., Hutchings, G. J., Sananes, M. T. and Volta J. C., 1994. *Journal of Chemical Society*, pp. 1093.

Ensminger, D. and Bond, L. J., 2012. *Ultrasonic: Fundamentals, Technologies and Applications.* 3rd Ed. London: CRC Press.

Fadhel, A., Pollet, P., Liotta, C. L., and Erkert, C. A., 2010. Combining the benefits of homogeneous and heterogeneous catalysis with tunable solvents and near critical water. *Molecules,* 15, pp. 8400 – 8424.

Felthouse, T. R., Burnett, J. C., Horrell, B., Mummey, M. J. and Kuo, Y. J., 2001. *Maleic Anhydride, Maleic Acid and Fumaric Acid* [Online]. Available at: http://www.southalabama.edu/chemistry/barletta/felthouse.pdf [Accessed: 21st February 2014].

Feng, R., Yang, X., Ji, W., Chen, Y. and Au, C., 2007. VPO catalysts supported on H_3PO_4 treated ZrO_2 highly active for *n*-butane oxidation. *Journal of Catalysis*, 246(1), pp. 166 – 176.

Fernandez, R. J., Vega, A. Diez, F. V., 2010. Partial oxidation of *n*-butane to maleic anhydride over VPO in a simulated circulating fluidised bed reactor. *Applied Catalysis A: General*, 376, pp. 76 – 82.

Frey, J. et al., 2009. Vanadium phosphorus on mesopores supports: model catalyst for solid state NMR studies of the selective oxidation of *n*-butane. *Solid State Nuclear Magnetic Resonance*, 35, pp. 130 – 137.

Goh, C. K., Taufiq Yap, Y. H., Hutchings, G. J., Dummer, N. and Bartley, J., 2008. Influence of Bi - Fe additive on properties of vanadium phosphate catalysts for *n*-butane oxidation to maleic anhydride. *Catalysis Today*, 131(1), pp. 408 – 412.

Grand View Research., 2013. Maleic Anhydride Market Analysis by Application and Segments Forecasts to 2020 [Online]. Available at: http://www.grandviewresearch.com/press-release/global-maleic-anhydride-market [Accessed: 21st February 2014].

Guilhoume, M., Roullet, M., Pajonk, G., Grzybowska, B. and Volta, J. C., 1992. *New Development in Selective Oxidation by Heterogeneous Catalysis*, 1st ed. Netherlands: Elsevier.

Guliants, V. V., Benziger, J. B., Sundaresan, S. and Yao, N., 1995. Evolution of the active surface of the vanadyl pyrophosphate catalyst. *Catalyst Letter*, 32, pp. 379 – 386.

Guliants, V. V. and Carreon, M. A., 2005. Vanadium-Phosphorus-Oxides: fundamentals of *n*-Butane oxidation to synthesis of new phases. *Catalysis*, 18, pp. 1 – 45.

Haber, J., 1994. Catalysis: Where science and industry meet. *Pure & Appl. Chem*., 66(8), pp. 1597 – 1620.

Haber, J., Zazhigalov, V. A., Stoch, J., Bogutskaya, L. V. and Batcherikova, I. V., 1997. Mechanochemistry: the activation method of VPO catalyst for *n*-butane partial oxidation. *Catalysis Today*, 33, pp. 39 – 47.

Harding, W. D., Birkeland, K. E. and Kung, H. H., 1994. Selective oxidation of butane on phosphorus - modified silica supported vanadia catalysts. *Catalysis Letters*, 28(1), pp. 1 – 7.

Haber, J., Block, J. H. and Delmon, B., 1995. Manual of methods and procedures for catalyst characterization. *Pure & Appl. Chem*, 67, pp. 1257 – 1306.

Hiyoshi, N., Yamamoto, N., Ryumon, N., Kamiya, Y. and Okuhara, T., 2004. Selective oxidation of *n*-butane in the presence of vanadyl pyrophosphate synthesised by intercalation exfoliation-reduction of layered $VOPO_4 \cdot 2H_2O$ in 2-butanol. *Journal of Catalysis*, 221(1), pp. 225 – 233.

Huang, W. J. and Cheng, Y. L., 2008. Effect of characteristics of activated carbon on removal of bromate. *Separation and Purification Technology*, 59, pp. 101 – 107.

Hutchings, G. J., 1991. Effect of promoters and reactant concentration on the selective oxidation of *n*-butane to maleic anhydride using vanadium phosphorus oxide catalysts. *Applied Catalysis*, 72(1), pp. 1 – 32.

Hutchings, G. J., 1993. Vanadium phosphorus oxide catalysts for the selective oxidation of *n*-butane to maleic anhydride. *Catalysis Today*, 16(1), pp. 139 – 146.

Hutchings, G. J. and Higgins, R., 1996. Effect of promoters on the selective oxidation of *n*-butane with Vanadium Phosphorus Oxide Catalysts. *Journal of Catalysis*, 162(2), pp. 153 – 168.

Hutchings, G. J. et al., 1997. Improved method of preparation of vanadium phosphate catalysts. *Catalysis Today*, 33(3), pp. 16 – 171.

Imai, H., Kamiya, Y. and Okuhara, T., 2007. Selective oxidation of *n*-butane over nanosised crystallites of $(VO)_2P_2O_7$ synthesised by an exfoliation reduction process of $VOPO_4 \cdot 2H_2O$ in a mixture of 2-butanol and ethanol. *Journal of Catalysis*, 251(1), pp. 195 – 203.

Irmawati, R. et al., 2004. Effect of calcination temperatures on physicochemical properties of vanadium - antimony mixed oxide catalysts. *Catalysis Today*, 93, pp. 631 – 637.

Ishimura, I., Sugiyama, S. and Hayashi, H., 2000. Vanadyl hydrogenphosphate sesquihydrate as a precursor for preparation of $(VO)_2P_2O_7$ and cobalt incorporated catalysts. *Journal of Molecular Catalysis*, 158(2), pp. 559 – 565.

Joensen, P., Frindt, R. F. and Morrison, S. R., 1986. Single layer MoS_2. *Materials Research Bulletin*, 21(4), pp. 457 – 461.

Johnson, J. W., Johnston, D. C., Jacobson, A. J. and Brody, J. F., 1984. Preparation and characterisation of vanadyl hydrogen phosphate hemihydrate and its topotactic transformation to vanadyl pyrophosphate. *Journal of the American Chemical Society*, 106(26), pp. 8123 – 8128.

Kamiya, Y., Nishikawa, E., Okuhara, T. and Hattori, T., 2001. Catalytic property of vanadyl pyrophosphates for selective oxidation of *n*-butane at high *n*-butane concentrations. *Applied catalysis A: General*, 206(1), pp. 103 – 112.

Kamiya, Y., Kijima, Y., Ohkura, T., Satsuma, A. and Hattori, T., 2003. Selective oxidation of *n*-butane over iron doped vanadyl pyrophosphate prepared from lamellar vanadyl *n*-hexylphosphate. *Applied Catalysis A: General*, 253, pp. 1 – 13.

Kamiya, Y., Ryumon, N., Imai, H. Okuhara, T., 2006. Nanosized crystallites of vanadyl pyrophosphate as highly selective catalyst for *n*-butane oxidation. *Catalysis Letter*, 111(3-4), pp. 159 – 163.

Keller, S. W., Kim, H. N. and Mallouk, T. E., 1994. *Chem. Soc.*, 116, pp. 8817.

Kiely, C. J. et al., 1995. Electron microscopy studies of vanadium phosphorus oxide catalysts derived from $VOPO_4 \cdot 2H_2O$. *Catalysis Letters*, 33 (3–4), pp. 357 – 368.

Kiely, C. J. et al., 1996. Characterisation of variations in vanadium phosphate catalyst microstructure with preparation route. *Journal of Catalysis*, 162(1), pp. 31 – 47.

Kleinfeld, E. R. and Furgson, G. S., 1994. *Science*, 265, pp. 370.

Klug, P. H. and Alexander, L. E., 1974. *X-ray diffraction procedures for polycrystalline and amorphous materials*. 2nd ed. New York: John Wiley & Sons.

Leong, L. K., Chin, K. S. and Taufiq Yap, Y. H., 2011. The effect of bi promoter on vanadium phosphate catalysis synthesised via sesquihydrate route. *Catalysis Today*, 164, pp. 341 – 346.

Leong, L. K., Chin, K. S. and Taufiq Yap, Y. H., 2012. Effect of varying reflux duration on the physicochemical and catalytic performance of vanadium phosphate catalyst synthesised via vanadyl hydrogen phosphate sesquihydrate. *Applied Catalysis A: General*, 415, pp. 53 – 58.

Leonowicz, M. E., Johnson, J. W., Brody, J. F., Shannon, H. F. and Newsam, J. M., 1985. Vanadyl hydrogen phosphate: $VOHPO_4 \cdot 4H_2O$ and $VOHPO_4 \cdot 0.5H_2O$. *Journal of Solid State Chemistry*, 56(3), pp. 370 – 378.

Li, X., Ji, W., Zhao, J., Zhang, Z. and Au, C., 2006b. A comparison study on the partial oxidation of *n*-butane and propane over VPO catalysts supported on SBA- 15, MCM - 41, and fumed SiO_2. *Applied Catalysis A: General*, 306, pp. 8 – 16.

Lin, M. M., 2001. Selective oxidation of propane to acrylic acid with molecular oxygen. *Applied Catalysis A: General*, 207, pp. 1 – 16.
Lopez, J. M., 2006. The selective oxidative activation of light alkanes from supported vanadia to multicomponent bulk V containing catalyst. *Topics in Catalysis*, 41, pp. 1 – 13.

Luciani, S., 2009. *Structural changes and dynamic behavior of vanadium oxide-based catalysts for gas-phase selective oxidations*. PhD Thesis. University of Bologna, Italy.

Martinez, M. L., Moiraghi, L., Agnese, M. and Guzman, C., 2003. Making and some properties of activated carbon produced from agricultural industrial residues. *The Journal of Argentine Chemical Society*, 91(4-6), pp. 103 – 108.

Mason, T. J., Paniwnyk, L. and Lorimer, J. P., 1996. The uses of ultrasound in food technology. *Ultrasonic Sonochemistry*, 3(3), pp. 253 – 260.

Mason, T.J and Tiehm, A., 2001. *Advances in Sonochemistry*. 1st ed. Netherlands: Elsevier Science.

Matsuura, I. and Yamazaki, M., 1990. *New Developments in Selective Oxidation*, 2nd ed. Netherlands: Elsevier.

Mohd. Iqbaldin, M. N. et al., 2013. Properties of coconut shell activated carbon. *Journal of Tropical Forest Science*, 25(4), pp. 497 – 503.

Nakamura, M., Kawai, K. and Fujiwara, Y., 1974. The structure and the activity of vanadyl phosphate catalysts. *Journal of Catalysis*, 34(3), pp. 345 – 355.

Nasirtabrizi, M. H., Ziaei, Z. M., Jadid, A. P. and Fatin, L. Z., 2013. Synthesis and chemical modification of maleic anhydride copolymers with phthalimide groups. *International Journal of Industrial Chemistry*, 4(1), pp. 4 – 11.

Nie, W. et al., 2001. A study on VPO specimen supported on aluminium - containing MCM-41 for partial oxidation of *n*-butane to MA. *Catalysis Letters*, 76(3-4), pp. 201 – 206.

Nie, W. Y., Wang, Z. Y., Ji, W. J. and Chen, C. T., 2003. Comparative studies on the VPO specimen supported on mesoporous Al-containing MCM-41 and large pore silica. *Applied Catalysis A: General*, 244(2), pp. 265-272.

Niwa, M. and Murakami, Y., 1982. Reaction mechanism of ammoxidation of toluene IV oxidation state of vanadium oxide and its reactivity for toluene oxidation. *Journal Catalysis*, 76, pp. 9 – 16.

Okuhara, T. and Misono, M., 1993. *Catalysis Today*, 16, pp. 61

Okuhara, T., Ryumon, N., Yamamoto, N. and Hiyoshi, N., 2002. A highly selective vanadyl pyrophosphate synthesised by exfoliation- reduction in mixed alcohols for *n*-butane oxidation. *Studies in Surface Science and Catalysis*, 145, pp. 271 – 274.

Olivares-Marin, M., Gonzalez, C. F., Garcia, A. M. Serrano, V. G., 2006. Preparation of activated carbon from cheery stones by activation with potassium hydroxide. *Applied Surface Science*, 252, pp. 5980 – 5983.

Overbeek, R. A., Pekelharing, A. R., Dillen, A. J. and Geus, J. W., 1996. Preparation, characterisation and testing of newly developed silica-supported VPO catalysts. *Applied Catalysis A: General*, 135(2), pp. 231 – 248.

Parsons, S. A. and Jefferson, B., 2006. *Activated carbon: Introduction to potable water treatment processes*, 1st ed. USA: Blackwell Publishing.

Patience, G. S. and Bockrath, R. E., 2010. Butane oxidation process development in a circulating fluidised bed. *Applied Catalysis A: General*, 376, pp. 4 – 12.

Pena-Farfal, C. et al., 2004. *Analytical Chemistry*, 549, pp. 3541 – 3547.

Pierini, B. T. and Lombardo, E. A., 2005. Structure and properties of Cr promoted VPO catalysts. *Materials Chemistry and Physics*, 92, pp. 197 – 204.

Poli, G. et al., 1981. The chemistry of catalysts based on vanadium-phosphorus oxides: Note II: The role of the method of preparation. *Applied Catalysis*, 1, pp. 395 – 404.

Prather, K., 2004. Enzyme classification systems. *BioCatalysis.* pp. 2.
Ruitenbeek, M. et al., 1998. Effects of silica and titania supports on the catalytic performance of VPO catalysts. *Elsevier Science Publication*, 118, pp. 52.
Redhead, P. A., 1962. Thermal desorption of gases. *Vacuum*, 12(4), pp. 203 – 211.

Richard, W. T. and Loomis, A. L., 1927. The chemical effects of high frequency sound waves. *Journal of the American Chemical Society*, 49(12), pp. 3086 – 3100.

Rownaghi, A. A., Taufiq Yap, Y. H. and Rezaei, F., 2010. Innovative process for the synthesis of vanadyl pyrophosphate as a highly selective catalyst for *n*-butane oxidation. *Chemical Engineering Journal*, 165, pp. 328 – 335.

Sananes, M. T., Hutchings, G. J. and Volta, J. C., 1995. On the role of the $VO(H_2PO_4)_2$ precursor for *n*-butane oxidation into maleic anhydride. *Journal of Catalysis*, 154(2), pp. 253 – 260.

Santos, H. M. and Capelo, J. L., 2009. *Ultrasound in Chemistry: Analytical Applications*. 2nd ed. Germany: WILEY-VCH

Sasaki, T., Nakano, S. Yamauchi, S. and Watanabe, M., 1997. *Chem. Matt.*, 9, pp. 602.

Sodeinde, Q. A., 2012, Preparation of a locally produced activated carbon from coconut shell and its use in reducing hexamine cobalt (III). *International Journal of Chemical Engineering and Applications*, 3(1), pp. 1 – 5.

Stefani, G., Budi, F., Fumagalli, C. and Suciu, D., 1990. *New Developments in Selective Oxidation*, 1st ed. London: Elsevier Publication.

Suslick, K. S., Hammerton, D. A. and Cline, R. E., 1986. *J. Am. Chem. Soc.*, 108, pp. 5641.

Suslick, K. S., 1988. *Ultrasound: It's Chemical, Physical and Biological Effects*, 1st ed. New York: VCH Publishers.

Suslick, K. S. and Doktycz, S. J., 1990. *Advances in Sonochemistry*, 1st ed. New York: JAI Press.

Suslick, K. S., 1997. *Handbook of Heterogeneous Catalysis*, 2nd ed. Weinheim: Wiley-VCH.

Suslick, K. S. and Crum, L. A., 1997. *Sonochemistry and sonoluminescene in encyclopedia of acoustic*, 1st ed. New York: Wiley Interscience.

Suslick, K. S. et al., 1999. Acoustic cavitation and its chemical consequences. *Phil. Trans. R. Soc. Lond. A*., 357, pp. 335 – 353.

Tan, I. A., Ahmad, A. L. and Hameed, B. H., 2008. Preparation of activated carbon from coconut husk: Optimisation study on removal of 2,4,6-trichlorophenol using response surface methodology. *Journal of Hazardous Material*, 153, pp. 709 – 717.

Taufiq Yap, Y. H. et al., 2001. The effect of the duration of *n*-butane/air pre-treatment on the morphology and reactivity of $(VO)_2P_2O_7$ catalysts. *Catalysis Letters*, 74, pp. 99 – 104.

Taufiq Yap, Y. H., Leong, L. K., Hussien, M. Z., Irmawati, R. and Hamid, S. B., 2004. Synthesis and characterisation of vanadyl pyrophosphate catalyst via vanadyl hydrogen phosphate sesquihydrate precursor. *Catalysis Today*, 93, pp. 715 – 722.

Taufiq Yap, Y. H., Goh, C. K., Hutchings, G. J., Dummer, N. and Bartley, J. K. 2006. Effect of mechanochemical treatment to the vanadium phosphate catalysts derived from $VOPO_4 \cdot 2H_2O$. *Journal of Molecular Catalysis*, 260(1), pp. 24 – 31.

Taufiq Yap, Y. H., Rownaghi. A. A., Hussien, M. Z. and Irmawati, R., 2007. Preparation of vanadium phosphate catalyst from $VOPO_4 \cdot 2H_2O$: Effect of microwave irradiation on morphology and catalytic property. *Catalyst Letter*, 119, pp. 64 – 71.

Taufiq Yap, Y. H. and Saw, C. S., 2008. Effect of different calcinations environments on the vanadium phosphate catalysts for selective oxidation of propane and *n*-butane. *Catalysis Today*, 131(1), pp. 285 – 291.

Taufiq Yap, Y. H., Nurul Suziana, N. M. and Hussein, M. Z., 2011. Influences of the various metal dopants for the nanosized vanadium phosphate catalysts. *Catalysis Letters*, 141(1), pp. 136 – 148.

Taufiq Yap, Y. H., Joshua Hoh, J. R. and Wong, Y. C., 2011. Synthesis of nanostructured vanadium phosphate catalyst using sonochemical route for partial oxidation of n-butane. *Journal of Applied Sciences*, 11(13), pp. 2370 – 2375.

Thornycroft, J. and Barnaby, S. W., 1985. Torpedo boat destroyers. *Institution of Civil Engineering*, 122, pp. 51.

Tsuchiya, Y., Hamashima, Y. and Sodeoko, M., 2006. A new entry to Pd-H chemistry: Catalytic asymmetric conjugate reduction of enones with EtOH and a highly selective enantioselective synthesis of warfarin. *Organic Letter*, 8(21), pp. 4851 – 4854.

Unnikrishnan, R. P., Demessie, E. S. and Varma, R. S., 2003. Alternative routes for catalyst preparation: use of ultrasound and microwave irradiation for the preparation of vanadium phosphorus oxide catalyst and their activity for hydrocarbon oxidation. *Applied Catalysis A: General*, 252, pp. 1 – 8.

Vale, G., Rial-Otero, R., Mota, A., Fonseca, L. and Capelo, J. L., 2008.Ultrasonic-assisted enzymatic digestion (USAED) for elemental determination and elemental speciation: A Tutorial. *Talanta*, 75(4), pp. 872 – 884.

Van Dillen, A. J., Terorde, R. J., Lensveld, D. J., Geus, J. W. and Jong, K. P., 2003. *Journal of Catalysis*, 216, pp. 257.

Viswanathan, B., Sivasanker, S. and Ramasamy, A.V., 2002. *Catalysis: principle and application*, 1st ed. New Delhi: Narosa Publishing House.

Vollhardt, P. and Schore, N., 2009. *Organic chemistry: structure and function*, 6th ed. New York: W. H. Freeman and Company.

Volta, J. C., 1982. Intercalation compounds as precursor for oriented catalyst: The MoO_3 graphite system in propylene oxidation. *Carbon*, 20(2), pp. 135.

Wibetoe, G., Takuwa, D. T., Lund, W. D. and Sawula, G., 1999. *Journal of Analytical Chemistry*, 363, pp. 46.

Wong, Y. C. and Taufiq Yap, Y. H., 2011. VOPO4·2H2O and the vanadium phosphate catalyst produced by sonochemical route. *Asian Journal of Chemistry*, 23(9), pp. 3853 – 3858.

Yamamoto, N., Hiyoshi, N. and Okuhara, T., 2002. Thin layered sheets of $VOHPO_4 \cdot 0.5H_2O$ prepared from $VOPO_4 \cdot 2H_2O$ by exfoliation reduction in alcohol. *Chemistry of Materials*, 14(9), pp. 3882 – 3888.

Yamazoe, N., Morishige, H. and Teraoka, Y., 1988. *Successful Design of Catalyst*, 2nd ed. Netherlands: Elsevier.

Zazhigalov, V. A., Zaitsev, Y. P., Belousov, V. M. and Parlitz, B., 1986. Studies of immobilised VPO/SiO_2 catalysts. *Reaction Kinetics and Catalysis Letters*, 32(1), pp. 209 – 214.

Zazhigalov, V. A. et al., 1996. *n*-butane oxidation on VPO catalysts: influence of alkali and alkaline- earth metal ions as additions. *Applied Catalysis A: General*, 134(2), pp. 225 – 137.

Zazhigalov, V. A., Diyuk, E. A., Sidorchuk, V. V. and Mironyuk, T. I., 2009. Synthesis of vanadium phosphorus oxide catalyst supported on pyrogenic silica and titanium dioxide. *Kinetika*, 50(4), pp. 608 – 617.

Zhou, Z. Q., Xu, H. Y., Ji, W. J. and Chen, Y., 2004. Preparation of novel composite VPO/fumed silica catalyst for partial oxidation of *n*-butane. *Catalysis Letter*, 96(3), pp. 221 – 226.

APPENDIX A

Support Calculation

Calculation for Coconut Shell Activated Carbon (CSAC) support used

$$\text{VPO/CSAC} = \frac{\text{Weight of } VOPO_4 \cdot 2H_2O}{\text{Weight of } VOPO_4 \cdot 2H_2O + \text{Weight of CSAC support}}$$

Example of calculation:

10 wt% VPO/CSAC
VPO/CSAC = 0.10

$$0.10 = \frac{10.0\ \text{g}}{10.0\ \text{g} + \text{Weight of CSAC support}}$$

$$10.0\ \text{g} + \text{Weight of CSAC support} = \frac{10.0\ \text{g}}{0.10}$$

$$10.0\ \text{g} + \text{Weight of CSAC support} = 100.0\ \text{g}$$

$$\text{Weight of CSAC support} = 100.0\ \text{g} - 10.0\ \text{g}$$

$$\text{Weight of CSAC support} = 90.0\ \text{g}$$

Thus, 90.0 g of CSAC was added during wetness impregnation to produce 10 wt% of CSAC supported VPO catalyst (10 wt% VPO/CSAC).

Denotations	Mass of $VOPO_4 \cdot 2H_2O$ used in first stage (grams)	Mass of CSAC (grams)
10 wt% VPO/AC	10.0	90.0
20 wt% VPO/AC	10.0	40.0
30 wt% VPO/AC	10.0	23.3
40 wt% VPO/AC	10.0	15.0
10 wt% UVPO/AC	10.0	90.0
20 wt% UVPO/AC	10.0	40.0
30 wt% UVPO/AC	10.0	23.3
40 wt% UVPO/AC	10.0	15.0

APPENDIX B

Solution Preparation for Redox Analysis

1. Preparation of 0.1 M sulphuric acid, H_2SO_4

$$1\text{ L of concentrated } H_2SO_4\ (95\% - 98\%) = 1.84\text{ kg}$$
$$= \frac{1840\text{ g}}{1000\text{ cm}^3}$$
$$= 1.84\text{ g cm}^{-3}$$

Molecular weight of H_2SO_4 = 2(1.00 g mol^{-1}) + 32.07 g mol^{-1} + 4(16.00 g mol^{-1})
= 98.07 g mol^{-1}

$$\text{Concentration of } H_2SO_4 = \frac{1.84\text{ g cm}^3}{98.07\text{ g mol}^{-1}} \times \frac{95}{100} \times 1000$$
$$= 17.82\text{ mol L}^{-1}$$
$$= 17.82\text{ M}$$

$M_1V_1 = M_2V_2$
Where: M_1 = Concentration of H_2SO_4 (95% - 98%)
V_1 = Volume of H_2SO_4 (95% - 98%)
M_2 = Concentration of diluted H_2SO_4
V_2 = Volume of diluted H_2SO_4

(17.82 M)(V_1) = (0.1 M)(1000 cm^3)
V_1 = 5.61 cm^3

Thus, 5.61 ml of (95% - 98%) H_2SO_4 was diluted to 1000 ml to prepare 0.1 M H_2SO_4.

2. Preparation of 2.0 M sulphuric acid, H_2SO_4

$M_1V_1 = M_2V_2$
Where: M_1 = Concentration of H_2SO_4 (95% - 98%)
V_1 = Volume of H_2SO_4 (95% - 98%)
M_2 = Concentration of diluted H_2SO_4
V_2 = Volume of diluted H_2SO_4

(17.82 M)(V_1) = (2.0 M)(1000 cm^3)
V_1 = 112.23 cm^3

Thus, 112.23 ml of (95% - 98%) H_2SO_4 was diluted to 1000 ml to prepare 2.0 M H_2SO_4.

3. Preparation of 0.01 N potassium permanganate, $KMnO_4$

Normality, N (eq L^{-1}) = M (mol L^{-1}) x n (eq mol^{-1})
$MnO_4^- + 8H^+ + 5e^- \leftrightarrow Mn^{2+} + 4H_2O$

$$\text{Molarity, M} = \frac{\text{N (eq L}^{-1})}{\text{n (eq mol}^{-1})}$$
$$= \frac{0.01 \text{ eq L}^{-1}}{5 \text{ eq mol}^{-1}}$$
$$= 0.002 \text{ mol L}^{-1}$$

Molecular weight of $KMnO_4$ = 39.10 g mol^{-1} + 54.94 g mol^{-1} + 4(16.00 g mol^{-1})
= 158.04 g mol^{-1}

Weight of $KMnO_4$ in 1000 cm^3 diluted 0.1 M H_2SO_4
= 0.002 mol L^{-1} x 158.04 g mol^{-1}
= 0.3161 g L^{-1}

Thus, 0.3161 g of $KMnO_4$ was transferred into 1000 ml volumetric flask, dissolved with 0.1 M H_2SO_4 then top up to 1000 ml.

4. Preparation of 0.01 N ammonium iron (II) sulphate, $(NH_4)_2Fe(SO_4)_2 \cdot 6H_2O$

Normality, N (eq L^{-1}) = M (mol L^{-1}) x n (eq mol^{-1})
$Fe^{2+} + e^- \leftrightarrow Fe^{3+}$

$$\text{Molarity, M} = \frac{\text{N (eq L}^{-1})}{\text{n (eq mol}^{-1})}$$
$$= \frac{0.01 \text{ eq L}^{-1}}{1 \text{ eq mol}^{-1}}$$
$$= 0.01 \text{ mol L}^{-1}$$

Molecular weight of $(NH_4)_2Fe(SO_4)_2 \cdot 6H_2O$
= 2(14.00 g mol^{-1}) + 20(1.00 g mol^{-1}) + 55.85 g mol^{-1} + 2(32.07 g mol^{-1}) + 14(16.00 g mol^{-1})
= 391.99 g mol^{-1}

Weight of $(NH_4)_2Fe(SO_4)_2 \cdot 6H_2O$ in 1000 cm^3 diluted 0.1 M H_2SO_4
= 0.01 mol L^{-1} x 391.99 g mol^{-1}
= 3.9199 g L^{-1}

Thus, 3.9199 g of $(NH_4)_2Fe(SO_4)_2 \cdot 6H_2O$ was transferred into 1000 ml volumetric flask, dissolved with 0.1 M H_2SO_4 then top up to 1000 ml.

5. Preparation of diphenylamine, $(C_6H_5)_2NH$ indicator

1.0 g of $(C_6H_5)_2NH$ was weighed and dissolved in few ml of concentrated H_2SO_4 in a 100 ml volumetric flask then continued top up to 100 ml.

6. Preparation of sample solution

   0.10 g of sample was weighed and dissolved in few ml of 2M H_2SO_4 in a 100 ml volumetric flask then continued top up to 100 ml.

APPENDIX C

Solution Preparation for ICP-OES Analysis

1. Preparation of 8.0 M nitric acid, HNO_3

$$1\text{ L of concentrated } HNO_3\ (65\%) = 1.390\text{ kg}$$
$$= \frac{1390\text{ g}}{1000\text{ cm}^3}$$
$$= 1.390\text{ g cm}^{-3}$$

Molecular weight of HNO_3 = 1.00 g mol^{-1} + 14.01 g mol^{-1} + 3(16.00 g mol^{-1})
= 63.01 g mol^{-1}

$$\text{Concentration of } HNO_3 = \frac{1.390\text{ g cm}^3}{63.01\text{ g mol}^{-1}} \times \frac{65}{100} \times 1000$$
$$= 14.339\text{ mol L}^{-1}$$
$$= 14.339\text{ M}$$

$M_1V_1 = M_2V_2$
Where: M_1 = Concentration of HNO_3 (65%)
V_1 = Volume of HNO_3 (65%)
M_2 = Concentration of diluted HNO_3
V_2 = Volume of diluted HNO_3

(14.339 M)(V_1) = (8.0 M)(1000 cm^3)
V_1 = 557.92 cm^3

Thus, 557.92 ml of (65%) HNO_3 was diluted to 1000 ml to prepare 8.0 M HNO_3.

2. Preparation of sample solution

0.01 g of sample was weighed and dissolved in few ml of 8M HNO_3 in a 100 ml volumetric flask then continued top up to 100 ml.

3. Preparation of blank HNO_3 standard

10 ml of concentrated HNO_3 was measured and placed in a 100 ml volumetric flask then top up with deionised water to the mark.

4. Preparation of stock solution of phosphorus, P

Relative molecular weight of Ammonium Dihydrogen Phosphate, $NH_4H_2PO_4$
$= 14.01\ g\ mol^{-1} + 6(1.00\ g\ mol^{-1}) + 30.9738\ g\ mol^{-1} + 4(16.00\ g\ mol^{-1})$
$= 115.0255\ g\ mol^{-1}$

50 ppm of stock solution for P $= 50\ mg\ L^{-1}$
$= 0.05\ g\ L^{-1}$

$$\text{Number of mole of P} = \frac{0.05\ g\ L^{-1}}{39.9738\ g\ mol^{-1}}$$
$= 1.6145 \times 10^{-3}\ mol\ L^{-1}$

Mass of $NH_4H_2PO_4 = (1.6145 \times 10^{-3}\ mol\ L^{-1}) \times (115.0255\ g\ mol^{-1})$
$= 0.1857\ g\ L^{-1}$

Thus 0.1857 g of $NH_4H_2PO_4$ was transferred into 1000 ml volumetric flask and top up with distilled water.

5. Preparation of standard solution of phosphorus, P

$M_1V_1 = M_2V_2$
Where: M_1 = Concentration of stock solution (50 ppm)
V_1 = Volume of stock solution
M_2 = Concentration of standard solution
V_2 = Volume of standard solution

Example of calculation:

Determination of the volume required to prepare 10 ppm standard solution

$(50\ ppm)(V_1) = (10\ ppm)(250cm^3)$
$V_1 = 50\ cm^3$

Thus 50 ml of stock solution for phosphorus was dissolved in 10 ml of 8M HNO_3 then diluted to 250 ml with deionised water to produce 10 ppm of standard solution of phosphorus.

Standard solution for P	Volume of stock solution required (ml)
10 ppm	50
20 ppm	100
30 ppm	150

6. Preparation of stock solution of vanadium, V

Relative molecular weight of Ammonium Metavanadate, NH_4VO_3
$= 14.01\ g\ mol^{-1} + 4(1.00\ g\ mol^{-1}) + 50.9415\ g\ mol^{-1} + 3(16.00\ g\ mol^{-1})$
$= 116.9780\ g\ mol^{-1}$

50 ppm of stock solution for V = 50 mg L^{-1}
= 0.05 g L^{-1}

$$\text{Number of mole of V} = \frac{0.05 \text{ g L}^{-1}}{50.9415 \text{ g mol}^{-1}}$$
= 9.8155 x 10^{-4} mol L^{-1}

Mass of NH_4VO_3 = (9.8155 x 10^{-4} mol L^{-1}) x (116.9780 g mol^{-1})
= 0.1148 g L^{-1}

Thus 0.1148 g of NH_4VO_3 was transferred into 1000 ml volumetric flask and top up with distilled water.

7. Preparation of standard solution of vanadium, V

$M_1V_1 = M_2V_2$
Where: M_1 = Concentration of stock solution (50 ppm)
V_1 = Volume of stock solution
M_2 = Concentration of standard solution
V_2 = Volume of standard solution

Example of calculation:

Determination of the volume required to prepare 10 ppm standard solution

(50 ppm)(V_1) = (10 ppm)(250cm^3)
V_1 = 50 cm^3

Thus 50 ml of stock solution for vanadium was dissolved in 10 ml of 8M HNO_3 then diluted to 250 ml with deionised water to produce 10 ppm of standard solution of vanadium.

Standard solution for V	Volume of stock solution required (ml)
10 ppm	50
20 ppm	100
30 ppm	150

APPENDIX D

XRD Calculation

Crystallite size measurements using powder XRD technique

$$\text{Crystallite Size, T (Å)} = \frac{0.89\lambda}{FWHM\ (rad) \times \cos\theta}$$

$$\text{where: FWHM (rad)} = \text{FWHM (°)} \times \frac{\pi}{180°}$$

$\lambda_{\text{Cu K}\alpha}$ = 1.54 Å

Example of calculation:

For VPO-150B0E, 2θ = 22.8977° and FWHM (°) = 1.18950

$$\text{FWHM (rad)} = 1.18950 \times \frac{\pi}{180°}$$
$$= 0.0276$$

$$\text{T (Å)} = \frac{0.89 \times 1.54\ \text{Å}}{0.0276 \times \cos 11.44885}$$
$$= 67.35929\ \text{Å}$$

Series 1: VPO-150B0E

2θ	θ	FWHM (°)	FWHM (rad)	T (Å)
22.8977	11.44885	1.18950	0.02076	67.35929
28.4804	14.24020	0.61020	0.01065	132.77461
29.9405	14.97025	0.60110	0.01049	135.23294

Series 1: VPO-120B30E

2θ	θ	FWHM (°)	FWHM (rad)	T (Å)
22.9077	11.45385	1.20160	0.02097	66.68217
28.4971	14.24855	0.66960	0.01169	121.00070
29.9620	14.98100	0.66250	0.01156	122.70581

Series 1: VPO-90B60E

2θ	θ	FWHM (°)	FWHM (rad)	T (Å)
22.8896	11.44480	1.28190	0.02237	62.50310
28.4899	14.24495	0.63860	0.01115	126.87249
29.9782	14.98910	0.62000	0.01082	131.12206

Series 2: VPO-U1R24

2θ	θ	FWHM (°)	FWHM (rad)	T (Å)
22.8001	11.40005	1.33750	0.02334	59.89539
28.4119	14.20595	0.54680	0.00954	148.14703
29.8898	14.94490	0.52900	0.00923	153.64634

Series 2: VPO-U2R24

2θ	θ	FWHM (°)	FWHM (rad)	T (Å)
22.8180	11.40900	1.38690	0.02421	57.76380
28.4166	14.20830	0.62640	0.01093	129.32253
29.9130	14.95650	0.59440	0.01037	136.74850

Series 2: VPO-U3R24

2θ	θ	FWHM (°)	FWHM (rad)	T (Å)
22.8288	11.41440	1.45430	0.02538	55.08776
28.4125	14.20625	0.63190	0.01103	128.19576
29.9043	14.95215	0.60630	0.01058	134.06178

Series 3: 10 wt% VPO/CSAC

2θ	θ	FWHM (°)	FWHM (rad)	T (Å)
22.9191	11.45955	1.29360	0.02258	61.94102
28.4400	14.22000	0.61120	0.01067	132.54553
29.9013	14.95065	0.59140	0.01032	137.43844

Series 3: 20 wt% VPO/CSAC

2θ	θ	FWHM (°)	FWHM (rad)	T (Å)
22.9048	11.45240	1.31980	0.02303	60.70987
28.4200	14.21000	0.62660	0.01094	129.28223
29.9725	14.98625	0.60140	0.01050	135.17558

Series 3: 30 wt% VPO/CSAC

2θ	θ	FWHM (°)	FWHM (rad)	T (Å)
22.8822	11.44110	1.33440	0.02329	60.04323
28.4655	14.23275	0.64650	0.01128	125.31538
29.9419	14.97095	0.60940	0.01064	133.39151

Series 3: 40 wt% VPO/CSAC

2θ	θ	FWHM (°)	FWHM (rad)	T (Å)
22.8595	11.42975	1.35240	0.02360	59.24170
28.4685	14.23425	0.65790	0.01148	123.14475
29.9148	14.95740	0.61930	0.01081	131.25085

Series 4: 10 wt% UVPO/CSAC

2θ	θ	FWHM (°)	FWHM (rad)	T (Å)
22.8400	11.42000	1.4865	0.02594	53.89554
28.4320	14.21600	0.6625	0.01156	122.27984
29.8800	14.94000	0.6251	0.01091	130.02249

Series 4: 20 wt% UVPO/CSAC

2θ	θ	FWHM (°)	FWHM (rad)	T (Å)
22.8800	11.44000	1.5241	0.02660	52.56963
28.4100	14.20500	0.6798	0.01186	119.16219
29.8200	14.91000	0.6564	0.01146	123.80517

Series 4: 30 wt% UVPO/CSAC

2θ	θ	FWHM (°)	FWHM (rad)	T (Å)
22.8400	11.42000	1.5667	0.02734	51.13660
28.4400	14.22000	0.6934	0.01210	116.83274
29.8800	14.94000	0.6612	0.01154	122.92356

Series 4: 40 wt% UVPO/CSAC

2θ	θ	FWHM (°)	FWHM (rad)	T (Å)
22.8800	11.44000	1.5967	0.02787	50.17935
28.4200	14.21000	0.6996	0.01221	115.79223
29.8000	14.90000	0.6898	0.01204	117.80507

APPENDIX E

XRD Profiles

Series 3: 10 wt% VPO/CSAC

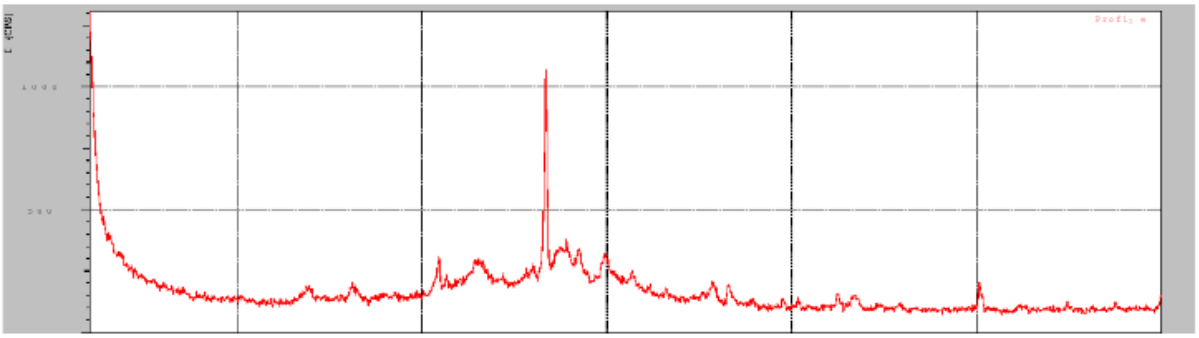

Series 3: 20 wt% VPO/CSAC

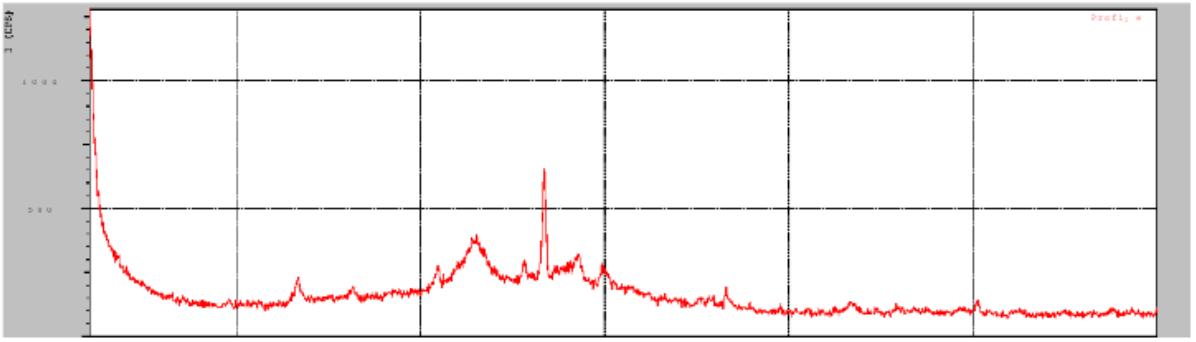

Series 3: 30 wt% VPO/CSAC

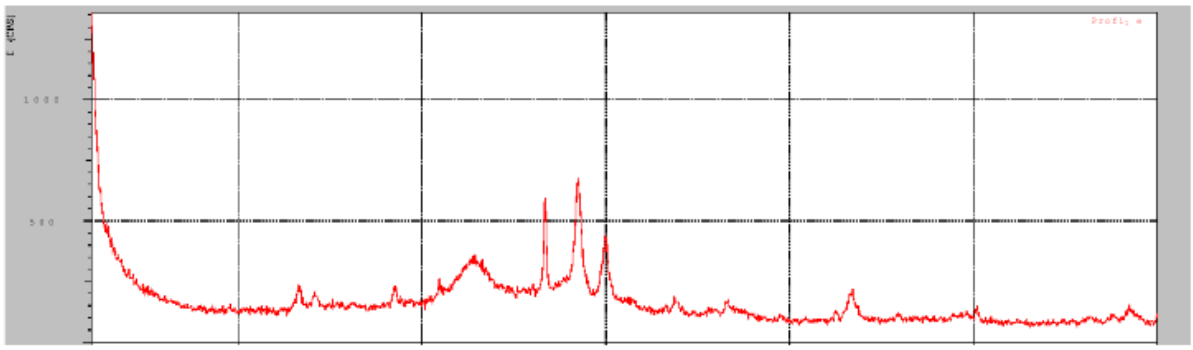

Series 3: 40 wt% VPO/CSAC

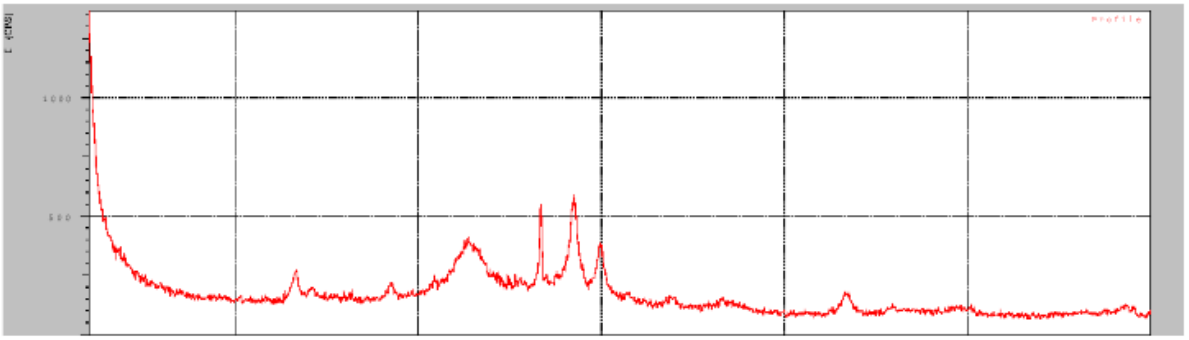

10 wt% UVPO/CSAC

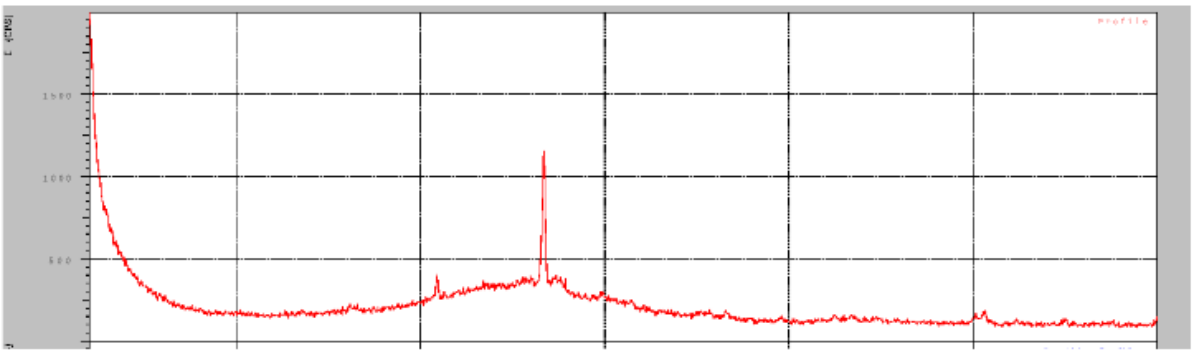

20 wt% UVPO/CSAC

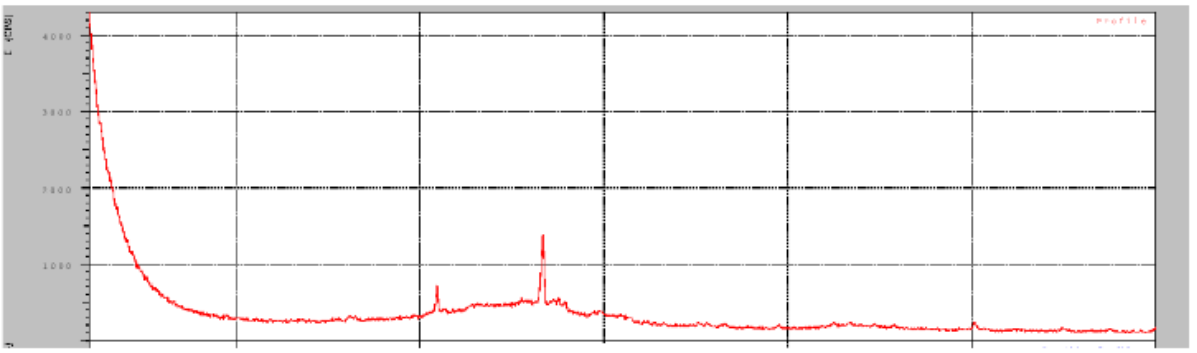

30 wt% UVPO/CSAC

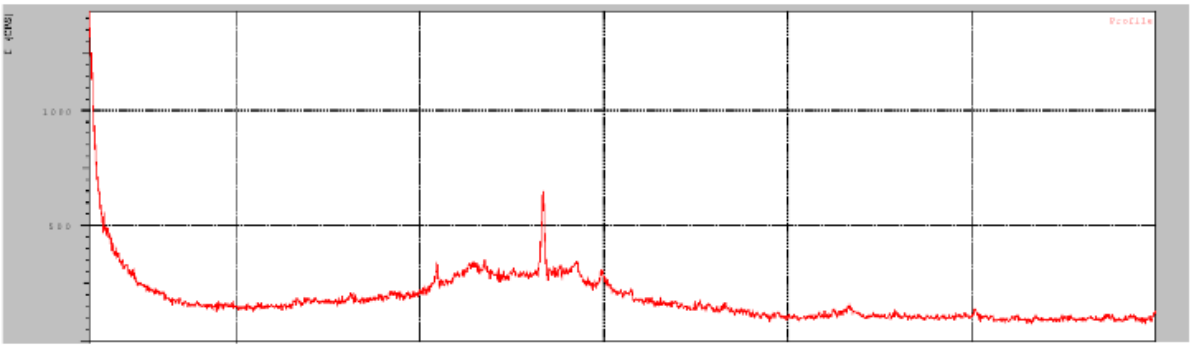

40 wt% UVPO/CSAC

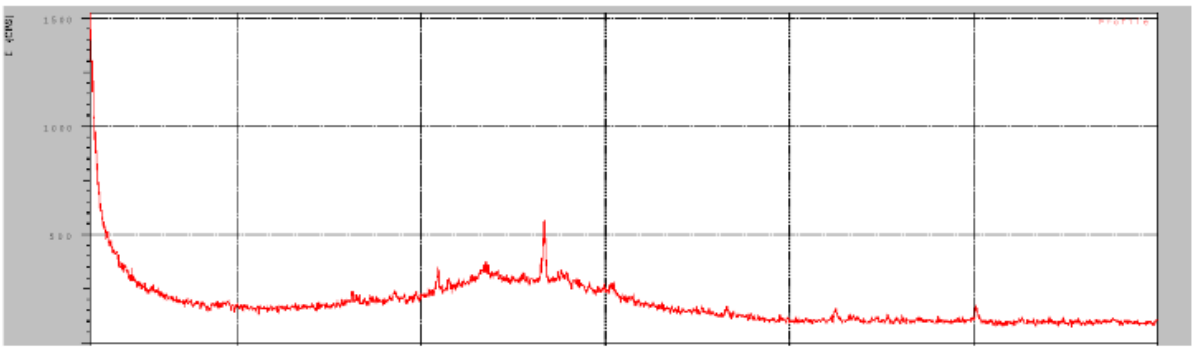

APPENDIX F

Adsorption Desorption Isotherm Sample

Series 1: VPO-150B0E

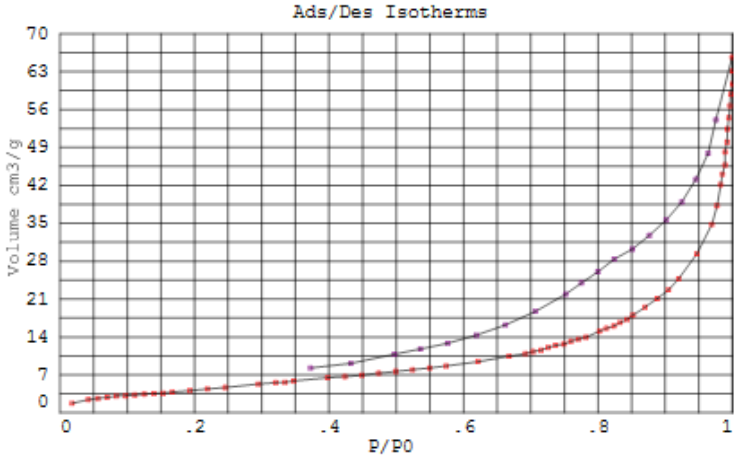

*** Sample information	***
Company Name :	UTAR
Operator :	Prakas
Date :	4/12/2012
Sample name :	VPO-150B0E
Preparation :	
Sample mass (g) :	.4785
Sample density (g/cm3) :	0
*	*
*	*
*	*
*	*
*	*
*	*
*	*
*	*
*	*
*	*
*	*
***	***

*** Acquisition parameters			***
Adsorption ----------	1st	2nd	3rd
Desired points :	15	10	12
Equilibrium deviation :	0.2	0.5	0.7
Equilibrium Time (min) :	3	3	3
P/P0 regions :	0.33	0.75	Sat.
Piston filling volume :--	-	-	-
Max Ads pressure :			1000
Min Sat pressure :			740
Initial load pressure :			600
Desorption ----------		1st	2nd
Desired points :		15	10
Equilibrium deviation :		0.9	0.5
Equilibrium Time (min) :		3	3
P/P0 regions :		0.75	
Piston filling volume :--		-	-
Last Des pressure :			300
Analysis type :		Ads + Des	
Saturation pressure :		PT100	
Pre-run time (min) :			10
Run Time (hh:mm) :			11:43

*** Analytical conditions	***
Gas molecolar weight (g/mol) :	28.01
Gas molecolar area (A²) :	16.2
Gas ads. density (g/cm3) :	.8086
Gas lqd.srf. tens. (Dyne/cm) :	8.85
Monolayer thickness (Å) :	3.54
Blank slope (cm3/Torr²) :	3.022064E-06
Blank intercept (cm3/Torr) :	.1162863
Instrument hysteresis :	1.0009757
2nd vir. burette temperature :	-262
2nd vir. piston temperature :	-3.1
Burette temperature (°C) :	-196
Correct slope/Intercept :	No
*	*
*	*
*	*
*	*
*	*
*	*
*	*
***	***

R E S U L T S

Calculation Method < B.E.T. >

<B.E.T.> Initial-final P/P0 :	.04 - .3
Specific surface calculations	
Monolayer volume (cm3/g) :	3.9101837
Specific surface area (m²/g) :	17.021809
C value of BET equation :	25.6455
Correlation factor :	.9963603
Pore specific volume (cm3/g) :	.04528944
Pore specific volume at P/P0 :	.95
Total Adsorbed volume (cm3/g) :	65.67462
(Dol./Heal)	
Cumulative area max. (m²/g) :	30.606199
Pore volume max. (cm3/g) :	.071522497

APPENDIX G

EDX Calculation

Series 1: VPO-150B0E

Atomic % of Phosphorus (P)	Atomic % of Vanadium (V)	P/V Atomic Ratio
31.65	27.41	1.155
31.68	27.46	1.154
31.66	27.41	1.155
31.60	27.45	1.151
31.62	27.42	1.153
31.63	27.41	1.154
31.67	27.40	1.156
31.61	27.41	1.153
31.66	27.40	1.155
31.68	27.41	1.156
Average P/V Atomic Ratio		1.154

Series 1: VPO-120B30E

Atomic % of Phosphorus (P)	Atomic % of Vanadium (V)	P/V Atomic Ratio
31.15	27.91	1.116
31.11	27.92	1.114
31.12	27.90	1.115
31.15	27.93	1.115
31.10	27.99	1.111
31.13	27.92	1.115
31.15	27.91	1.116
31.10	27.90	1.115
31.11	27.96	1.113
31.12	27.96	1.113
Average P/V Atomic Ratio		1.114

Series 1: VPO-90B60E

Atomic % of Phosphorus (P)	Atomic % of Vanadium (V)	P/V Atomic Ratio
30.25	28.64	1.056
30.23	28.69	1.054
30.24	28.67	1.055
30.21	28.67	1.054
30.23	28.69	1.054
30.23	28.64	1.056
30.22	28.66	1.054
30.22	28.68	1.054
30.21	28.65	1.054
30.24	28.67	1.055
Average P/V Atomic Ratio		1.054

Series 1: VPO-60B90E

Atomic % of Phosphorus (P)	Atomic % of Vanadium (V)	P/V Atomic Ratio
33.27	22.48	1.480
33.21	22.49	1.477
33.24	22.46	1.480
33.25	22.43	1.482
33.24	22.49	1.478
33.29	22.48	1.481
33.20	22.46	1.478
33.24	22.44	1.481
33.21	22.44	1.480
33.24	22.45	1.481
Average P/V Atomic Ratio		1.480

Series 1: VPO-30B120E

Atomic % of Phosphorus (P)	Atomic % of Vanadium (V)	P/V Atomic Ratio
34.65	22.45	1.543
34.69	22.48	1.543
34.67	22.48	1.542
34.65	22.49	1.541
34.62	22.46	1.541
34.68	22.49	1.542
34.69	22.46	1.545
34.64	22.43	1.544
34.63	22.44	1.543
34.66	22.44	1.545
Average P/V Atomic Ratio		1.543

Series 1: VPO-0B150E

Atomic % of Phosphorus (P)	Atomic % of Vanadium (V)	P/V Atomic Ratio
34.85	22.15	1.573
34.89	22.18	1.573
34.87	22.18	1.572
34.85	22.19	1.571
34.82	22.16	1.571
34.88	22.19	1.572
34.89	22.16	1.574
34.84	22.13	1.574
34.83	22.14	1.573
34.86	22.14	1.575
Average P/V Atomic Ratio		1.573

Series 2: VPO-U1R24

Atomic % of Phosphorus (P)	Atomic % of Vanadium (V)	P/V Atomic Ratio
30.84	27.98	1.102
30.85	27.99	1.102
30.87	27.96	1.104
30.88	27.99	1.103
30.84	27.99	1.102
30.85	27.96	1.103
30.84	27.98	1.102
30.86	27.97	1.103
30.88	27.96	1.104
30.89	27.96	1.105
Average P/V Atomic Ratio		1.103

Series 2: VPO-U2R24

Atomic % of Phosphorus (P)	Atomic % of Vanadium (V)	P/V Atomic Ratio
30.59	28.55	1.071
30.59	28.56	1.071
30.58	28.57	1.070
30.59	28.57	1.071
30.60	28.59	1.070
30.62	28.60	1.071
30.61	28.54	1.073
30.60	28.56	1.071
30.58	28.57	1.070
30.58	28.54	1.071
Average P/V Atomic Ratio		1.071

Series 2: VPO-U3R24

Atomic % of Phosphorus (P)	Atomic % of Vanadium (V)	P/V Atomic Ratio
30.15	28.94	1.042
30.13	28.99	1.039
30.14	28.97	1.040
30.11	28.97	1.039
30.13	28.99	1.039
30.13	28.94	1.041
30.12	28.96	1.040
30.12	28.98	1.039
30.11	28.95	1.040
30.14	28.97	1.040
Average P/V Atomic Ratio		1.040

Series 3: 10 wt% VPO/CSAC

Atomic % of Phosphorus (P)	Atomic % of Vanadium (V)	P/V Atomic Ratio
30.55	28.21	1.083
30.58	28.26	1.082
30.56	28.21	1.083
30.50	28.25	1.080
30.52	28.22	1.082
30.53	28.21	1.082
30.57	28.20	1.084
30.51	28.21	1.082
30.56	28.20	1.084
30.58	28.21	1.084
Average P/V Atomic Ratio		1.083

Series 3: 20 wt% VPO/CSAC

Atomic % of Phosphorus (P)	Atomic % of Vanadium (V)	P/V Atomic Ratio
30.95	27.91	1.109
30.98	27.90	1.110
30.96	27.91	1.109
30.99	27.90	1.111
30.92	27.92	1.107
30.93	27.91	1.108
30.97	27.90	1.110
30.99	27.91	1.110
30.96	27.90	1.110
30.98	27.91	1.110
Average P/V Atomic Ratio		1.110

Series 3: 30 wt% VPO/CSAC

Atomic % of Phosphorus (P)	Atomic % of Vanadium (V)	P/V Atomic Ratio
31.35	26.91	1.165
31.30	26.96	1.161
31.36	26.91	1.165
31.30	26.95	1.161
31.32	26.92	1.163
31.33	26.91	1.164
31.37	26.90	1.166
31.31	26.91	1.164
31.36	26.90	1.166
31.38	26.91	1.166
Average P/V Atomic Ratio		1.164

Series 3: 40 wt% VPO/CSAC

Atomic % of Phosphorus (P)	Atomic % of Vanadium (V)	P/V Atomic Ratio
31.55	26.31	1.199
31.58	26.36	1.198
31.56	26.31	1.200
31.59	26.30	1.201
31.52	26.32	1.198
31.53	26.31	1.198
31.57	26.30	1.200
31.59	26.31	1.201
31.56	26.30	1.200
31.58	26.31	1.200
Average P/V Atomic Ratio		1.200

Series 4: 10 wt% UVPO/CSAC

Atomic % of Phosphorus (P)	Atomic % of Vanadium (V)	P/V Atomic Ratio
30.29	28.54	1.061
30.28	28.59	1.059
30.26	28.57	1.059
30.29	28.57	1.060
30.29	28.59	1.059
30.23	28.54	1.059
30.27	28.56	1.060
30.26	28.58	1.059
30.26	28.55	1.060
30.28	28.57	1.060
Average P/V Atomic Ratio		1.060

Series 4: 20 wt% UVPO/CSAC

Atomic % of Phosphorus (P)	Atomic % of Vanadium (V)	P/V Atomic Ratio
30.35	27.81	1.091
30.38	27.86	1.090
30.36	27.81	1.092
30.30	27.85	1.088
30.32	27.82	1.090
30.33	27.81	1.091
30.37	27.80	1.092
30.31	27.81	1.090
30.36	27.80	1.092
30.38	27.81	1.092
Average P/V Atomic Ratio		1.091

Series 4: 30 wt% UVPO/CSAC

Atomic % of Phosphorus (P)	Atomic % of Vanadium (V)	P/V Atomic Ratio
30.55	26.71	1.144
30.58	26.76	1.143
30.56	26.71	1.144
30.50	26.75	1.140
30.52	26.72	1.142
30.53	26.71	1.143
30.57	26.70	1.145
30.51	26.71	1.142
30.56	26.70	1.145
30.58	26.71	1.145
Average P/V Atomic Ratio		1.143

Series 4: 40 wt% UVPO/CSAC

Atomic % of Phosphorus (P)	Atomic % of Vanadium (V)	P/V Atomic Ratio
31.35	26.21	1.196
31.38	26.26	1.195
31.36	26.21	1.196
31.30	26.25	1.192
31.32	26.22	1.195
31.33	26.27	1.193
31.37	26.25	1.195
31.31	26.28	1.191
31.36	26.26	1.194
31.38	26.25	1.195
Average P/V Atomic Ratio		1.194

APPENDIX H

EDX Profiles

Series 3: 10 wt% VPO/CSAC

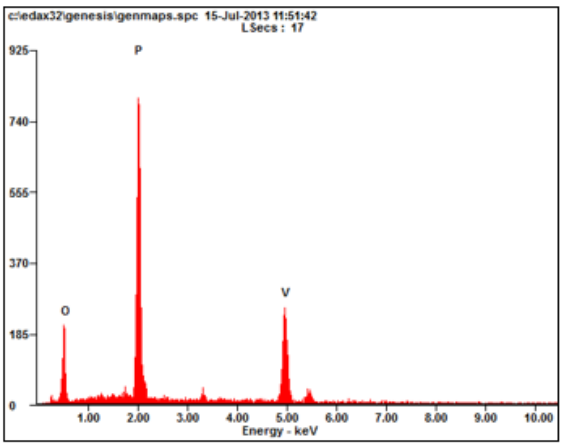

Element	Wt%	At%
OK	22.51	41.24
PK	31.09	30.55
VK	47.22	28.21
Matrix	Correction	MThin

Series 3: 20 wt% VPO/CSAC

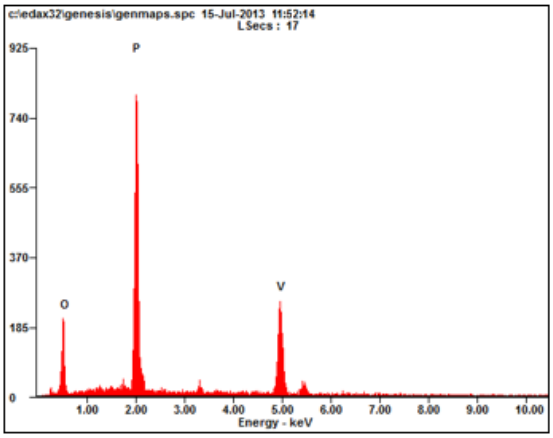

Element	Wt%	At%
OK	22.51	41.14
PK	31.55	30.95
VK	46.79	27.91
Matrix	Correction	MThin

Series 3: 30 wt% VPO/CSAC

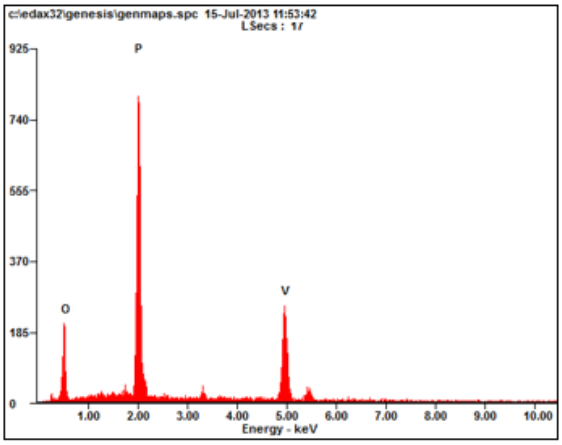

Element	Wt%	At%
OK	22.19	41.74
PK	32.26	31.35
VK	45.55	26.91
Matrix	Correction	MThin

Series 3: 40 wt% VPO/CSAC

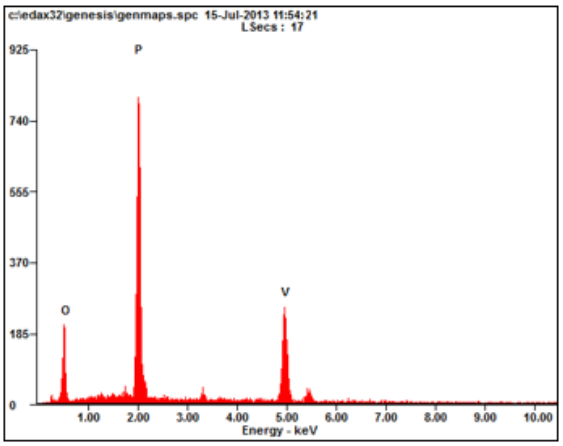

Element	Wt%	At%
OK	22.52	42.14
PK	32.66	31.55
VK	44.80	26.31
Matrix	Correction	MThin

Series 4: 10 wt% VPO/CSAC

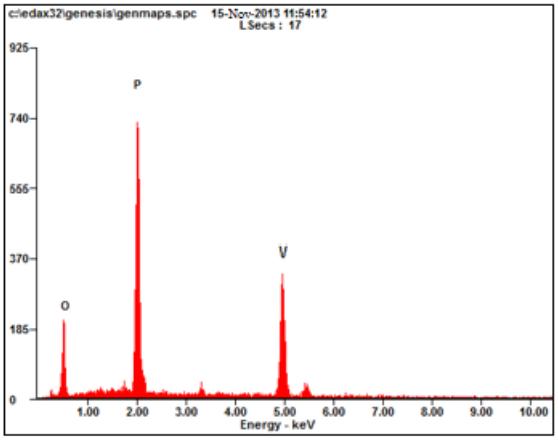

Element	Wt%	At%
OK	21.59	41.17
PK	30.75	30.29
VK	47.66	28.54
Matrix	Correction	MThin

Series 4: 20 wt% VPO/CSAC

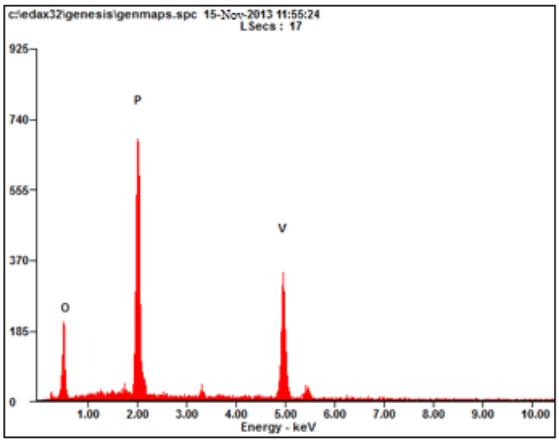

Element	Wt%	At%
OK	22.12	41.84
PK	31.06	30.35
VK	46.81	27.81
Matrix	Correction	MThin

Series 4: 30 wt% VPO/CSAC

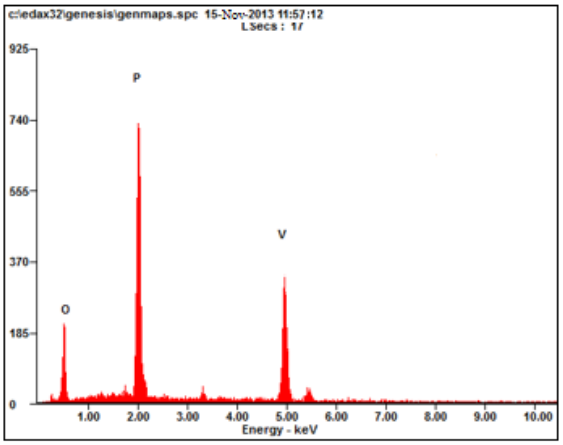

Element	Wt%	At%
OK	22.87	42.74
PK	31.64	30.55
VK	45.50	26.71
Matrix	Correction	MThin

Series 4: 40 wt% VPO/CSAC

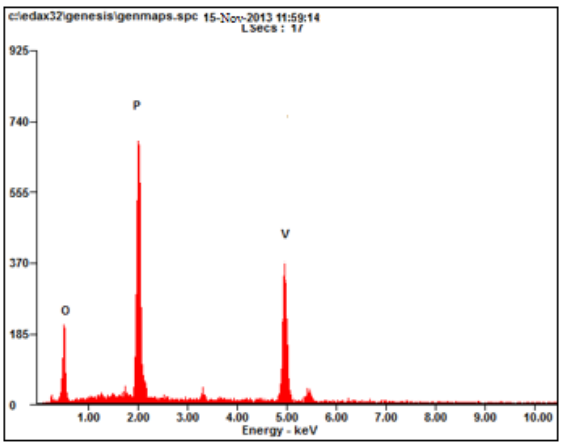

Element	Wt%	At%
OK	22.75	42.44
PK	32.53	31.35
VK	44.73	26.21
Matrix	Correction	MThin

APPENDIX I

ICP-OES Calculation

Calculation of P/V Atomic ratio from ICP-OES Analysis

$$\frac{\mathrm{P}}{\mathrm{V}} = \frac{\text{Concentration of P/Atomic weight of P}}{\text{Concentration of V/Atomic weight of V}}$$

Example of calculation:

For VPO-150B0E, [P] = 18.79 mg/L and [V] = 26.64 mg/L

$$\frac{\mathrm{P}}{\mathrm{V}} = \frac{\left(\frac{18.79\ \mathrm{mg/L}}{1000}\right)/30.9738\ \mathrm{g/L}}{\left(\frac{26.64\ \mathrm{mg/L}}{1000}\right)/50.9415\ \mathrm{g/L}}$$

$$= 1.16$$

Series 1

Samples	Concentration of Phosphorus, P (mg/L)	Concentration of Vanadium, V (mg/L)	P/V Atomic Ratio
VPO-150B0E	18.79	26.64	1.16
VPO-120B30E	19.43	29.59	1.08
VPO-90B60E	19.44	30.74	1.04
VPO-60B90E	20.78	26.29	1.30
VPO-30B120E	22.69	26.85	1.39
VPO-0B150E	23.58	26.93	1.44

Series 2

Samples	Concentration of Phosphorus, P (mg/L)	Concentration of Vanadium, V (mg/L)	P/V Atomic Ratio
VPO-R24R24	19.44	30.74	1.04
VPO-U1R24	21.77	33.15	1.08
VPO-U2R24	25.47	39.89	1.05
VPO-U3R24	29.55	47.18	1.03

Series 3

Samples	Concentration of Phosphorus, P (mg/L)	Concentration of Vanadium, V (mg/L)	P/V Atomic Ratio
10 wt% VPO/CSAC	12.61	19.75	1.05
20 wt% VPO/CSAC	23.73	36.82	1.06
30 wt% VPO/CSAC	26.83	39.75	1.11
40 wt% VPO/CSAC	29.30	41.54	1.16

Series 4

Samples	Concentration of Phosphorus, P (mg/L)	Concentration of Vanadium, V (mg/L)	P/V Atomic Ratio
10 wt% UVPO/CSAC	20.98	33.18	1.04
20 wt% UVPO/CSAC	32.21	49.51	1.07
30 wt% UVPO/CSAC	34.57	50.76	1.12
40 wt% UVPO/CSAC	36.35	51.54	1.16

APPENDIX J

Redox Calculation

Calculation of oxidation state of vanadium by using redox titration

According to Niwa and Murakami,

$T_1 = V^{4+} + 2V^{3+} = 20[MnO_4]V_1$ (1)
$T_2 = V^{5+} + V^{4+} + V^{3+} = 20[Fe^{2+}]V_2$ (2)
$T_3 = V^{5+} = 20[Fe^{2+}]V_3$ (3)

(2) – (3): $V^{4+} + V^{3+} = 20[Fe^{2+}]V_2 – 20[Fe^{2+}]V_3$ (4)
(1) – (4): $V^{3+} = 20[MnO_4]V_1 – 20[Fe^{2+}]V_2\ Z + 20[Fe^{2+}]V_3$ (5)

Substitute (5) into (1):

$V^{4+} = 20[MnO_4]V_1 – 2V^{3+}$
$V^{4+} = 20[MnO_4]V_1 – 2(20[MnO_4]V_1 + 20[Fe^{2+}]V_2 + 20[Fe^{2+}]V_3)$
$V^{4+} = 40[Fe^{2+}]V_2 – 40[Fe^{2+}]V_3 – 20[MnO_4]V_1$ (6)

Substitute (5) and (6) into (2):
$V^{5+} = 20[Fe^{2+}]V_2 – V^{4+} – V^{3+}$
$V^{5+} = 20[Fe^{2+}]V_2 – (40[Fe^{2+}]V_2 – 40[Fe^{2+}]V_3 – 20[MnO_4]V_1) –$
$(20[MnO_4]V_1 – 20[Fe^{2+}]V_2 – 20[Fe^{2+}]V_3)$
$= 20[Fe^{2+}]V_3$ (7)

From (5):

$V^{3+} = 20(0.01)V_1 – 20(0.01)V_2 – 20(0.01)V_3$
$= 0.2V_1 – 0.2V_2 + 0.2V_3$ (8)

From (6):

$V^{4+} = 40(0.01)V_2 – 40(0.01)V_3 – 20(0.01)V_1$
$= 0.4V_2 – 0.4V_3 + 0.2V_1$ (9)

From (7):

$V^{3+} = 20(0.01)V_3$
$= 0.2V_3$ (10)

The average oxidation state of vanadium is calculated as:

$$V_{AV} = \frac{3V^{3+} + 4V^{4+} + 5V^{5+}}{V^{3+} + V^{4+} + V^{5+}}$$

Example of calculation:

For VPO-150B0E, $V_1 = 10.40\ cm^3$, $V_2 = 12.90\ cm^3$ and $V_3 = 3.30\ cm^3$

From (8):
$V^{3+} = 0.2V_1 - 0.2V_2 + 0.2V_3$
$= 0.2(10.40) - 0.2(12.90) + 0.2(3.30)$
$= 0.16\ cm^3$
$\approx 0\ cm^3$ (Since no peaks attributed to V^{3+} were detected from the XRD analysis, this value is always taken as 0)

From (9):
$V^{4+} = 0.4V_2 - 0.4V_3 + 0.2V_1$
$= 0.4(12.90) - 0.4(3.30) + 0.2(10.40)$
$= 1.76\ cm^3$

From (10):
$V^{5+} = 0.2V_3$
$= 0.2(3.30)$
$= 0.66\ cm^3$

$$V_{AV} = \frac{3(0) + 4(1.76) + 5(0.66)}{0 + 1.76 + 0.66}$$
$= 4.273$

$$\text{Percentage of } V^{4+} = \frac{V^{4+}}{V^{3+} + V^{4+} + V^{5+}} \times 100$$
$$= \frac{1.76}{0 + 1.76 + 0.66} \times 100$$
$= 72.73\%$

Percentage of V^{5+} = 100% - Percentage of V^{4+}
= 100% - 72.73%
= 27.27%

Series 1

Sample	V_1 (cm^3)	V_2 (cm^3)	V_3 (cm^3)	V^{4+} (%)	V^{5+} (%)	V_{AV}
VPO-150B0E	10.40	12.90	3.30	72.73	27.27	4.273
VPO-120B30E	7.33	14.63	3.10	83.54	16.46	4.165
VPO-90B60E	6.50	15.00	2.80	86.47	13.53	4.135
VPO-60B90E	4.07	12.10	9.00	19.16	80.84	4.808
VPO-30B120E	3.90	15.30	12.25	15.22	84.78	4.848
VPO-0B150E	3.30	16.00	13.20	14.84	85.16	4.852

Series 2

Sample	V_1 (cm^3)	V_2 (cm^3)	V_3 (cm^3)	V^{4+} (%)	V^{5+} (%)	V_{AV}
VPO-R24R24	6.50	15.00	2.80	86.47	13.53	4.135
VPO-U1R24	7.50	14.10	3.40	80.35	19.65	4.197
VPO-U2R24	7.10	14.80	3.10	84.02	15.98	4.160
VPO-U3R24	6.00	15.50	2.50	88.89	11.11	4.111

Series 3

Sample	V_1 (cm^3)	V_2 (cm^3)	V_3 (cm^3)	V^{4+} (%)	V^{5+} (%)	V_{AV}
10 wt% VPO/CSAC	5.50	14.10	5.80	65.68	34.32	4.343
20 wt% VPO/CSAC	4.90	15.40	5.70	71.78	28.22	4.282
30 wt% VPO/CSAC	4.10	17.70	5.60	78.21	21.79	4.218
40 wt% VPO/CSAC	4.10	18.90	5.50	80.50	19.50	4.195

Series 4

Sample	V_1 (cm^3)	V_2 (cm^3)	V_3 (cm^3)	V^{4+} (%)	V^{5+} (%)	V_{AV}
10 wt% UVPO/CSAC	5.50	16.10	3.80	88.89	11.11	4.111
20 wt% UVPO/CSAC	5.30	16.40	3.50	83.41	16.59	4.166
30 wt% UVPO/CSAC	5.10	16.70	3.20	85.42	14.58	4.146
40 wt% UVPO/CSAC	4.90	17.10	3.00	87.25	12.75	4.127

APPENDIX K

TPR Calculation

Calculation of reduction activation energy

$E_a = 0.066T_m$ where T_m: Maximum reduction temperature (Kelvin)

$\chi = Ae^{\left(\frac{-E_a}{R \times T_m}\right)}$ where A: 1×10^{13}
R: 0.001987 kcal $K^{-1}mol^{-1}$

$[H_2] = \frac{P}{R \times T}$ where P: Presure (0.009869 atm)
R: 82.056 $cm^3 atm\ K^{-1}mol^{-1}$
T: Ambient temperature (298 K)

$E_r = RT_m \ln\left[\frac{A(H_2)}{\chi}\right]$ where R: 0.001987 kcal $K^{-1}mol^{-1}$

Example of calculation:

For VPO-150B0E, V^{5+} peak reduction temperature = 880 K

$E_a = 0.066(880)$
$= 58.080$ K

$\chi = (1 \times 10^{13})e^{\left[\frac{-58.080}{(0.001987)\times(880)}\right]}$
$= 0.03754\ s^{-1}$

$[H_2] = \frac{0.009869}{(82.056) \times (298)}$
$= 4.036 \times 10^{-7}$ mol cm^3

$E_r = (0.001987)(880) \ln\left[\frac{(1 \times 10^{13})(4.036 \times 10^{-7})}{(0.03754)}\right]$
$= 32.3363$ kcal mol^{-1} x 4.184 J/cal
$= 135.295\ kJmol^{-1}$

Calculation of amount of oxygen species removed

Example of calculation:

For VPO-150B0E, amount of oxygen species removed from V^{5+} peak
= 414.256 μmol/g
= 414.256 x 10^{-6} mol/g
= (414.256 x 10^{-6} mol/g) x (6.02 x 10^{23} atom/mol)
= 2.494 x 10^{20} atom/g

Calculation for the ratio of oxygen removed

Example of calculation:

For VPO-150B0E:
Amount of oxygen species removed from V^{5+} peak = 2.494 x 10^{20} atom/g
Amount of oxygen species removed from V^{4+} peak = 9.607 x 10^{20} atom/g

$$\text{Ratio of } V^{4+}/V^{5+} \text{ oxygen species removed} = \frac{9.607 \text{ x } 10^{20}}{2.494 \text{ x } 10^{20}}$$
$$= 3.852$$

$$\text{Ratio of } V^{5+}/V^{4+} \text{ oxygen species removed} = \frac{2.494 \text{ x } 10^{20}}{9.607 \text{ x } 10^{20}}$$
$$= 0.259$$